The University Of Sheffield.

Department of Mechanical Engineering

Gas Turbine CO_2 Enhancements on Carbon Capture and Storage

Kelachi Omehia

December 2020

Professor Mohamed Pourkashanian| Professor Derek Ingham| Professor Lin Ma| Dr Kevin Hughes| Dr Alastair Clements| Dr Stavros Michailos| Dr Karen Finney.

Thesis submitted to the University of Sheffield in fulfilment of the requirement for the degree of Doctorate of Philosophy (PhD)

Declaration of Authorship

I confirm that:

i. This work was carried out under supervision of the Department of Mechanical Engineering as part of the fulfilment of the requirements of the Doctoral of Philosophy (PhD);
ii. Where any published work was consulted, this has been clearly stated;
iii. Where I have quoted from the work of others, the source has been provided. With the exception of such quotations, the thesis is entirely my own work;
iv. I have acknowledged all sources of help required for the purpose of this work;
v. Where any part of the thesis has previously been submitted for a degree or any other qualification at the University, this has been clearly stated;
vi. Where any work resulting from this work have been published, it has been clearly stated;

Journal Publications

Chapter 4 is associated with the following publication, still yet to be submitted;

- Omehia, K. C., Michailos, S., Hughes, K. J., Ingham, D. B., & Pourkashanian, M. (2020). Modelling CO_2 Injection in PACT MGT using characteristic maps.

Chapter 6 is associated with the following publication;

- Omehia, K. C., Clements, A. G., Michailos, S., Hughes, K. J., Ingham, D. B., & Pourkashanian, M. (2020). Techno-economic assessment on the fuel flexibility of a commercial scale combined cycle gas turbine integrated with a CO2 capture plant. *International Journal of Energy Research*, *44*(11), 9127-9140.

Conference Presentations

The presentations in conferences attended throughout this project are;

- Performance evaluation of PACT Pilot-Plant Micro Gas Turbine (2017 UKCCSRC ECR Winter School, Nottingham)
- Impact of natural gas composition variation on the performance of PACT Pilot-Plant Micro Gas Turbine (2017 UKCCSRC Biannual Meeting, London).

Acknowledgement

The author would like to acknowledge the UKCCSRC for the PACT facility in Beighton, Sheffield, where most of the experiment work implemented in the thesis was carried out.
I would like to thank Professor Mohamed Pourkashanian, Professor Derek Ingham and Dr Kevin Hughes for the support provided during the course of the project, which led to the successful completion of this thesis.
I would like to acknowledge Dr Stavros Michailos, Dr Clements Alastair, Dr Maria Elena Diego for their guidance throughout this project.
I would also like to thank my friends and research colleagues from the Energy 2050 group, especially Abdul'Aziz Aliyu, with whom I started my research journey and helped create an unforgettable experience whilst undergoing the project.
Finally, I would like to say a specially thanks to my family for the financial funding and sponsorship, as well as the mental care provided during the period of the PhD programme.

Abstract

The objective of this research was to investigate the impact of increasing the CO_2 concentration in the exhaust flue gas in gas turbines via exhaust gas recirculation (EGR) and selective exhaust gas recirculation study (S-EGR). The gas turbine types explored are the micro gas turbine (MGT) and the combined cycle gas turbine (CCGT). Both gas turbines were integrated with a chemical absorption capture plant operated using MEA, in order to determine the reduction in carbon emissions into the atmosphere. Modelling the CCGT, involved a fuel flexibility study as well as a techno-economic analysis carried out to determine the cost of electricity (COE) and cost of CO_2 avoided (COA) to ascertain the economic and energy savings involved as well as the emission reductions. The study on the MGT, entailed the experimental and modelling analysis of S-EGR via CO_2 injection into the compressor inlet, with a maximum CO_2 injection flowrate of 300 kg/h. The experimental campaign carried out on the MGT and capture plant were based at the LCCC, in Sheffield. The performance of the MGT is investigated over a range of power outputs (100 kWe to 60 kWe) and the emission properties are recorded. It was observed that the CO_2 flue gas concentration increased from 1.8 mol% to 9.6 mol% and 1.5 mol% to 11.6 mol% at 100 kWe and 60 kWe respectively, which improved the performance of the integrated capture plant, indicating that S-EGR operation in the MGT could reduce the specific reboiler duty by 15% whilst increasing the liquid-gas ratio, at a constant capture rate of 90%, thus, reducing overall energy costs. The CCGT study entailed the modelling of fuel flexibility via increasing the CO_2 content in the fuel from a conventional natural gas composition with 1 mol% CO_2 to a maximum CO_2 content of 10 mol%. Then, an Exhaust Gas Recirculation (EGR) study, involving a 35% EGR ratio stream from the exhaust to the compressor inlet, in which the CO_2 content in both the fuel and the air were increased. In both studies, the CCGT is integrated to a capture plant, to reduce the emissions from the power plant. The results indicate that implementing EGR in a CCGT provides better working conditions for the integrated capture plant, when operating with various fuel compositions. The COE and COA associated with EGR implemented CCGT's are noticeably lower and thus proving its high energy savings and emission reductions.

Table of Contents

Nomenclature

A	Area
Ar	Argon
CH_4	Methane
C_2H_6	Ethane
C_3H_8	Propane
C_4H_{10}	Butane
CO_2	Carbon Dioxide
Cp	Specific Heat Capacity at constant pressure
Cv	Specific Heat Capacity at constant volume
h	Enthalpy
H	Head
L/G	Liquid/Gas
$\dot{m}$	Mass flowrate
M	Mach number
N	Rotational Speed
N_2	Nitrogen
NO_x	Nitrogen Oxides
O_2	Oxygen
P	Pressure
PR	Pressure Ratio
Q	Heat
R	Universal Gas Constant
T	Temperature
Z	Compressibility factor
ε	Effectiveness
η	Efficiency
υ	Velocity of the fluid
γ	Specific Heat Ratio

Abbreviations

ACP	Amine Capture Plant
AMP	2-Amino-2-methyl-1-propanol
ASU	Air Separation Unit
BPV	Bypass Valve
CCS	Carbon capture and Storage
CCGT	Combined Cycle Gas Turbine
CDT	Compressor Discharge Temperature
CFD	Computational Fluid Dynamics
COA	Cost of CO_2 Avoided
COE	Cost of Electricity
CHP	Combined Heat and Power
DCC	Direct Contact Cooler
DEA	Diethanolamine
DOE	Department of Energy
EGR	Exhaust Gas Recirculation
FTIR	Fourier Transform Infra-red
GHG	Greenhouse Gas
HAT	Humidified Air Turbines
HEX	Heat Exchanger
HRSG	Heat Recovery Steam Generator
IEA	International Energy Agency
IEO	International Energy Outlook
IGCC	Integrated gasification Combined Cycle
IPCC	Intergovernmental Panel on Climate Change
ISO	International Organization for Standardization
LHV	Lower Heating Value
LVR	Lean Vapour Recompression
MEA	Monoethanolamine

MDEA	Methyl diethanolamine
NETL	National Energy Technology Laboratory
NGCC	Natural Gas Combined Cycle
OECD	Organization for Economic Cooperation and Development
PACT	Pilot-scale Advanced Capture Technology
PES	Primary Energy Saving
SCADA	Supervisory Control and Data Acquisition
S-EGR	Selective Exhaust Gas Recirculation
SFC	Supplementary Firing Cycle
TIT	Turbine Inlet Temperature
TOC	Total Overnight Cost
TOT	Turbine Outlet Temperature
TPC	Total Plant Cost
UKCCSRC	UK Carbon Capture and Storage Research Centre

1. Introduction

This chapter introduces the energy demand in a growing global economy. Also highlighted are the environmental impact of greenhouse gas (GHG) emissions and its cause. There is focus on the major contribution to these emissions and the methods aimed at reducing these emissions.

1.1. Background

As shown in Figure 1.1 [1], there is an observed increase in global temperatures over the last 79 years, which has raised concerns regarding the future of the planet. Figure 1.1, shows the temperature anomalies observed over a 139-year period. The negative anomalies indicate a reduction in global temperatures and the positive anomalies indicate an increase in global temperatures. The annual variations are paired with a LOWESS smooth (non-parametric regression analysis that relies on a k-nearest neighbour model) [1], which gives an effective smoothing of approximately five years. The Intergovernmental Panel on Climate Change (IPCC) 5th Assessment Report (AR5), 2014, confirmed the 4th Assessment Report's assertion that global warming of our climate system is associated with an observed increase in anthropogenic GHG concentrations due to increased human activities [2]. Hence, the importance in developing GHG mitigation technology [3].

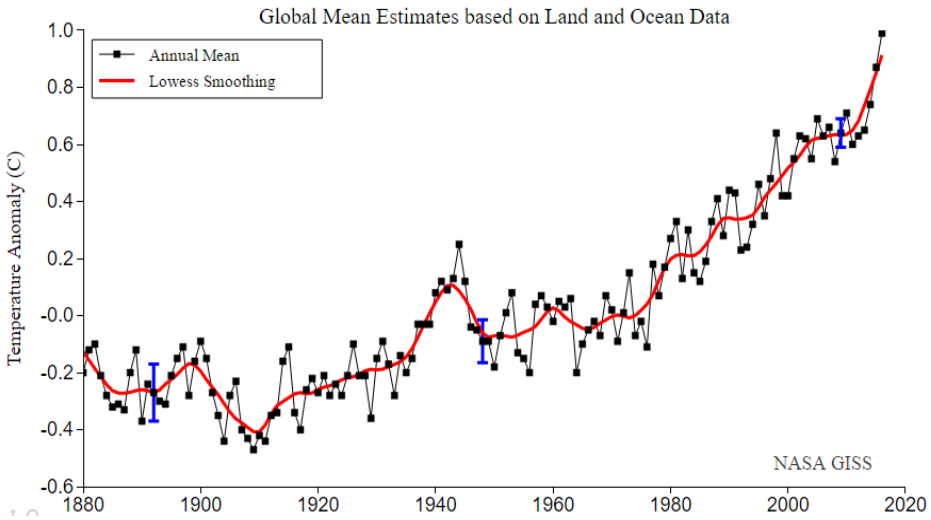

Figure 1.1: Temperature anomaly as a function of the year (1961-1990) [1].

The synthesis report by the IPCC confirms that much of the increase in global temperatures can be attributed to the influence of human activities such as the use of fossil fuels, cement production and gas flaring [2]. These daily human activities that require energy generation lead to an increase in the anthropogenic GHG into the atmosphere with CO_2 emissions contributing to about 78% of the global GHG emissions [2]. Figure 1.2 shows the increasing trend in atmospheric CO_2 concentration in parts per million as measured at the Mauna Loa Observatory, Hawaii [4].

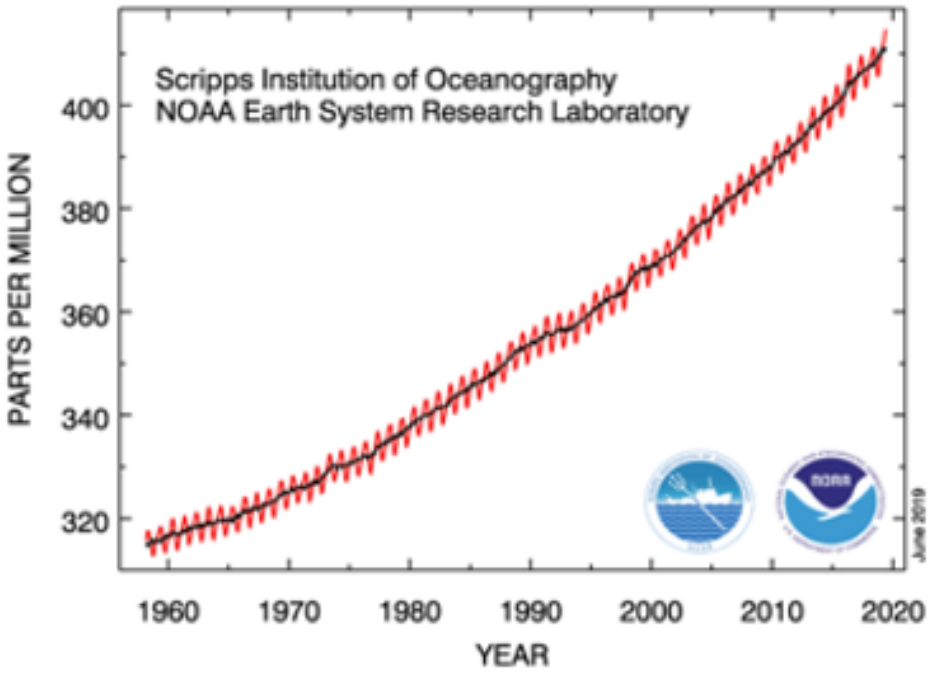

Figure 1.2: Atmospheric CO_2 concentration as a function of the time as measured at the Mauna Loa Observatory, Hawaii (latest CO_2 reading of June 2019 is 414.42ppm) [4].

It is observed that the CO_2 emissions have significantly increased from a value of 315 ppm in 1960 to a level above 414.42 ppm in 2019 according to the daily measurements of CO_2 emissions as illustrated in Figure 1.2 [4]. This increase in atmospheric CO_2 is considered to be mostly energy-related. As shown in Figure 1.3 [2], electricity and heat production related GHG emissions account for 25% of the total emissions from the five major economic sectors in 2010 followed by Agriculture Forestry and Other Land Use (AFOLU).

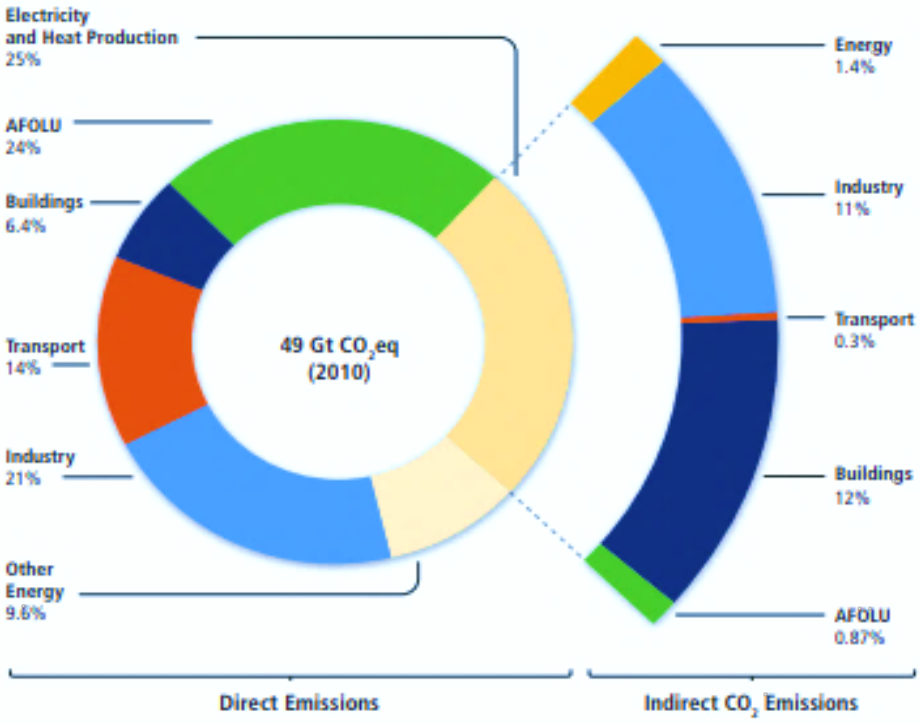

Figure 1.3: GHG emissions from the major economic sectors [2].

Energy demand is expected to increase in the coming years as a result of the growing population and the development of global economies. Also, there is an established correlation between the increase in energy demand and the increase in CO_2 concentration in the atmosphere, as a result of the increase in carbon-intensive energy generation. The largest increase in energy demand is expected to take place in developing countries where there is a 46% to 58% predicted increase in energy consumption between 2004 to 2030 [5].

The International Energy Outlook (IEO) 2013 [6] also projects an increase in global energy consumption by 56% between 2010 and 2040 [6]. Figure 1.4, shows the projected trend of energy consumption from 1990 to 2040. The energy consumption is measured in Quadrillion Btu where 1 Quadrillion Btu is equivalent to 1.005 ExaJoules. As shown in Figure 1.4 [5], most of the growth in energy consumption occurs in non-OECD (Organization for Economic Cooperation and Development) Asian countries. Furthermore, the center of gravity of energy consumption in developing Asian countries is expected to grow over the next 20 years, with the Asian middle classes accounting for much of the growth in global

GDP compared to other developing countries [7]. In these countries, the demand for energy is driven by strong, long-term economic growth and rapidly growing populations [6, 8].

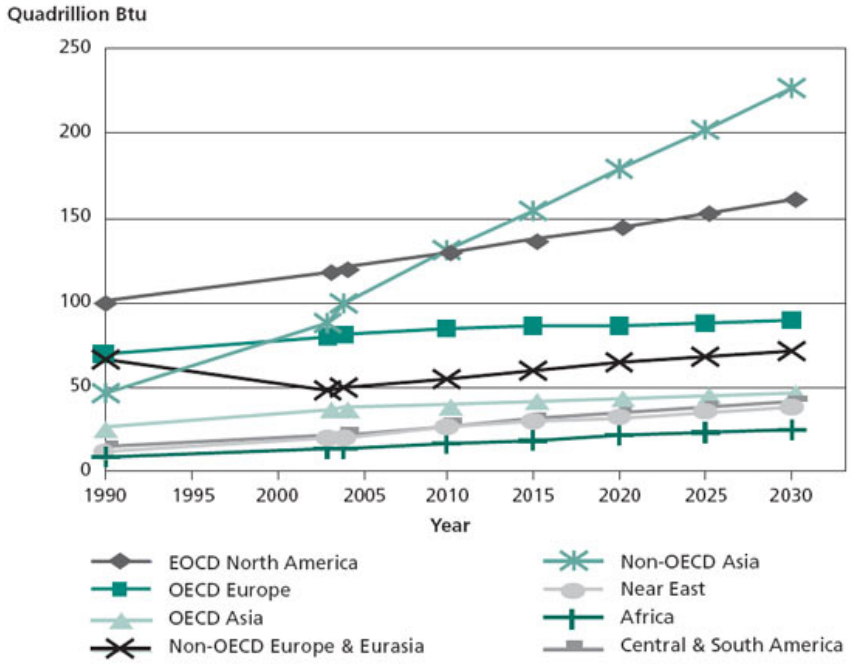

Figure 1.4: Market energy consumption for OECD and non-OECD countries from 1990-2030 [5].

The energy consumption in industrialized countries, where there is a stable economy and the population growth is slow, is projected to grow at a relatively lower rate compared to developing countries. It is projected that approximately half of the increase in global energy consumption by 2030 will be for energy generation and for transportation [5]. The trend in energy consumption will inherently affect the energy market. Currently, there is a move to energy generation processes with low carbon emissions to deal with the increasing trend of GHGs that affect the environment. These have led to the focus on carbon emission reduction technologies. Currently, there are five approaches considered and adopted by various countries to reduce their CO_2 emissions [9, 10] and these are as follows:

i. Improving energy efficiency in power plants with the use of new technologies.
ii. Increase usage of low carbon fuels such as biogas.
iii. Use of renewable energy such as wind and solar energy.
iv. Application of geoengineering approaches, such as afforestation (planting new trees in barren land) and reforestation (restocking trees in existing woodlands).
v. Carbon Capture Utilisation and Storage (CCUS).

In many parts of the world, GHG emission concerns and energy supply security have enabled government policies that support the development of renewable energy generation [6, 11]. This has led to renewable energy being the fastest growing energy generation processes available with a predicted average growth of 2.8% annually from 2010 to 2040 [6].

As the development of renewable energy sources continues to increase, the benefits and advantages associated with these energy sources have been made clear. However, the challenges associated with renewables still persist. This is due to the novelty associated with renewables, unclear control, and higher capital expenditure compared to conventional fossil fuel technologies [12]. Wind and solar power costs have been slightly reduced in recent years, due to the increase in efficiency-to-cost ratio of renewable technologies and the decrease in initial cost related to materials and manufacturing process assemblies [12]. Another challenge associated with renewable energy generation is the variability in energy generation patterns exhibited, which creates problems when integrating these energy sources with the grid [12]. The intermittence of wind and solar energy hinders the economic competitiveness of these technologies as there might not be the availability of energy at times of great importance [6]. Other problems associated with renewable energy sources are its inability to provide flexible and dispatchable power, which will become increasingly important with increase in global energy demand [13]. Studies have been carried out looking into the intermittency of renewable energy sources. In a United Kingdom study, wind installations operated at less than 20% of their potential output for approximately 40% of a given year [14].

Also, there is predicted to be a global increase in energy generation form nuclear power from 2.3 trillion kWh in 2012 to 3.1 trillion kWh in 2040 and to 4.5 trillion kWh in 2040 as stated in the IEO 2016 [11]. This growth is attributed to the GHG emission concerns and the energy supply security in non-OECD countries [6, 11]. However, due to the aftermath of the March 2011 disaster at Fukushima Daiichi in Japan, there is predicted to be a strong decline in the nuclear energy generations share from 25% in 2015 to 15% by 2040 in OECD countries [8]. This is mainly due to the current policies aimed at the retirement of nuclear capacity in OECD countries [6].

Although renewable energy is the fastest growing energy source, fossil fuels are still expected to meet much of the world's energy demands [8, 11]. As shown in Figure 1.5, petroleum and other liquids remain to be the largest source of energy till 2040, although there is a predicted decline in market energy consumption from 33% in 2012 to 30% in 2040 [8, 11]. On a global scale, the petroleum and liquids consumption increases in the industrial and transportation sectors, particularly motor gasoline and distillate fuel oil, whilst experiencing a decline in the residential and energy generation sector [8, 11 and 15]. It is expected that fossil fuels will retain approximately 80% of the world energy consumption through 2040 with natural gas being the fastest-growing fossil fuel [16].

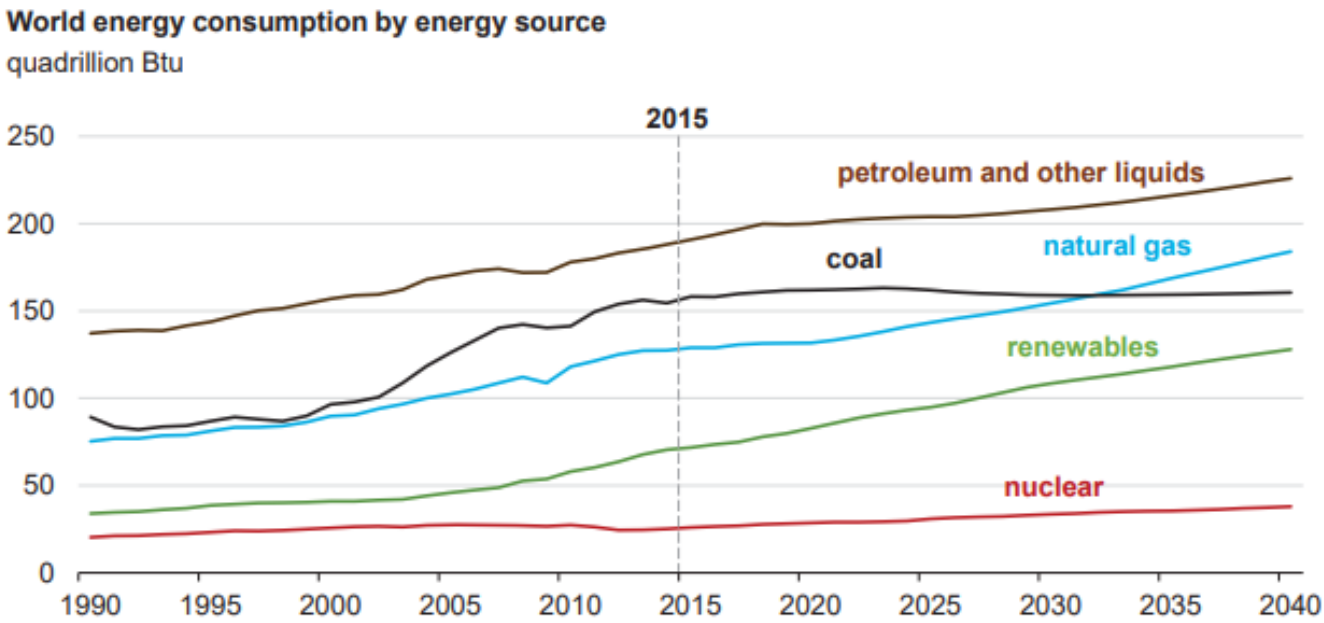

Figure 1.5: World energy consumption by various energy sources, 1990 – 2040 [8].

1.1.1. Petroleum and other liquids

According to the IEO 2017 Reference case, the world's consumption of petroleum and other liquid fuels will increase from 95 million barrels per day in 2015 to 113 million barrels per day in 2040 [8]. All growth in the petroleum and liquids energy utilisation is attributed to the transportation and industrial sectors of the economy [6, 11]. Furthermore, the increase in consumption is more prevalent in non-OECD countries compared to OECD countries, with demand rising by 1.3% per year, where a strong economic and population growth increases its demand [8]. This will lead to a growth in CO_2 emissions from petroleum and liquid consumption worldwide.

The IEO 2017 predicts that OPEC (Organization of the Petroleum Exporting Countries) will invest in incremental production, so as to increase or maintain their share of the global liquids production through to 2040 [8, 11]. However, the use of petroleum and liquids in the energy generation sector will experience a decline due to factors such as the predicted high oil prices and the relatively lower cost for natural gas which will introduce a need to use alternative energy sources [8].

1.1.2. Coal

The use of coal shows the slowest growth worldwide within the time frame shown in Figure 1.5 [8]. The global consumption of coal remains roughly the same after 2015 as shown in Figure 1.5 [8], with India and China using the largest amounts in energy generation, and together with the United States, they account for 70% of the world coal use [6, 11]. Reliability in supply is the main reason for the use of coal in developing countries. Coal is mainly used for electricity production and this accounts for 45% of the world coal consumption in 2012 and this will decrease to 32% by 2040 due to the increased demand in low CO_2 emitting fossil fuels such as natural gas [11]. The industrial sector accounted for 26% of the total coal used in 2012 and this will decrease to 24% in 2040.

The carbon content of coal is greater than other fossil fuels, such as natural gas, and therefore it emits more CO_2 during combustion. This is because natural gas is more energy dense, therefore it has a lower rate of CO_2 emission. Coal became the leading source of world energy-related CO_2 emissions in 2006 and it has been predicted that it would remain the leading source through 2040, nevertheless it is expected to decrease from 43% in 2012 to 38% in 2040 [17].

1.1.3. Natural Gas

Natural gas, which main constitutes of methane, ethane, propane, butane, carbon dioxide, nitrogen and small amounts of hydrogen, accounts for the largest increase in world energy consumption, with an increase from 120 trillion cubic feet (Tcf) in 2012 to 203 Tcf in 2040 [11]. This is as a result of the abundant natural gas resources available and its robust production [11, 16].

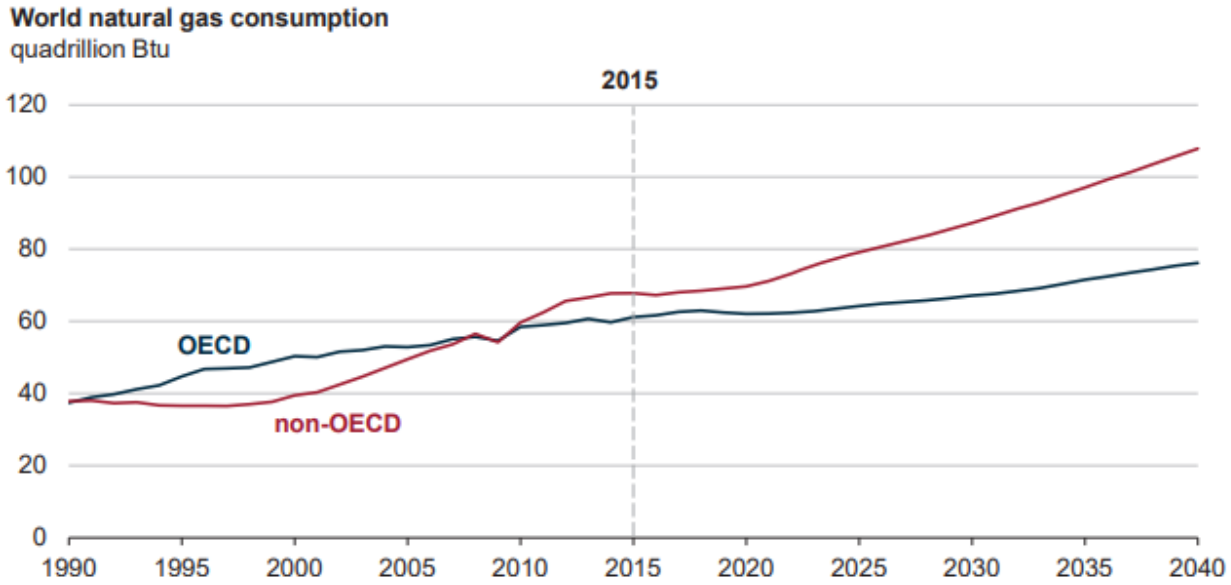

Figure 1.6: Natural gas consumption comparison between OECD and non-OECD countries [8].

As shown in Figure 1.6, natural gas consumption is predicted to keep growing in both OECD and non-OECD countries from 2015 to 2040, with the majority of its growth occurring in non-OECD countries [8] due to its growing demand energy for its economic and population growth. Furthermore, the global natural gas consumption is expected to increase in non-OECD countries from 53% in 2015 to 59% in 2040 [8]. It is predicted that natural gas will remain a key fossil fuel in energy generation and the industrial sector in many countries, with these sectors accounting for nearly 75% of the projected global natural gas consumption [8, 11]. The increase in natural gas consumption is driven by the predicted low natural gas prices, which will reduce the competitiveness of coal-fired energy generation. Since this is at the expense of the growth in renewables, there is projected increase in natural gas-fired energy generation [15]. Natural gas production in the United States from shale gas and tight oil plays an important role in the future of natural gas production. However, the negative environmental impacts associated with shale gas such as fracking, (which can lead to air and water pollution as well as seismic activities due to the high pressures used) are not being factored in. The technological advancements and improvements in industry practices reduces resource development cost and increases the natural gas production volume [15]. In the future, the increasing

natural gas supply from the United States, Canada and China is predicted to come from shale formations, which will help supply global markets [6, 8, and 15]. Advancements in the horizontal drilling and hydraulic fracturing techniques will provide newly discovered natural gas resources, supporting the global growth in natural gas consumption [11].

As of 2015, 50% of the natural gas production is accounted for by shale resource development. By 2040, shale resource development is projected to account for nearly 70% of the United State natural gas production, 50% of China's natural gas production, and in the future, most of the natural gas resources from Canada are expected to come from tight oil resources from regions within the country [8]. The IEO 2013 [6] predicts the tight and shale gas resources in Canada and China will account for more than 80% of their total domestic production in 2040. According to the IEO 2016 [11], there is an average increase in energy-related CO_2 emissions from liquid fuels, natural gas and coal from 1990 to 2040. However, the energy-related CO_2 emission growth is slowed after 2012 by a gradual shift from coal towards natural gas [8], and this is because natural gas combustion produces less greenhouse gas emissions compared to coal and petroleum products [11]. Thus, the carbon footprint of natural gas is observed to be better than coal and other petroleum products.

In OECD countries, energy-related CO_2 emissions remain stagnant through to 2040 whilst in non-OECD countries, the CO_2 emissions are predicted to grow at a rate of 1% a year from 2015 to 2040 [8]. With the high fuel operational flexibility and reduced capital cost of new gas-fired power plants, natural gas continues to be an attractive fossil fuel for energy generation [15]. As governments begin looking towards the implementation of cleaner and lower CO_2 emission strategies, the push to natural gas to displace coal and other fuels will be encouraged. However, to further reduce the energy-related CO_2 emissions, low carbon technologies will have to be implemented. In the past, there have been climate policy protocols and conventions aimed at reducing the release of dangerous anthropogenic gases (caused by human interference) into the climate system. The major agreement put into force after the United Nations Framework Convention on Climate Change (UNFCCC) in 1992, was the Kyoto Protocol in Japan, 1997 [18], which set binding targets for industrialized countries for reducing greenhouse gas emissions.

1.2. Carbon Capture

To reduce the CO_2 emissions from energy generation plants and reduce the greenhouse gas emissions, there are several techniques which can be employed. The separation of CO_2 for capture requires the modification of traditional power plant processes. There are four main processes currently used in the capture of CO_2 from power plants and these are as follows;

i. Post-combustion capture.
ii. Pre-combustion capture.
iii. Oxyfuel combustion.
iv. Chemical looping.

1.2.1. Post-combustion capture

This process removes the CO_2 from the exhaust flue gas from the power plant after combustion. Post-combustion capture is usually retrofitted in existing power plants and has been proven to work at small-scale with CO_2 recovered at rates up to 800 tons per day [10]. On a further note, there are two commercial-scale coal fired power plants currently operating with retrofitted post-combustion CCS, which are; The Sask's Power Boundary Dam Plant in Canada and the NRG Petra Nova Plant in USA [19]. The major drawback with post-combustion capture is the high cost and the energy penalty associated with the process [20]. Hence, post-combustion capture increases the cost of electricity (COE) by 32% in gas-fired plants and 65% in coal-fired plants [21].

The most used and viable technique is the absorption technique which involves the use of chemical solvents to absorb the CO_2 [9]. The CO_2 is separated from the exhaust flue gas by passing through a continuous scrubbing system, consisting of an absorber and a desorber. The solvents can be regenerated through a stripping or regenerative process by heating. Examples of common solvents are monoethanolamine (MEA), diethanolamine (DEA) and potassium carbonate (K_2CO_3) [22].

1.2.2. Pre-combustion capture

This process involves the pre-separation of the CO_2 from the fuel before combustion. This process is mostly used in Integrated Gasification Combined Cycle (IGCC) power plants [10]. For coal-fired plants, the gasification process is conducted in a gasifier under a low oxygen level, forming a synthetic gas (syngas) which consists mainly of CO and H_2. The syngas then undergoes a water-gas shift reaction with steam to form more H_2 with the CO gas being converted to CO_2 [9]. Natural gas, containing mainly methane (CH_4), can be reformed to syngas containing H_2 and CO and the rest of the process is similar to that described for coal. The equations highlighting these processes are as follows [9];

$$Coal \overset{gasfication}{\Longrightarrow} CO + H_2$$
$$CH_4 + H_2O \overset{reform}{\Longrightarrow} CO + 3H_2$$
$$CO + H_2O \overset{water-gas\ shift}{\Longrightarrow} H_2 + CO_2 \quad (1.1)$$

There are two types of reforming for natural gas, namely steam reforming and auto thermal reforming. The reactors for both steam reforming and auto thermal reforming, generate a blend of CO and H_2, which will vary based on the technology and operating parameters implemented [23]. Steam reforming is an endothermic reaction, where some of the natural gas is used for firing in the reformer furnace to provide the heat required for the reforming reaction. Auto thermal reforming is a combination of steam reforming and partial oxidation. Partial oxidation is an exothermic reaction and hence provides some energy required for the endothermic steam reforming reaction [23].

After reforming and the water-gas shift reaction, the CO_2 is separated from the hydrogen in the reactor by CO_2 separation technologies, such as chemical absorption and the pure stream of CO_2 is compressed and sent for storage or utilisation [9, 23]. In the case of natural gas fired power plants, the cost of CO_2 avoided is 112 $/ *ton* CO_2 for pre-combustion capture compared to a 58 $/ *ton* CO_2 for post-combustion capture as

highlighted in a study by the IEA (International Energy Agency) greenhouse gas R&D programme (2006) [24]. Also, the cost of electricity obtained was 9.7 c/kWh and 8 c/kWh for pre-combustion and post-combustion capture respectively.

1.2.3. Oxyfuel combustion

This type of combustion refers to a process where the fuel combustion takes place with an oxygen (typically 95% pure) and CO_2 rich recycled flue gas rather than air to produce an exhaust flue gas containing a lower concentration of nitrogen, leading to substantial reduction in thermal NO_x formation [9, 25]. The pure oxygen used in this process is obtained from an air separation unit (ASU) [9], and the low amount of NO_x in oxy-fuel combustion is due to the negligible amount of nitrogen in the oxidant [25]. Oxy-fuel combustion with pure oxygen occurs at temperatures as high as 3500°C, which is far too high for materials used in power plants. This temperature is controlled by the proportion of flue gas recycled into the combustion chamber to about 1300°C in typical gas turbine cycles and 1900°C in oxy-fuel coal-fired boilers using current technology [3].

The flue gas from this process consists only of water vapour and CO_2, as well small amount of pollutants, such as SO_2 [26]. As SO_2 can lead to corrosion problems, it is removed via flue gas desulphurization methods [9]. After condensation of water vapour from the exhaust flue gas, the flue gas would then contain 80-98% of CO_2, depending on the type of fuel used [3], which is then compressed, dried, transported and stored [26].

The main energy penalty in oxy-fuel combustion occurs due to the oxygen supply for the combustion process which comes from an energy intensive ASU [27]. This affects the cost of CO_2 avoided and the cost of electricity when compared to other capture technologies. In the case of natural gas fired power plants, the cost of CO_2 avoided is 102 $\$/ ton\ CO_2$ for oxy-fuel combustion capture compared to a 58 $\$/ ton\ CO_2$ for post-combustion capture as highlighted in a study by the IEA greenhouse gas R&D programme (2006) [24]. Also, the cost of electricity obtained was 10 c/kWh and 8 c/kWh for oxy-fuel combustion and post-combustion capture respectively.

1.2.4. Chemical looping combustion

This process involves an indirect combustion system that avoids contact between the fuel and the oxidant. A metal oxide is used as an oxygen carrier as a replacement of pure oxygen directly for the combustion. The process involves two stages in two reactors: a reduction (fuel) column and an oxidation (air) column. In the first column, the metal oxide is reduced to a metal while the oxygen released is used to oxidize the fuel to CO_2 and water. In the second column, the reduced metal oxide is oxidized with air and recycled in the process. The exhaust flue gas from the reduction reaction consists mainly of CO_2 and water and the exhaust flue gas from the oxidation reaction consists mainly of N_2 and unused O_2 [28]. A pure stream of CO_2 for separation can be obtained by condensing out the water [9], with no extra energy needed for separation.

There are various metal oxides that can be used for this process (as oxygen carriers), including Fe_2O_3, NiO, CuO and MN_2O_3. Their effectiveness has been studied by researchers, such as Ishida et al. [29] and Cho et al. [30], with focus on the conversion rate of the oxygen carrier. However, most investigations have been conducted with Fe_2O_3 [28].

Table 1.1

Advantages and Disadvantages of CO_2 Capture technologies [9].

Capture technology	Advantages	Disadvantages
Pre-combustion	Full mature technology and hence high CO_2 concentration absorption efficiency.	Efficiency decay problems associated with hydrogen-rich gas turbine fuel.
Post-combustion	Mature technology compared to others and easily retrofitted.	Low CO_2 concentration affects capture efficiency.
Oxy-fuel combustion	High CO_2 concentration that enhances absorption efficiency. Low NO_x in flue gas.	- Corrosion problems - High energy penalty
Chemical Looping	Main combustion product is CO_2, hence neglecting the need for intensive air separation.	Technology still under development.

1.3. Challenges of Carbon Capture Technologies with Fossil Fuels

The adaptation of these carbon capture technologies for energy generation depends on the energy source and system being used, as each carbon capture technology is easier to deploy with some energy sources compared to others. In oxy-fuel combustion, the energy being used by the air separation unit is high, which leads to a high efficiency drop in the system due to a high energy penalty [9]. Although the cost of carbon capture with oxyfuel is lower than for conventional pulverised coal plants, due to the lower flue gas flowrate and increased concentration of CO_2 in the exhaust flue gas. However, the cost of the ASU and flue gas recirculation reduces its economic advantage [31]. In pre-combustion capture, there are temperature-associated heat transfer problems and issues that lead to efficiency decay that occur due to the use of a hydrogen-rich gas turbine fuel. Also, there is a high capital cost for the pre-combustion sorbents currently available [9]. Chemical looping is a process in the early stages of development and as such, there is inadequate large scale operational experience [9, 31]. Post-combustion capture with

amines has proven to have the greatest near-term potential to reducing GHG emissions [31], due to its ability to be retrofitted with existing power plants. As well as the numerous research with both pilot and industrial scale operational facilities which have demonstrated its feasibility and practicality.

The two main parameters used in defining the performance of carbon capture technologies are the energy penalty and the capture efficiency. The capture efficiency is the percentage of CO_2 emissions captured from the flue gas introduced into the capture plant. Whilst the energy penalty is the energy required by the capture plant to regenerate the amine to be used in the CO_2 capture process. Both parameters define the operation of the capture plant and are thus paramount in understanding the performance of the system.

However, the main challenge with post combustion capture is the high cost and energy penalty involved with low CO_2 emitting fuels, which affect the capture efficiency of the system [9]. Another reason for low CO_2 emissions, is the lean pre-mixed combustion chamber in the gas turbine, which ensures ultra-lean combustion is taking place. This occurs due to combustion temperature reduction and leads to emissions reductions from the gas turbine (NO_x included). As a result, the low emissions also contribute to a decrease in energy penalty in the capture plant, due to higher CO_2 partial pressures in the flue gas which favours the capture reaction [32].

In this project, two main processes are investigated to combat the high energy penalties associated with integrating post-combustion capture with natural gas power generation. They involve increasing the CO_2 concentration in the exhaust of the gas turbine via Exhaust Gas Recirculation (EGR) and Selective Exhaust Gas Recirculation (S-EGR). The first process involved S-EGR of CO_2 into the air intake of the compressor, in a micro gas turbine (MGT). In this study, a MGT is modelled, and investigated with S-EGR via CO_2 injection. The techniques and methodology employed to ensure an accurate depiction of the operation of the MGT under S-EGR conditions are detailed in this work. The increased CO_2 content flue gas in passed through a novel CO_2 capture plant for CO_2 removal. The impact of S-EGR on the capture plant is also studied and reviewed in this project.

In the second process, the CO_2 concentration in the fuel (fuel flexibility) is increased, to simulate the combustion of high CO_2 content natural gas. In this study, the increase in CO_2 concentration in the fuel is investigated, with the implementation of EGR on the CCGT. The study details the impact of varying CO_2 concentrations on a gas turbine with EGR, with a focus on the technical and economic viability study of the process. These processes are investigated with focus on the performance of these systems, when integrated to post-combustion CO_2 capture plants.

1.4. Research Objectives

The proposed research will contribute to both experimental and modelling knowledge on the impact of EGR and S-EGR on gas turbines when integrated to a post-combustion capture system. With the use of EGR and S-EGR in gas turbines, we aimed at improving the performance of an integrated post-combustion capture systems.

To investigate this, a set of research objectives are set out to determine the benefits both thermodynamically and economically, associated with the inclusion of EGR and S-EGR in gas turbines coupled to a post-combustion capture system.

The objectives of this thesis involve investigating the effect of S-EGR in a MGT via the injection of CO_2 in the MGT and investigating the effect of EGR in a CCGT, operating with varying fuel compositions. Other objectives involve investigating the effect of increased CO_2 concentration in the flue gas on the performance of a two-absorber CO_2 capture plant, resulting from EGR and S-EGR processes. Another performance parameter in the two-absorber capture plant which is analysed is the amine concentration. This helps provide a better understanding of the capture process.

This research suggests an approach to accurately develop a process model of the micro gas turbine (MGT), available at the PACT (Pilot-scale Advanced CO_2 Capture Technology) facility in Beighton, Sheffield. To validate this modelling process, baseline experimental data will be obtained from the PACT facility. For the capture process, process modelling will be carried out on a new two-absorber post-combustion capture plant, available at the

same PACT facility, for the purpose of capturing the CO_2 from the gas turbine emissions. This enhancement from a one-absorber post-combustion plant, is aimed at improving the CO_2 absorption capacity of the capture process.

Investigating the effect of S-EGR and EGR will involve modifications to the micro gas turbine available at the PACT facility, which has to be replicated in the model, thus highlighting the importance of the modelling methodology represented in this thesis.

It is intended that the economic viability this modification will be taking into consideration, hence a techno-economic study is carried out on the CCGT coupled to a capture plant. In addition, the impact of higher CO_2 content fuels will be investigated and documented, to understand the cost and emissions benefits associated with the use of EGR in commercial-scale gas turbines coupled to a post-combustion capture plant.

The novelties of this research are as follows:

i. Improves the methodological flaws associated with characteristic maps, by using Matlab to analyse the effect of varying CO_2 injection flow rates in a MGT.
ii. Resolves a gap in the literature, regarding the process modelling of a two-absorber pilot-scale CO_2 capture plant with increasing CO_2 content flue gas and increasing amine concentration, based on experimental data available at the PACT facility.
iii. Resolves a gap in knowledge regarding the technical and economic analysis of a standalone CCGT and CCGT modified with EGR, integrated with CCS, whilst operating with high CO_2 content fuels.

1.5. Research Questions

i. Can process modelling of a micro gas turbine be performed accurately with the implementation of characteristic map?
ii. How does S-EGR via CO_2 injection affect the performance of a micro gas turbine?
iii. How can the characteristic maps be scaled to accommodate the implementation of S-EGR on a gas turbine?

iv. How does a post-combustion CO_2 capture plant perform with higher CO_2 concentration in the flue gas?

v. How does a post-combustion CO_2 capture plant perform when operating higher amine concentrations?

vi. What effect does EGR on CCGT performance, whilst operating with higher CO_2 content fuels?

vii. What are the cost and emission reductions associated with commercial-scale CO_2 capture plant benefit from both EGR and operating with higher CO_2 content fuels?

1.6. Research Limitations

Within the timeframe of this project, there have been some unexpected and unplanned natural occurrences that have led to a delay in collation of results and submission of the thesis. These include a flood in the PACT, Sheffield in November 2019 (third year of the project) and the National Lockdown that started in March 2020 due to the COVID-19 global pandemic. The flood led to the closure of the PACT centre which caused a re-direction of the project towards complete modelling as it was no longer possible to finish the planned experimental campaign. The lockdown due to COVID-19, caused a delay in modelling as the University had to be shut down with no access to the research offices for research students/staff, hence restricting access to the software as the modelling software could only be accessed on the University network. This was later remedied using the remote desktop connection, which was set up at home for continuation of the project. These delays caused an estimated overall delay of six months in the estimated project deadline. The PACT flood caused a three-month setback from November 2019 to February 2020, during which other modelling work was considered and carried out. The COVID-19 pandemic caused a further three-month setback as modelling work could not be carried out effectively due to problems with the operating the software from home, which was later rectified with remote desktop connection.

1.7. Thesis Outline

Chapter 1: Introduction – This chapter focuses on the need for the research study being carried out and research gaps being filled by the research study in this thesis. The global energy use and the different fossil fuels used in the growing economy for energy generation, as well as the various climate change mitigation techniques available.

Chapter 2: Literature review – This chapter introduces a critical review of literature relating to work that has been carried out on studies similar to the research topic of this thesis. The different studies are compared and their final conclusions are investigated to highlight topic areas of interests and novelty which are used to develop this research study. The research techniques and equations used in this research study are also highlighted, to show the thermodynamic principles applied in the systems used in this research study. The research gaps are highlighted in this chapter as well as the approaches being taken to perform this research study.

Chapter 3: Experimental methodology –This chapter highlights the procedures and steps used in the experimental set-up for both the micro gas turbine and the CO_2 capture plant, as well as instrumentation errors and accuracy. The instruments and their operation in experimental analysis are reviewed, as well as the start-up and shut-down procedures for both systems.

Chapter 4: MGT modelling methodology - This chapter highlights the modelling approach undertaken to investigate the effect of increasing the CO_2 flowrate into the compressor air intake. A model of the MGT is created with Aspen Plus with each component operated by characteristic maps. The model is validated with the manufacturer's data as well as with literature.

Chapter 5: Modelling the effect of selective exhaust gas recirculation on micro gas turbines – Building up from Chapters 3 and 4, this chapter focuses on the modelling aspect of the CO_2 S-EGR. The characteristic maps are scaled using thermodynamic principles for each CO_2 flowrate to provide accurate results which correspond to the experimental data.

Chapter 6: Modelling the effect of selective exhaust gas recirculation on pilot scale amine-based CO_2 capture plant – This Chapter entails the modelling of a two-absorber pilot scale CO_2 capture plant using Aspen Plus. The study investigates the effect of increasing the CO_2 concentration in the flue gas at different amine strengths.

Chapter 7: Techno-economic study of EGR and fuel flexibility on a Commercial Scale Gas Turbine integrated with CCS – This chapter focuses on the performance and economic analysis on a commercial scale NGCC (Natural Gas Combined Cycle) integrated with a CO_2 capture plant using amines (30% MEA). The process model was developed in gPROMS and using a capital cost scaling methodology, the economic impact of operating with higher CO_2 content fuels was analysed as opposed to operating with EGR. Both models were integrated to a CO_2 capture plant for greenhouse gas mitigation purposes.

Chapter 8: Conclusion and Future Remarks – This chapter highlights all the conclusions from the thesis as well as the future work that could be carried out.

2. Literature Review

In this chapter, a literature review is performed on the gas turbine as a system, as well as its operation and its different variations. Also, a review is performed on the CO_2 capture and storage (CCS) technologies, which provide a long-term solution to reduce the greenhouse gas emissions from energy generating plants (gas turbine in this project). A further review is performed on the thermodynamics of the gas turbine and CO_2 capture system which are implemented in this project. As mentioned in Section 1.3, the application of CCS leads to an increase in energy penalties in the system. However, there are different techniques which can be implemented to reduce this penalty, which are discussed in detail in this chapter.

2.1. Gas Turbine System

The history of the gas turbine system can be traced to 1867, with a German called Werner von Siemens, who presented the first 'dynamo' after having discovered the principle of electrodynamics [33]. Fast-forward to 1891, Charles E.L. Brown succeeded in transmitting 220kW of power 175km from Lauffen/Neckar to Frankfurt/Main, Germany. In the context of the evolutionary move from piston to rotating engines, first exercised in the field of steam engines, the design target for the future of the gas turbine system became clearer, with the theme being a move from the boiler, condenser, water pumps, and no auxiliary equipment towards a more stable system [33].

Further development of the gas turbine took place in the early 1900's with pioneering work done in Germany. Holzwart built the most successful series of early stage gas turbines between 1908 and 1933 with a steadily increasing power output up to 5MW. The first industrial application of the gas turbine was installed in a steel works in Hamborn, Germany, in 1933 [34]. In the history of energy conversion, the gas turbine technology has proven to be an efficient technology, with a simple gas turbine changing 30 – 40% of its fuel input into shaft output [35]. The first practical gas turbine used to generate electricity

was at Neuchatel, Switzerland in 1939 and was developed by the Brown Boveri Company [36].

As discussed in Section 1.1, with the current threat of global warming, due to the increase in greenhouse gas emissions from energy generation sources (such as gas turbines) operating with fossil fuels, there is a global shift towards low carbon emitting fossil fuels used in power generation such as natural gas. This corresponds to the global increase in the natural gas demand for fossil fuel combustion to generate electricity.

The gas turbine is considered to be at the heart of a natural gas power plant as it generates electricity by converting the fuel to mechanical energy, which is then used to generate electricity. The power and efficiency characteristics of a gas turbine are the result of a complex interaction of different turbomachines and a combustion system [37].

The conversion of heat released by burning the fuel into mechanical energy first involves compressing air in an air compressor, then injecting and burning the fuel at approximately constant pressure, and then expanding the hot gas in a turbine to generate power [37]. As a result of the complex interaction of the gas turbine technology, a part of the turbine power is used to drive the compressor. The remaining power is used as output shaft power to turn the energy conversion device called a generator [36].

There are different investigations that analyze the performance of different gas turbines. Ashley De Sa et al. [38] have studied the performance of a gas turbine at varying ambient temperatures. In this study, the performance of the gas turbine is investigated whilst exposed to changes in ambient conditions which deviate from the ISO (International Organization for Standardization) conditions. The aim of this study was to establish an assessment for local power generation planning, installation and forecasting.

Thamir et al. [39] performed an analysis on the thermal impact of the operating conditions on the performance of a combined cycle gas turbine. In this study, they developed a thermodynamic model of each component in the system, using thermodynamic equations that define the operation of each component in the model. Cameretti et al. [40] conducted research on a micro gas turbine equipped with exhaust gas recirculation and checked the performance of the micro gas turbine when supplying renewable bio fuels.

There are different types of gas turbines available for various applications. Conventional gas turbines range from a size of one or a few MWe to more than 350MWe [41]. The application of the gas turbine depends on the amount of power needed from the gas turbine. For large scale, industrial applications that require large power outputs, the most commercial based gas turbine is the combined cycle gas turbine (CCGT) that generates about 300MWe. For research purposes and small industrial purposes, another gas turbine referred to as a micro gas turbine (MGT) is used which generates a lower power output.

2.2. Combined Cycle Gas Turbine (CCGT)

In this gas turbine, not all the energy generated is converted to mechanical energy via the shaft, instead some energy is available in the exhaust gas. The only limitation is that the final exhaust temperature should not be reduced below the dew point to avoid corrosion from the sulphur in the fuel burnt [42]. The combined cycle gas turbine power plants are operated by a Brayton cycle based topping cycle and a Rankine cycle based bottoming cycle. The CCGT can achieve a thermal efficiency of around 60%, in contrast to a single cycle steam power plant which is limited to efficiencies of about 35-42%. [43]

The combined cycle gas turbine (CCGT) is comprised of a gas turbine, a heat recovery steam generator and a steam turbine as shown in Figure 2.1. The heat recovery steam generator (HRSG) is used to produce steam which is used to augment the shaft power produced in the steam turbine and hence increase the efficiency of the combined cycle. Alternatively, the exhaust heat may be used to produce hot water for factory or district heating, or hot steam for some chemical processes [42].

Many researchers have focused on improving the modeling of the CCGT utilizing the Brayton cycle gas turbine and Rankine cycle steam turbine. Kaushika et al. [44] investigated the optimum performance of a CCGT by modeling and simulation. Ibrahim et al. [39] carried out research on the thermal impact of operating conditions on the performance of a CCGT. They studied effects of variations such as ambient temperature, compression ratio, turbine inlet temperature, isentropic efficiencies for both compressor and turbine and mass flow rate of steam on the overall efficiency and power output.

The HRSG comprises of the economizer, the superheater and the evaporator. The purpose of the heat exchangers in the HRSG of a CCGT is to transfer heat from the gas turbine from the exhaust to the water or steam of the bottoming rankine cycle (steam turbine) [45]. The most common type of HRSG in a CCGT is the drum type HRSG with forced circulation. They are vertical, and the exhaust gas flow is vertical with horizontal tubes bundles suspended in the steel structure which supports the drums [46].

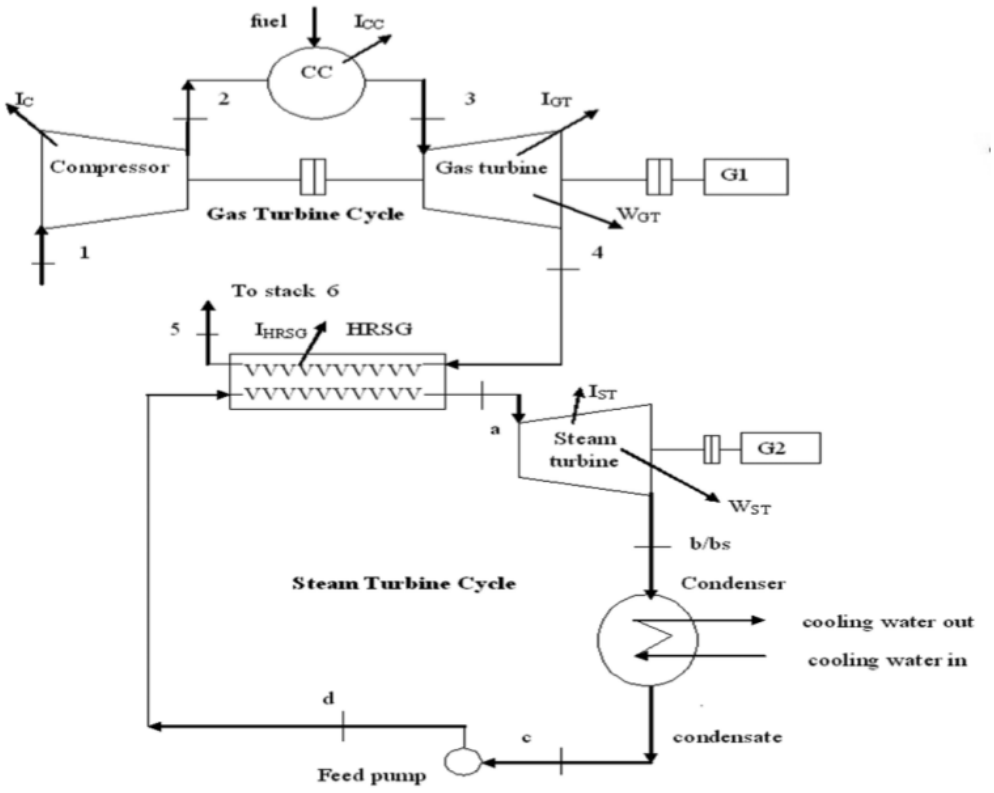

Figure 2.1: Schematic diagram of a CCGT cycle [47].

As shown in Figure 2.1, the gas cycle generates an exhaust gas with heat which is then transferred in the HRSG and the heat is used to power the steam cycle turbine. The temperature-entropy (T-S) plot of a commonly used CCGT is presented in Figure 2.2 and the systematic modeling of the two cycles are also presented [47].

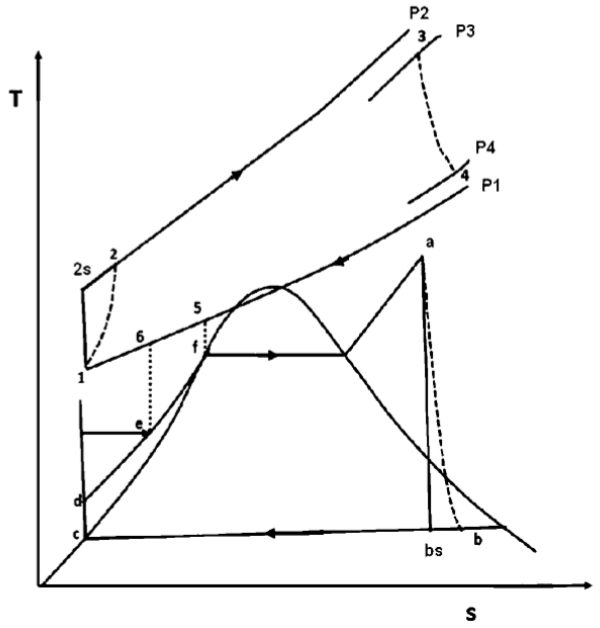

Figure 2.2: T-S diagram of the CCGT cycle [48].

Figure 2.2 shows a temperature-entropy diagram for a CCGT with two cycles (Brayton and Rankine). The process 1-2-3-4-1 forms the Brayton cycle while the process a-b-c-d-a forms the Rankine cycle. The process 1-2 is the adiabatic compression of air in the compressor and 1-2s is the isentropic compression. The process a-b is the adiabatic expansion of the steam in the steam turbine and a-bs is the isentropic expansion. The dotted lines shown in the figure highlight the actual gas and steam cycles while the single lines highlight the ideal gas and steam cycles. The point e is the feed water temperature to the HRSG and f is the saturation temperature corresponding to the steam pressure in the evaporator section. Between points 5 and 6, the exhaust gas is taken to the stack and emitted [48].

2.2.1. Brayton Topping Cycle

The major components of the Brayton topping cycle are the compressor, combustion chamber and the turbine. In these chambers, air is sucked in, pressurized and heated up for a later expansion process.

The compressor efficiency can be calculated by taking into account the deviation of the actual gas cycle from the ideal gas cycle. The isentropic efficiency (η_c) can be given as follows [43]:

$$\eta_c = \frac{T_{2s} - T_1}{T_2 - T_1} \tag{2.1}$$

where T_1 is the compressor inlet temperature, T_2 is the temperature at the end of isentropic compression and T_{2s} is the temperature at the end of actual compression. The actual temperature of at the outlet of the compressor can be calculated by taking into account the compressor efficiency and the specific heat ratio for air (γ_a) [43]:

$$T_2 = T_1 \left[1 + \frac{\left(\frac{P_2}{P_1}\right)^{\frac{\gamma_a - 1}{\gamma_a}} - 1}{\eta_c} \right] \tag{2.2}$$

The compressor work, neglecting the blade cooling can be calculated as follows [43]:

$$W_c = \frac{c_{pa} \text{ x } T_1 \left(\left(\frac{P_2}{P_1}\right)^{\frac{\gamma_a - 1}{\gamma_a}} - 1 \right)}{\eta_m \, x \, \eta_c} \tag{2.3}$$

where η_m is the mechanical efficiency of the compressor and c_{pa} is the specific heat of air which can be determined based on the working temperature.

The combustion chamber is where high pressure air is fed from the compressor before being passed to the turbine. In the combustion chamber, the fuel is ignited in the presence of the compressed air to produce a gas which goes to the turbine.

The basic combustion principle is based on the energy balance principle. Applying the principle of energy balance, we obtain [43]:

$$m_a c_{pa} T_2 + m_f \text{ x } LHV + m_f c_{pf} T_f = \left(m_a + m_f\right) c_{pg} \text{ x } TIT \tag{2.4}$$

where m_f is the mass flow rate of fuel (kg/s), m_a is the mass flow rate of air (kg/s), TIT is the turbine inlet temperature, LHV is the lower heating value, c_{pf} is the specific heat of the fuel, c_{pg} is the specific heat of the flue gas and T_f is the temperature of the fuel.
The high temperature gas mixture from the combination of the compressed air and the ignited fuel is expanded when it enters the turbine. The gas is expanded down to exhaust pressure, and producing a shaft work output in the process [43].

The isentropic efficiency of the turbine (η_T) can be expressed as follows:

$$\eta_T = \frac{T_3 - T_{4s}}{T_3 - T_4} \tag{2.5}$$

The exhaust gas temperature of the gas turbine can be expressed as follows:

$$T_4 = T_3\left[1 - \eta_T\left(R_{pg}\right)\right] \tag{2.6}$$

where R_{pg} can be expressed using the specific heat for the gas (γ_g):

$$R_{pg} = 1 - \frac{1}{\left(\frac{P_2}{P_1}\right)^{\frac{\gamma_g - 1}{\gamma_g}}} \tag{2.7}$$

$T_4 = T_{g1}$, where T_{g1} is the inlet gases temperature of the Heat Recovery Steam Generator.
The total work output of the turbine (W_T) is expressed as follows:

$$W_T = c_{pg} \text{ x } TIT \text{ x } \eta_T \text{ x } \frac{R_{pg}}{\eta_m} \tag{2.8}$$

Hence the net work output of the gas turbine is given by:

$$W_{net} = W_T - W_c \tag{2.9}$$

2.2.2. Heat Recovery Steam Generator (HRSG)

The HRSG is analysed by applying the energy balance for gas and water in each part of the HRSG, the gas temperature and water properties [39].

Applying energy balance, the heat available with exhaust gases (Q_a) from the gas turbine can be given as follows [43]:

$$Q_a = m_g \text{ x } c_{pg} \text{ x } \left(T_{g1} - T_{g4}\right) \text{ x } h_{1f} \tag{2.10}$$

where T_{g1} is the exhaust temperature entering the HRSG, T_{g4} is the exhaust temperature from the HRSG and h_{1f} is the heat loss factor which typically ranges from 0.98 to 0.99 [49]. The steam obtained from the HRSG expands to the condenser pressure in the steam turbine.

The superheater duty is expressed as follows:

$$Q_{sh} = m_s \left(h_{sh} - h_s\right) = m_g \text{ x } c_{pg} \text{ x } \left(T_{g1} - T_{g2}\right) \text{ x } h_{1f} \tag{2.11}$$

2.2.3. Rankine Bottoming Cycle

This steam turbine cycle can be captured in terms of the mass and energy conservation equations, semi-empirical relations and thermodynamic state conservation [39, 43]. The energy balance, heat rejected and pump work can be found in Mohanty et al., [43].

The net output of the steam turbine plant is given by:

$$W_{snet} = W_s - W_p \tag{2.12}$$

The thermal efficiency of the steam cycle is given by:

$$\eta_{total} = \frac{W_{snet}}{Q_a} \tag{2.13}$$

2.3. Micro Gas Turbine

The other type of gas turbine is the micro gas turbine (MGT). The MGT is a single shaft low-pressure gas turbine that comes as either a simple gas cycle or a combined heat and power cycle system. MGTs thermodynamically differ from large scale GTs such as the CCGT, mainly in the type of turbomachinery used, the presence of a recuperator and the high rotational speed of the shaft [41].

MGTs came into the automotive market between 1950 and 1970. The first MGT was based on a gas turbine designed to be used in generators of missile launching stations, aircraft and bus engines, among other commercial means of transport. However, for a variety of reasons, the MGT did not achieve great success in the automotive segment [50]. The interest in the market for stationary power spread in the mid-1980 and accelerated in the 1990s, with the reuse in the automobile market in hybrid vehicles and when the demand for distributed generating technologies increased [51]. This lead to an increase in the use of the MGT in the energy market. Some companies in the United States, United Kingdom and Sweden have recently introduced in the world market commercial units of MGTs. Among these companies are: Allied Signal, Elliot Energy Systems, Capstone, Ingersoll-Rand Energy Systems & Power Recuperators Works TM, Turbec, Brownman Power and ABB Distributed Generation & Volvo Aero Corporation [50].

The main technical barriers to the implementation of the MGT are its low efficiency in its basic configuration when compared to an equal power output reciprocating engine. Also, the efficiency of the MGT decreases at partial load and the use of fuels with lower LHV such as biogas also reduces the efficiency [52]. In addition, MGTs require power conditioning to produce electricity at grid frequency and this will inherently increase installation and maintenance cost. The non-technical barriers to the implementation of the MGT are that the maintenance requires more skilled personnel compared to reciprocating engines [52].

The current set of MGTs performance range is 15 to 300kWe with an efficiency of 25-30%, pressure ratio of 3 to 5 and a maximum cycle temperature of 800 to 1000^{0}C [50, 52]. The MGT can be used for power generation in the industrial, commercial and residential sectors. They could be used for continuous power generation; premium power; emergency standby; remote power; combined heat and power; mechanical drive; and wastes and bio-fuels [52]. Pilavachi et al. [52] highlights the market potential for the MGT in industries such as chemicals, food and drink, pulp and paper and textiles.

However, the largest use for micro-turbines is in the combined heat and power sector, where the exhaust gas from the MGT, which has a high temperature, is used to produce

heat for other purposes such as industrial heating [52]. Inclusion of the CHP in the gas turbine will increase the overall efficiency of the gas turbine, often exceeding 80%.

The main advantage of the MGT lies in the small power output, their low environmental impact in terms of pollutants (NO_x), and operation and maintenance costs [41]. The easy operation and installation [50] of the MGT makes it the most efficient and reliable system used for research purposes.

The technology of MGTs is not new, as researchers such as Ali et al. [53] and Nikpey et al. [54] have conducted research attaining to the impact of the operating conditions on the performance of a micro gas turbine and a detailed thermodynamic analysis on a micro gas turbine. This thesis is mainly focused on the performance analysis of the MGT because of its advantages for research stated earlier as well as it provides a realistic recommendation for commercial-scale gas turbines.

Although thermodynamically different, MGTs share an identical set-up of a compressor, combustion chamber and a turbine, when compared to larger scale gas turbines [55]. However, to increase the electrical efficiency of the MGT to an acceptable value, the temperature of the compressed air entering the combustor is increased using the heat from the turbine exhaust system. This is done using an air-to-air heat exchanger referred to as a recuperator or a regenerator. This allows the net electrical cycle efficiency to be increased to as much as 30% compared to the average net efficiency of un-recovered (un-regenerated) MGTs are 17% [56].

2.3.1. Turbec T100

The MGT used in the analysis in this thesis is a Turbec T100 series 3 and comprises of six components [57]:

i. Generator and Electrical Systems
ii. Compressor, Turbine and Combustion chamber
iii. Recuperator/Regenerator
iv. Valve Connection to the CCP
v. Exhaust Gas/Water Heat Exchanger
vi. Control System

The Turbec T100 is typically fueled by natural gas, but the use of other fuels such as biogas, syngas, diesel, kerosene, methanol, LPC is also possible. The MGT uses a high-speed generator to produce electricity with the compressor and the turbine both placed on the same shaft as the generator. A recuperator/regenerator is connected to the MGT to improve the electrical efficiency [56, 57].

The Turbec T100 uses a radial centrifugal compressor to compress ambient air with a pressure ratio of about 4.5:1. The compressed air is preheated by a recuperator before it enters the combustion chamber where it is mixed with the fuel. The combustion chamber is of lean pre-mix emission type with low emissions of pollutants. The premixing of the air and the fuel enables clean combustion to occur at a relatively low temperature. Injectors are used to control the air-fuel ratio and the air-fuel mixture in the primary zone of the combustion chamber. In order to achieve low levels of CO, hydrocarbons and NO_x, the air-fuel mixture needs to be maintained in the combustion chamber for a relatively long period to allow for complete combustion [58]. The mixed gas then leaves the combustion chamber to the turbine where expansion occurs and the energy generated is used to drive the compressor and generator which are mounted on the same shaft as the turbine [56, 57].

The electrical power is generated by a permanent magnet rotating at high speed. The generator is water-cooled, and designed for high conversion efficiency. The frequency AC power from the generator is rectified and converted to DC and then converted to three-phase AC for export to the grid [56, 57]. The generator also acts as an electrical starter during start-up where power is taken from the grid until the turbine reaches its generating conditions.

The turbine consumes 330kW of natural gas and generates about 100kW of electrical power at 33% electrical efficiency. When the heat exchanger is added to the system, an additional 150kW of thermal power is generated which increases the overall efficiency of the system to 77% [57].

A schematic of the heat flow around the Turbec T100 is shown in Figure 2.3:

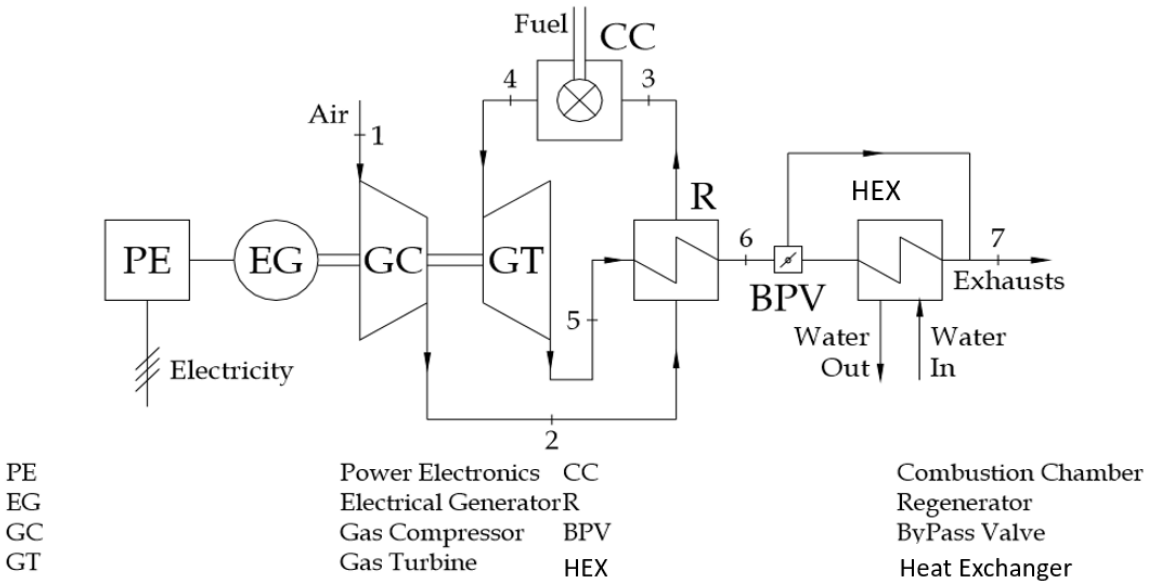

Figure 2.3: Schematic of a micro gas turbine [41].

The MGT can be operated in different operational modes:

- Non-cogeneration (electricity production only)
- Cogeneration (combined production of electrical and thermal energy)

In cogeneration mode, the MGT can be set to work with electrical or with thermal power priority or both. In the electrical priority operating mode, there is a 100% BPV (Bypass valve) opening which ensures that the HEX (heat exchanger) is skipped and the flue gas is taken out as exhaust whereas the thermal priority operating mode involves complete closure of the bypass valve (0% BPV opening), so that all the flue gases are passed though the HEX for thermal power recovery [41].

The main characteristic parameters of the MGT are as follows [41]:

i. Electrical power (PWR_{el})
ii. Thermal power (PWR_{th})
iii. Electrical efficiency (η_{el})

$$\eta_{el} = \frac{PWR_{el}}{\dot{m}_f * LHV} \tag{2.14}$$

iv. Thermal efficiency (η_{th})

$$\eta_{th} = \frac{PWR_{th}}{\dot{m}_f * LHV} \tag{2.15}$$

v. Total efficiency (η_{tot})

$$\eta_{tot} = \frac{PWR_{el} + PWR_{th}}{\dot{m}_f * LHV} = \eta_{el} + \eta_{th} \tag{2.16}$$

vi. Recuperator effectiveness (ε)

$$\varepsilon = \frac{T_{air,out} - T_{air,in}}{T_{gas,in} - T_{air,in}} \tag{2.17}$$

Where LHV is the lower heating value of the fuel, $T_{air,in}$ is the temperature of the air entering the combustor, $T_{air,out}$ is the temperature of the air leaving the recuperator into the combustor and $T_{gas,in}$ is the high temperature of the gas from the turbine entering the recuperator.

2.3.2. Micro Gas Turbine Performance

The maximum net power output in the MGT is limited by the temperature that the material of the turbine can support, associated with the cooling technology and the service life required. The main factors affecting the performance of the MGT are component efficiency and the gas temperature at the turbine outlet. Lee et al. [59] have carried out research on the MGT performance where they analyzed engine performance and component characteristics of a micro gas turbine. The performance parameters examined were the turbine outlet temperature, exhaust flue gas temperature, engine inlet temperature, compressor discharge temperature, compressor discharge pressure and fuel, and air flow rates [59].

During off-design operation of the MGT, the shaft speed changes during the power variation. At any given speed, there exists only a single operation condition, which satisfies

a specific turbine exit temperature; hence, full power is only available at maximum shaft speed [59]. Badran et al. [60] discussed the improvements on the gas turbine performance. An increase or decrease in the efficiencies of the compressor and turbine will have a great effect on the characteristics of the gas turbine. An increase in the compressor efficiency will decrease the work of the compressor and increase the expansion work of the turbine, hence improving the performance of the gas turbine system by increasing the net power output [60].

The operating conditions also vary with ambient conditions. An increase in ambient temperatures leads to an increase in the specific air consumption, which leads to more work being done by the compressor with a reduced net power output from the system and thus reducing the efficiency. The mass flow rate of the gases is also reduced [47, 60]. Researchers such as De Sa et al. [38] have focused on the performance of the gas turbine at varying ambient temperature. In their analysis, a correlation was developed between the ambient temperature and the decrease of the gas turbine power output. It was concluded that "for every 1 Kelvin increase in ambient temperature above ISO conditions, there is a 0.1% loss in thermal efficiency of the gas turbine system and 1.47 MW loss of power of the gross power generated".

2.3.3. Thermodynamics of a Micro Gas Turbine

The thermodynamics of the micro gas turbine is based on the Brayton cycle, of which in its ideal form consists of two isentropic processes and two isobaric processes. The arrangement of the simple gas turbine is such that the compressed air is ignited with the fuel in the combustion chamber at isobaric conditions. Expansion then occurs in the turbine from the hot gases from the combustion chamber, thus resulting in power generation.

The two isentropic processes represent the compression (compressor) and expansion (turbine) processes in the MGT [46]. The two isobaric processes represent the combustion process and the transfer of the exhaust gas from the turbine for other processes such as heat recovery (CHP). According to the first law of thermodynamics, energy can be converted from one form to another but total energy in the system must

remain constant. A simplified application of the first law of thermodynamics to the Brayton cycle has the following relationship [46];

Compressor:

$$W_c = \dot{m}_a(h_2 - h_1) \tag{2.18}$$

Turbine:

$$W_t = (\dot{m}_a + \dot{m}_f)(h_3 - h_4) \tag{2.19}$$

Total Work Output:

$$W_{cyc} = W_t - W_c \tag{2.20}$$

Heat added to the system:

$$Q_{2,3} = \dot{m}_f \text{ x } LHV = \left(\dot{m}_a + \dot{m}_f\right)(h_3) - \dot{m}_a h_2 \tag{2.21}$$

Overall cycle efficiency;

$$\eta_{cyc} = \frac{W_{cyc}}{Q_{2,3}} \tag{2.22}$$

2.3.4. Combined Heat and Power

CHP has always been of high significance for improving the efficiency of the energy sector in Europe, currently supplying about 10% of Europe's heat and electricity [61]. The use of CHP is targeted to increase to 30% of European electricity production in the long term according to COGEN Europe (The European Association for the Promotion of Cogeneration) [52].

The principal reasons for the ambitious targets set for the CHP is its contribution in the mitigation of greenhouse gas emissions. CHP reduces CO_2 emissions when compared with the separate production of heat and power. Currently, this saving can be up to 1000 tons of CO_2 per GWh of power production [52].

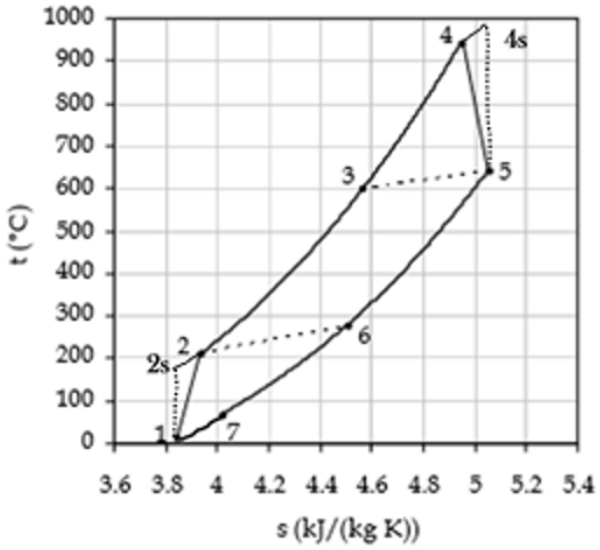

Figure 2.4: T-S Brayton cycle for a micro gas turbine with combined heat and power [41].

Figure 2.4 depicts the Brayton cycle for the MGT shown in Figure 2.3 for a BPV opening of 0%, which allows the gas to enter the heat exchanger. The performance of the cogeneration system can be evaluated by comparison with the separate production of heat and electricity. The most commonly used index is the PES (Primary Energy Saving) index, which quantifies the primary energy savings offered by the CHP operation compared with just normal operation of the MGT [41]. The PES index is calculated as follows:

$$PES = 1 - \frac{1}{\frac{\bar{\eta}_{el}}{\eta_{el\_ref}} + \frac{\bar{\eta}_{th}}{\eta_{th\_ref}}} \tag{2.23}$$

where;

- $\bar{\eta}_{el}$ and $\bar{\eta}_{th}$ are the electrical and thermal efficiencies of the cogeneration system averaged over a given period.
- η_{el_ref} and η_{th_ref} are the reference values of the efficiency for separate production of electrical and thermal energy.

A positive value of the index means that the primary energy consumption of the CHP system is lower compared to separate production over the time period considered [41].

2.4. Exhaust Gas Cycles

There are many advanced power generation cycles being developed and researched on, with the purpose of taking advantage of the thermodynamic characteristics of the system [62]. One of the advantages of these advanced gas cycles is the increase in CO_2 concentration in the flue gas, which provides a logical way of reducing the high electrical efficiency penalty caused by a CO_2 capture process [52], due to the increased CO_2 partial pressures incurred as there is more CO_2 in a specified volume of flue gas.

As mentioned earlier in Chapter 1 of the thesis, the concentration of CO_2 in the exhaust flue gas from the gas turbine is low and this has a large impact on the economic and technical viability of the carbon capture process [57]. To decrease the energy penalty, innovative cycle's configurations are considered to attain higher system performance [54]. The most promising cycles are the humidified air turbine (HAT) cycle, the exhaust gas recirculation (EGR) cycle and the supplementary firing cycle (SFC). These options all provide different changes in the operation and performance of the gas turbine with the main aim of reducing the associated energy penalty when integrated to a CO_2 capture plant.

2.4.1. Humidified Air Turbine (HAT)

This gas turbine cycle utilizes a higher mass flow to the expander/turbine via the injection of heated water into the compressed air flow before the combustion chamber [63]. Humidified air turbine cycles have a thermodynamic potential of electrical efficiencies similar to or higher than that of combined cycles [64].

The concept of HAT cycles was developed by Rao et al., [63]. According to Carrero et al., [65], the injection of water into the compressed air enables the recuperation of energy in the exhaust gas as well as augmenting the mass flow through the turbine for a given compressor input, thus increasing the electrical efficiency in the system.

Parente et al., [66], suggests the possibility of transforming a MGT into a micro Humid Air Turbine (mHAT), without major modifications to the system, except the combustion chamber. A thermodynamic assessment of a HAT cycle based on the MGT has been carried out by Parente et al. [66] which shows the potential for 5% and 50% increase in efficiency and specific power output respectively, compared to a standard recuperative MGT.

In addition to the components of the recuperative MGT case without CHP, a humidifier, an economizer, a heat exchanger and an EGC (Exhaust gas condenser) are added to the form the HAT cycle. Water is heated close to saturation point by the compressed air in the humidifier/saturation tower. The heated water enters at the top of the humidification tower and is brought in contact with the compressed air flowing in a counter-current manner that enters at the bottom of the tower [62]. Between the two counter current flows of the water and the compressed air, heat and mass are exchanged by direct contact. The evaporated water results in an increased mass flow of air leaving the humidifier and entering the recuperator [54]. The humidified air is then reheated in the recuperator before entering the combustion chamber. The hot exhaust gas from the combustion chamber is expanded in the turbine. After leaving the turbine, the excess heat in the exhaust gas is used to heat up the humidified air in the recuperator and to preheat the water flow to the humidifier in an economizer. To prevent water loss, most of the water content in the exhaust is condensed in an EGC and returned to the process.

2.4.2. Supplementary Firing Cycle (SFC)

The supplementary firing cycle (SFC) involves the combustion of additional fuel in the secondary combustion unit located at the exit of the gas turbine, Li et al.., [62]. This system leads to a reduction in efficiency compared to conventional NGCC's [62], however, it increases the power output of the gas turbine by around 30% during peak electricity demand as suggested by Kiameh et al., [67]. The overall system Lower heating value (LHV) efficiencies in supplementary firing cycles integrated with capture plants is about 43.1 - 48.1% compared to 50% in conventional CCGT's coupled with ACP's [62, 68 and 69]. This process involves the presence of a secondary combustion unit at the exit of the gas

turbine, where additional fuel and excess oxygen from the exhaust flue gas are burned [68, 70]. The combustion of the additional fuel, leads to the exhaust flue gas being re-heated for heat recovery in the HRSG to generate steam for the bottom rankine cycle [62]. The integration of supplementary firing is seen to also increase the temperature difference in the HRSG, thus increasing the flue gas temperature as well as increase the high-pressure steam production in the HRSG, leading to mitigating power losses due to steam extraction, as well as energy penalty reduction in the reboiler in the capture plant [70]. The increased temperature in the exhaust flue is also a limitation in the process, as it is a contributor to its lower efficiency and thermal stress is incurred in the HRSG tubes at temperatures above 800°C as suggested by Biliyok et al., [71]. Although, it can be increased to around 1300 °C, with the implementation of advanced alloys, insulated casings, high temperature-tolerant heat exchangers and water-cooled furnaces [62, 68 and 72]. The rise in temperature restriction has been found to increase the amount of fuel that can be burned, and further enhancing the CO_2 concentration in the exhaust flue gas [62, 72]. Also, a bottom rankine cycle with higher temperature capacity, such as a supercritical bottoming cycle may improve the efficiency [62].

The implementation of supplementary firing on a gas turbine integrated with carbon capture was proposed by Li et al., [62]. In this study, the concentration of CO_2 was reported to increase from 3.8 % mol to 6.7 % mol. However, with exhaust gas condensation, the CO_2 concentration could be further increased to 8.4 mol% [69]. The increase in CO_2 concentration is due to the combustion of the fuel in the secondary combustion chamber [68, 72]. This favors the chemical absorption process in the absorber column [69]. Other characteristics associated with supplementary firing are the resulting increased exhaust flue gas mass flow rate, which decreases the capital costs associated with the integration of a CO_2 capture plant [68, 70] and the reduction in reboiler duty due to the increase in steam production, thus returning the steam/rankine cycle to its full capacity while still meeting reboiler duty requirements [71]. The increase in exhaust flue gas flowrate, counteracts the benefits of high CO_2 concentration, which leads to the reduction in LHV efficiency [62]. However, with exhaust gas condensation, exhaust flue gas flowrate can be reduced [69].

Furthermore, the reduced O_2 content, due to supplementary firing causes amine solvent degradation [69]. However, keeping the O_2 concentration in the secondary combustion unit above 16 mol%, will assist in stabilizing combustion [62, 69], as most burners are not designed to operate below 21 mol% O_2. Also, work by Li et al., [62] and Ditaranto et al., [73], have reported high NO_x reductions in gas turbines with supplementary firing.

There are various studies suggesting the substitution of other fuels for fossil fuels with supplementary firing gas turbines such as biomass, with the benefit of venting the exhaust flue gas into the atmosphere without substantially contributing to increasing CO_2 emissions [70]. Researchers such as Gnanapragasam et al., [74] and Datta et al., [75]., have performed such investigations on NGCC plants and noted similar atmospheric CO_2 emissions reductions.

Other studies such as Bhattacharya et al., [76], have performance a comparative analysis on the performance of biomass firing in both NGCC and IGCC (Integrated Gasification Combined Cycle) plants, and concluded that the IGCC plant efficiency is lower than that of the NGCC, because the efficiency of the NGCC plant monotonically reduces with supplementary firing, whilst the maximum efficiency for the IGCC plant occurs at an optimum degree of supplementary firing.

2.4.3. Exhaust Gas Recirculation (EGR)

Gas turbines with exhaust gas recirculation are one of the most promising cycles which are currently under investigation. Together with reduced NO_x emissions, EGR benefits from being able to increase the CO_2 concentration and decrease the exhaust gas mass flow rate to be treated in the carbon capture process [54].

Although the literature is filled with creative gas turbine cycles, to aid in the removal of CO_2 from the exhaust flue gas by a capture many of these cycles require significant modifications to the gas turbine system [77]. The implementation of EGR simply requires redirecting some flue gas to facilitate the CO_2 removal process via increasing the CO_2 concentration.

The main technical challenges involved with the implementation of the EGR cycle is the replacement of the air inlet with exhaust flue gas which adversely affects some operating

parameters of the MGT, such as the flame stability, combustion efficiency, and hence results in increased amounts of carbon monoxide (CO) and unburned hydrocarbons (UHC).

Substantial amount of research has been conducted on the performance of the MGT with EGR cycle implemented. Akram et al. [78] discussed the effect of EGR on the performance of a pilot-scale CO_2 capture unit. Cameretti et al. [79] discussed the effect of NO_x through a CFD simulation of an EGR operated micro gas turbine. Cameretti et al., [80], also investigated the effect of EGR in a micro gas turbine operating with bio-fuels such as bio-ethanol and biogas. Cameretti et al., [80], concluded that bio-fuels can be operated in a MGT with low EGR ratios, to preserve an acceptable level of thermal efficiency, with the advantage of low NO_x emissions.

Li et al. [62] discussed the impact of EGR, HAT, SFC and EFC on the turbomachinery of a natural gas-fired power plant with post-combustion amine-based CO_2 capture. Further studies regarding the modelling of the MGT with EGR has been researched by Majoumered et al., [81] and Nikey et al., [82]. In these studies, a MGT was modelled with characteristic maps whilst the MGT was coupled to a chemical absorption CO_2 capture plant. Majoumered et al., [81] compared the EGR cycle and HAT cycle, with a Baseline MGT. This study highlighted that HAT cycles produced the highest efficiencies, however, with EGR there was marginal impact on the gas turbine turbo-machinery. However, with both cycles, the CO_2 capture process was considered to be less expensive when compared to the Baseline MGT. The effect of EGR ratio on the performance of the MGT coupled to a chemical absorption CO_2 capture plant was extensively investigated by Nikpey et al., [82]. Other studies such as Ali et al., [83], compared a HAT, STIG (Steam Injected Cycle) and EGR cycles using Aspen HYSYS. In this study, it was concluded that the CO_2 enrichment varied from 1.6 mol% to 3.7mol%, 1.8 mol% and 1.7 mol% for EGR, STIG and HAT cycles. Also, there was an observed decrease by 50% in the flue gas flowrate, which correlates to a small CO_2 capture system. Although, there is a decrease in electrical efficiency with EGR (9%), the benefits of EGR, when coupled to a CO_2 capture system outweighs the efficiency loss associated with the cycle.

Other methods of investigating EGR via CO_2 injection to the MGT inlet have been investigated by Ali et al., [84] and Best et al., [85] in a process called Selective Exhaust Gas Recirculation (S-EGR). Ali et al., [84], performed a modelling study on the effect of increasing CO_2 injection rate on the performance of the MGT and the downstream impact on the integrated CO_2 capture plant. The study aimed at providing a better understanding of EGR with the increase in CO_2 injection flowrate corresponding to an increase in EGR ratio. Alternatively, Best et al., [85], performed an experimental analysis on the MGT with EGR. The results obtained from Best et al., [85], validate the results observed by Ali et al., [84]. However, in the study conducted by Best et al., [85], a CO_2 capture plant was not included.

Commercially, the impact of EGR has been investigated by Li et al., [32], Ali et al., [86], Adams et al., [87] and Sipöcz et al., [88]. In these studies, a combined cycle was modified with exhaust gas recirculation and integrated to a CO_2 capture plant. Li et al., [32] performed a study on the impact of EGR on a natural gas combined cycle integrated to a MEA-based chemical absorption capture plant. A similar study was conducted by Ali et al., [86], that investigates the techno-economic implication of a natural gas combined cycle coupled to a MEA-based chemical absorption plant. Sipöcz et al., [88], compared a standard CCGT power plant integrated to a MEA-based chemical absorption plant to a CCGT with EGR and a plant configuration with additional alternative CO_2 removal process, comprising of absorber cooling and LVR (Lean vapour Recompression).

Other CCGT with S-EGR studies were carried out by Herraiz et al., [89], where two configurations for the CCGT with S-EGR, where investigated. The series and parallel configurations were observed to increase the net power output of the CCGT by 5.2% and 2.3% respectively. With the integration of an amine-based post combustion capture plant, the S-EGR in parallel, is observed to perform better than the series configuration, suggested by the higher power output and thermal efficiency associated with the configuration. Other CO_2 removal systems were investigated with the CCGT in parallel by Herraiz et al [90]. In this study, the use of structured adsorbents in a regenerative adsorption wheel configuration was considered for the application of S-EGR. The study investigated the practical feasibility of rotary adsorption with structured adsorbents for

the application of S-EGR with post combustion capture. The system was able to achieve a 97% selective CO_2 transfer efficiency and a 90% capture efficiency, with an 800 MWe CCGT.

The modelling of a commercial-scale CCGT with EGR and integrated to a MEA-based chemical absorption CO_2 capture plant, was detailed by Sander et al., [91]. In this study, the performance and operational behaviour of a CCGT coupled to a CO_2 capture plant is analysed. The net power output and electrical efficiency were observed to increase by 3.6% and 2.1% respectively, with the implementation of EGR. However, with the implementation of the CO_2 capture system, there is an observed 30% power loss due to steam extraction. This is due to less energy consumption from the CO_2 capture plant, as a result of the reduced exhaust gas flowrate and increased CO_2 concentration in the exhaust flue gas. In other studies, by Adams et al., [87], the individual components in the model were presented as well as the equations that define their operation. The CCGT was also operated under off-design conditions to determine the performance of the system under dynamic operation. A techno-economic study was also carried out in this study to determine the costs associated with dynamic operation of the CCGT. This study offered a detailed breakdown on the methodology in modelling EGR in a CCGT, coupled to a MEA-based CO_2 capture plant. Other part-load operations of the CCGT with S-EGR research have been carried out by Qureshi et al., [92]. Part-load operation of 80, 60 and 40% of a series, parallel and hybrid configurations for S-EGR n a 606 MWe CCGT coupled to a MEA-based CO_2 capture plant is analysed. In this study, the hybrid configuration had to highest CO_2 concentration in the flue gas and reduces the flue gas flowrate the most, highlighting its better performance, when compared to the series and parallel configuration.

Other studies carried out by Diego et al., [93, 4], have considered advanced configurations with CCGT's coupled with CO_2 capture plants. In this study, membranes were implemented in different two configurations; series and parallel, to investigate its CO_2 removal capacity. To provide an in-depth understanding in the application of these processes, further analysis on the economic cost was required on the NGCC's due to the complexity. In the EGR cycle, the exhaust gas from the turbine is recirculated and mixed with the air inlet upstream of the compressor. In this study, the total gross power output

was observed to increase with EGR, as well as the overall efficiency of the system and the CO_2 concentration in the exhaust flue gas. Other research, involving the use of membranes for CO_2 capture have been carried out by Merkel et al., [95], Russo et al., [96] and Baker et al., [97]. In the study by Merkel et al., [95], it was shown that the use of membranes can further enhance the CO_2 concentration in the flue gas from 4 mol% to 15-20 mol%, while reducing the minimum energy for CO_2 capture by 40%. In the studies by Russo et al., [96] and Baker et al., [97], the performance of the membrane was investigated with S-EGR, with focus on the membrane area and its permeability.

To maintain the efficiency, the recirculated stream is passed through an EGC, where it is cooled down before entering the compressor [54].

The level of exhaust gas recirculated is defined by the EGR ratio [54]:

$$EGR\ ratio = \frac{mass\ flow\ rate\ of\ the\ recirculated\ gas}{Total\ mass\ flow\ rate\ of\ the\ exhaust\ gas}\ \mathrm{X}\ 100 \tag{2.24}$$

As the EGR ratio increases, the CO_2 concentration in the exhaust gas increases and the mass flow decreases [62]. Since there is less oxygen available in the exhaust gases than in ambient air, the O_2 concentration before and after combustion decreases with increasing EGR ratio. From a combustion viewpoint, combustion chambers are usually built for air containing 21 mol% of O_2 and EGR considerably decreases the O_2 concentration [62]. Elkady et al. [98] studied the behavior of combustion in a DLN (Dry Low NO_x) combustor. The results obtained highlighted that low O_2 concentration in the combustion chamber could reduce the reaction rates, allow for combustion to spread over a large region and reduce peak flame temperature, which is not in favor of the oxidation of CO to CO_2. The study also highlights that the NO_x emissions are decreased by more than 50% with an EGR ratio of 35%.

2.5. Fuel Flexibility Review

Various researchers have conducted experimental and modelling work on different gas turbines with the different exhaust cycles as shown in Section 2.3.5, with the aim of reducing the energy penalty in the capture plant, when integrated. However, not much work has been conducted on the performance of the gas turbine integrated to a capture plant, whilst operating with different fuels.

There are various studies, which have been conducted on the performance of the gas turbine with various fuels implemented. Some studies considered in literature, include the use of alternative fuels instead of natural gas. Research has been carried out by Moliere et al., [99] on the technical considerations essential to the successful application of alternative fuels in gas turbines. The study focuses on the performance of the gas turbine when these fuels are implemented. The fuels investigated include coal-derived gases, non-conventional natural gas (weak gases and high CO_2 content gases) and liquid alternative fuels. Other systems such as IGCC's have also been investigated by Majoumerd et al., [100], where the fuels such as H_2-rich gas and cleaned syngas were implemented in a gas turbine and compared to baseline natural gas fuel. With no modification to the gas turbine, reduced performance of the gas turbine is expected for limited operational hours [101]. However, for uninterrupted gas turbine operation, some modifications will have to be implemented.

Most literature entail the performance of the gas turbine with biogas and bio-fuels such as Bohn et al., [102], that investigated the effect of biogas combustion on the performance of a micro gas turbine, whilst operating at a constant turbine inlet temperature and at a constant energy input to the combustor. Other researchers such as Nikpey et al., [103] have performed a modelling study, analysing a biogas-fueled micro gas turbine, and Nipkey et al., [101] has also performed experimental studies on a mixture of natural gas and biogas as a fuel with no engine modifications. Both studies investigate the performance of the MGT at decreasing methane concentrations and varying power loads, with the aim of mapping out an operational window at which the maximum possible level of biogas can be utilized for satisfactory performance of the engine [103].

Other researchers such as Cameretti et al., [40], have investigated the effect of a MGT modified with EGR whilst operating with bio-fuels. In this study, a CFD analysis was carried out on some solutions for the efficient employment of liquid and gaseous bio-fuels in lean-mixed combustion chambers in MGT's. Economically, Kang et al., [104], has performed an economic assessment of a 5MW-class gas turbine-based CHP, fueled with biogas, with the aim of determining the economic feasibility of operating the system.

Some researchers have directed their focus on the impact of natural gas composition on the performance of the MGT. Studies such as Abbott et al., [105], have investigated the effect of natural gas composition variability on the operation of the gas turbine. This study highlights the impact of varying fuel compositions on the wobbe index and the combustion dynamics within the system. Whilst other researchers such as Wasiu et al., [106], have investigated the effect of CO_2 content in natural gas on the performance characteristics of the engine. The limitations of the gas turbine regarding fuel variation have been documented by Nikpey et al., [101] and Abbott et al., [105], and with further variation in baseline fuel composition, the combustion chamber in the gas turbine is exposed to combustion flameout and over a period of time, component failure.

To apply fuel flexibility commercially, CCGT's will require further analysis due to the economic costs, thus, performing a techno-economic study would assist in identifying the benefits of fuel flexibility, which is considered in this thesis.

2.6. Post-Combustion CO_2 capture review

Technologies utilized for CO_2 capture are used in removing CO_2 from hydrocarbon gas streams in the oil and gas production business [107]. In this research, the CO_2 capture technique implemented is a post combustion CO_2 capture plant, as reviewed in Chapter 1 of the thesis. There are currently a range of technologies available for post combustion capture of CO_2, such as membranes, ionic liquids, enzyme-based systems and amine-based systems.

Membranes used in CO_2 capture allow the CO_2 in the exhaust flue gas to pass through, while blocking other components in the flue gas [9]. The main problem associated with

application of membranes are the low sensitivity of the membrane materials [108], making it difficult to achieve the specification required by the *International Energy Agency* (CO_2 recovery ratio of 80% or 90%) [109].

However, the development of polymeric membranes, as well as ceramic and metallic membranes can prove to produce significantly increased CO_2 separation and efficiency [9]. Various polymeric membranes have been reviewed by Brunetti et al., [108], where their CO_2 permeability and selectivity are compared. It was highlighted that only a few membrane materials possessed high CO_2 selectivities close to 100, and often the high selectivities corresponded with low CO_2 permeabilities. The study pointed out that the performance of the membrane is based on the composition, as well as the pressure of the flue gas. Researchers such as Korelskiy et al., [110], are currently looking into novel ceramic membrane materials, and have identified zeolite membranes as an attractive and promising technology, to replace polymeric membranes. This is due to their porous structure, thus displaying higher fluxes compared to polymeric membranes. This gives them the advantage of higher chemical and thermal stability compared to polymeric membranes [110].

There are various options in utilizing membranes in CO_2 capture. One concept, suggested by Figueroa et al., [31], involves the flow of the flue gas through a bundle of membrane tubes, while an amine solution would flow through the shell side of the bundle. As the flue gas flows through the tube, the CO_2 would be absorbed by the amine solution. This process blocks impurities to the amine, thus causing loss of amine as a result of stable salt formation. Other studies such as Diego et al., [93, 94], have investigated the implementation of membranes alongside other CO_2 capture technologies. Two different configurations for a membrane connected to an amine-based CO_2 capture plant were investigated, with the aim of increasing both the selectivity and permeability of the membrane. In this study, an amine-based capture plant is operated along with a membrane, with the membrane acting as a pre-concentrator and the amine-based CO_2 capture plant as the main CO_2 capture technology with limited energy input.

The use of ionic liquids for CO_2 capture is a novel method involving the use of a salts containing organic cations and either organic or inorganic anions [31]. The ionic liquids

dissolve gaseous CO_2 at high temperatures, thus neglecting the need for flue gas cooling. They are also physical solvents, therefore requiring less heat for the regeneration process.

Enzyme-based systems are a biological-based capture process that utilizes naturally occurring CO_2 reactions in living organisms [31]. One possibility is by the use of an enzyme-based system, which mimics the respiratory system in vertebrates [111]. The enzyme utilized is carbonic anhydrase (CA), which is the fastest, low-energy facilitator known for CO_2 [112]. CA was developed by Carbozyme Inc as a permeator, consisting of two microporous polypropylene hollow fiber membranes separated by a thin liquid membrane. The CA is attached to a hollow fiber wall to ensure the incoming CO_2 comes in contact with the CA to maximize conversion efficiency [111, 112].

Amine-based systems involve the use of chemical solvents in the CO_2 capture process. Commercially available solvents such as TEA (trimethylamine), DEA (diethanolamine), MDEA (methyl diethanolamine) and MEA (mooethanolamine) have shown to have different operating characteristics in the CO_2 capture plant. In literature, these various solvents are investigated and compared with the standard MEA solvent.

Studies such as Xue et al., [113], have performed a comparative study in the performance of MEA and DEA. This study concludes that the reboiler duty is more sensitive to lean loading in MEA compared to DEA, suggesting that the DEA has generally better performances. Other studies such as De Avila et al., [114], have conducted research into the thermal decomposition of MEA, DEA, TEA and MDEA. The data from the study showed that TEA was the most thermally stable, with the tertiary amines being more stable and the primary amines being the least stable. However, the study also shows that the CO_2 capture efficiency was inversely proportional to the thermal stability.

Other solvents being researched include AMP (2-Amino-2-methyl-1-propanol) and Pz (Piperazine). A study carried out by Fredriksen et al., [115], investigated the oxidative degradation of these solvents, when compared with MEA and DEA. Also, Koronaki et al., [116] carried out a parametric analysis, investigating the effect of inlet flue gas, liquid flow

rates, packing type, amine solution concentration, temperature of flue gas and liquid solvent on the performance of both AMP and MEA solvents.

Further research has been carried out on solvent mixtures. In a study by Rodriguez et al., [117], a mixture of DEA-MDEA was analyzed and compared to MEA and DEA solvents. The results from this study conclude that concentration of the DEA-MDEA mixture has a strong influence on the hydrodynamic behavior of the absorber column, related to the residence time and CO_2 capture efficiency.

In modelling an amine-based CO_2 capture plant, various studies have investigated the effect of changes in flue gas compositions, due to differences in power generation sources. Researchers such as Agbonghae et al., [118], have investigated the impact of varying flue gas conditions and compositions from four fossil fuel power generation sources on the performance an amine-based CO_2 capture plant. A techno-economic study was carried out to highlight the financial benefits and drawbacks associated with each process. Also, studies such as Rezazadeh et al., [119] and Akram et al., [120, 121], have investigated the effect of increasing CO_2 concentration in the flue gas through EGR in the gas turbine on the performance of the CO_2 capture plant.

In optimizing the performance of the amine-based CO_2 capture plant, various technologies have been considered in literature to develop the process, such as absorber intercooling and heat integration. Absorber intercooling involves single or multi solvent cooling stages, being applied to the absorber column, where a fraction of the solvent is cooled and returned to the absorber column [122, 123]. By inter-cooling the absorber column, the heat of absorption is released and the solvent temperature exiting the absorber column is reduced. This favors the absorption process via the high driving forces and increased absorption capacity of the solvent (rich loading) [122]. The driving force in this context can be defined as the differences in composition between the vapour phase (flue gas) and liquid phase (amine), caused by differences in partial pressures [124].

In a study by Amrollahi et al., [122], a CO_2 capture system with absorber inter-cooling was compared with a split-flow model and a system with the combination absorber inter-cooling and split flow. Other configurations compared were a chemical absorption process with LVR and absorber inter-cooling and LVR. The study concluded that the best

process was absorber inter-cooling with LVR as it produced the least power demands and the highest exergy efficiencies.

Studies have been conducted on this technique such as Knudsen et al., [125], that indicates the application of inter-stage cooling in the lower section of the absorber column has negligible impact on the performance of a MEA CO_2 capture system., whereas a reduction of up to 7% can be obtained with novel solvents. Other studies such as Li et al., [126], have obtained similar results with MEA as the solvent in an inter-cooling absorption system. However, the Li et al., [126], suggested a decrease in absorber column height, due to the increased driving force in the column at lower temperatures as described by Amrollahi et al., [122].

Other optimization process includes heat integration in the CO_2 capture plant, between different process streams [123]. This process involves the minimization of energy consumption whilst maximizing heat recovery [127]. There are four strategies in heat integration as suggested by Le Moullec et al., [123], which are; rich solvent splitting, rich solvent preheating, rich solvent flashing and parallel economizer agreement. The rich solvent splitting involves the rich amine stream is split into two flows. The first flow is pre-heated using a lean/rich heat exchanger and the second flow is maintained at a low temperature. The cold stream is injected at the top of the stripper column, whilst the heated stream is injected at an appropriate column height. Le Moullec et al., [123], noted that the higher temperature of the heated stream, the lower the injection height of the stripper. Rich solvent preheating involves heating the rich solvent above the maximum temperature in the economizer through heat transfer from the hot lean to the cold rich solvent. Rich solvent flashing entails the flashing of the hot rich solvent before its injection into the stripper. Finally, the parallel economizer agreement involves the splitting of the rich and lean solvent flow into two or more streams to be feed into heat exchangers.

2.7. Post-Combustion CO_2 Capture with MEA

In this thesis, the chemical absorption process is utilized, with MEA (monoethanolamine) implemented as the solvent in the amine capture plant. CO_2 capture using an alkanolamine

is one of the most widely used methods of CO_2 removal. Alkanolamines are classified as primary, secondary and tertiary amines depending on the number of hydrogen atoms attached to the nitrogen atom [128]. Each alkanolamine has one hydroxyl group and one amino group. The amino group reacts with the acid gases such as CO_2 due to its alkalinity and leads to absorption while the hydroxyl group increases its water solubility [129]. MEA (monoethanolamine) is classified as a primary alkanolamine because of its molecular formula $H_2NCH_2CH_2OH$, and due to it possessing two nitrogen atoms directly attached to a nitrogen atom. MEA is the most preferred solvent for CO_2 capture for exhaust gas streams with low concentrations of CO_2 and this is because of its low molecular weight which results in high solution capacity and a maximum absorption of CO_2 [129]. Although, MEA is the most preferred solvent, it has some disadvantages, such as its high corrosiveness when the concentration falls below 20% and the solutions are highly concentrated with acid gas. Another disadvantage is the high heat of reaction of MEA and CO_2, which results in high energy requirements for the stripping of CO_2 for regenerative purposes [129].

This process is an already available technology. MEA has been used as a solvent for non-selective removal of acidic gases from natural gas streams which are generally oxygen free for the past 60 years [107]. The process was modified to incorporate inhibitors to resist solvent degradation and equipment corrosion when applied to CO_2 capture from flue gas in which oxygen is present.

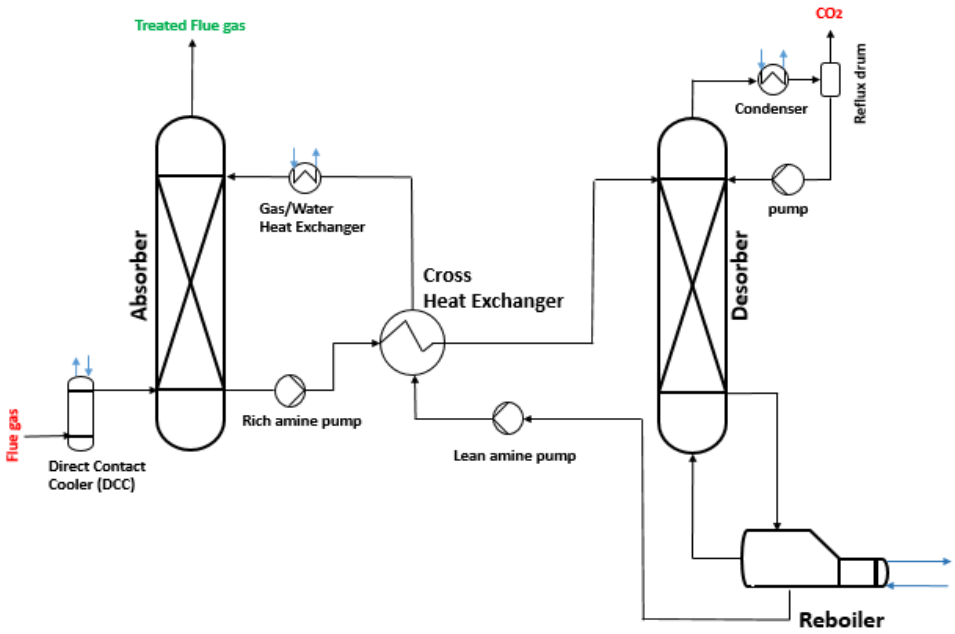

Figure 2.5: Schematic of the CO_2 amine capture plant [84].

A schematic of the CO_2 amine capture plant which will be used in this project is shown in Figure 2.5. The plant highlights the major components of the pilot-scale plant whereas for a large-scale plant, more components would be needed. The amine capture plant used in this project comprises of four major components; absorber column, stripper column, reboiler and cross heat exchanger. There are three main stages involved with CO_2 capture using MEA:

i. Flue gas cooling.
ii. Absorption of CO_2.
iii. MEA Regeneration.

The choice of solvent for this process depends on three factors, the rate of reaction of the solvent, the loading capacity and the regeneration duty. Compared to other primary alkanolamine, MEA has a lower regeneration duty, a high loading capacity and a fast rate of reaction with CO_2 [129].

2.7.1. Flue gas cooling

This process involves the flue gas being cooled (reduction in temperature) prior to contact with the MEA solution in the absorber [107]. The temperature of the exhaust gas leaving a micro gas turbine is about 70^0C, at this temperature the MEA will be ineffective in CO_2 capture and as such, the temperature of the flue gas entering the capture plant is maintained at 40^0C. To do this, usually a DCC (direct contact cooler) as shown in Figure 2.5 is used. After leaving the DCC, the flue gas is sent to a blower (fan) to increase the pressure of the flue gas before entering the absorber [119].

2.7.2. Absorption of CO_2

The absorber is the component of the capture plant where the CO_2 in the flue gas interacts with the MEA solvent and loses its CO_2 in a process called absorption. The absorber is a packed column in which the flue gas enters at the bottom of the absorber and interacts with the MEA solvent which enters the absorber at the top, in a counter-current contact flow [84, 120]. The loading of the CO_2 is measured on a molar basis using the equation [120]:

$$CO_2\ loading = \frac{wt\%\ CO_2 * 1.39}{wt\%\ MEA} \tag{2.25}$$

where 1.39 is the ratio of the molecular weight of MEA and CO_2 (MW_{MEA}/MW_{CO2}), wt% CO_2 is the weight percent of CO_2 and wt% MEA is the weight percent of MEA.

The treated gas leaves the absorber column and enters a water was column where any entrained droplets of the solvent that are carried by the treated gas are removed [120]. The temperature of the treated gas leaving the absorber is usually about 55^0C [107].

The lean amine used in the absorber refers to the MEA solvent without CO_2 contamination and the rich amine leaving the absorber refers to the MEA solvent after capturing CO_2.

2.7.3. MEA Regeneration

The rich amine leaves the bottom of the absorber and is pumped using the rich amine pump to the cross-heat exchanger where the rich amine is heated up using heat obtained

from the hot lean amine that exits the desorber (stripper) in a counter-current flow. This process allows the rich amine to be heated up and the lean amine being used in the absorber to be cooled down [84]. In the desorber, the rich amine flows downwards into the reboiler and counter to the direction of the upward flowing CO_2 vapor. At the reboiler at the bottom of the desorber, partial evaporation of the rich amine solvent occurs as the rich amine solvent is heated using pressurized hot water to a temperature of about 120^0C. At these high temperatures, there is a risk of thermal degradation but this risk does not outweigh the need for solvent recovery [120]. Most of the energy consumed in the capture plant is as a result of the reboiler energy consumption (Specific reboiler duty). This energy consumption is best defined using the equation [120]:

$$Q = \dot{m}_w * c_p * (T_{in} - T_{out}) \tag{2.26}$$

where Q is the energy consumption in KJ/hr, m_w is the mass flow rate of the pressurized hot water in kg/hr, c_p is the specific heat capacity of water in KJ/kgK, T_{in} is the inlet temperature of the pressurized water in ^{0}C and T_{out} is the outlet temperature of the pressurized water in ^{0}C.

The stripped solvent (lean amine) leaves the reboiler at a high temperature and is pumped into the cross-heat exchanger where it losses some heat to the rich amine solvent. To further cool the lean amine, a second heat exchanger is used. The lean amine is then used in the absorber for the absorption process [119, 120]. At the top of the desorber, the stripped CO_2 is cooled using a condenser and the droplets of water entrained in the CO_2 stream is also condensed. The stream then flows into a reflux drum where the gaseous CO_2 and condensed H_2O are separated. The condensed liquid is returned to the top of the desorber column while the concentrated CO_2 stream is sent for storage [120].

2.8. Chapter Conclusion

This chapter carries out a review of the various research conducted on gas turbines and post combustion capture plants. In these studies, the use of exhaust gas recirculation (EGR) and selective exhaust gas recirculation (S-EGR) were shown be the most desirable

system, when retrofitting a gas turbine to a post combustion capture plant, as they significantly reduce the energy penalty incurred by the capture plant. Other studies highlight the effect of various amines adaptable to the post combustion capture plant, with monoethanolamine (MEA) showing desirable absorbance and desorbance capacity.
Various researchers have conducted both process modelling and experimental studies around this study, with different operating conditions being investigated. However, there is lack of knowledge regarding the appropriate process modelling technique for a micro gas turbine with the use of characteristic maps, especially when modified with S-EGR. Also, the ramifications of EGR when operating with various fuels in the gas turbine is unclear.
To create an emphasis on the effect of EGR and S-EGR on post combustion capture, a two - absorber capture plant with MEA is implemented. Previous research conducted with MEA have shown high promise in the technology, however, the inclusion of two-absorbers for the purpose of further energy penalty reductions is unclear.
In this project, a detailed investigation is carried out on the performance of both a micro gas turbine (MGT) and a commercial scale gas turbine (CCGT). Both systems are integrated to a CO_2 capture plant operated with monoethanolamine (MEA) as the solvent, with the aim of reducing the CO_2 emissions from these fossil-fueled power generating techniques. This thesis outlines the methodologies and results in modelling different techniques implemented on the integrated gas turbine and CO_2 capture for improved operational efficiencies. Furthermore, experimental work on both the micro gas turbine and capture plant was conducted to assist in the modelling, which are also detailed and analysed in this thesis.
The feasibility of the project is highlighted in a techno-economic analysis where capital and operational cost of the different techniques are examined. This study provides a detailed understanding of the commercial implication of the techniques investigated in this thesis.

3. Experimental Methodology

In this chapter, the experimental procedures and set-up for the Micro Gas Turbine (MGT) manufactured by Turbec is presented, as well as the experimental set-up for the two-absorber amine capture plant.

3.1. Introduction

The use of small scale gas turbines has increased in recent years and this is likely to continue to increase [52]. MGTs are thermodynamically different from commercial scale gas turbines and as such a fair comparison between these two systems cannot be made [130], due to the different non-linear thermodynamic operations occurring in the different components of the commercial-scale gas turbine system. The small size of the micro gas turbine corresponds to a lower mass flow rate of air entering the compressor which is reflected in the small size of the component and its high rotational speed. Lower noise and lower emissions can also be attributed to the small size of the device.

Micro gas turbines offer a wide range of use, from research purposes to small scale generation of electricity. In the generation of electricity, several fuel options can be adapted instead of natural gas, such as biogas and diesel [131].

The introduction of micro gas turbines has extensive advantages in the development of research into the performance of gas turbines. This because of its small size and affordability, hence, ensuring it is easily purchasable by gas turbine research institutions. As stated earlier in Chapter 1, although thermodynamically different, MGTs share an identical set-up of a compressor, combustion chamber and a turbine, when compared to larger scale gas turbines. This enables data correlation in performance parameters between a MGT and a larger scale gas turbine.

The MGT used in this experiment is a Turbec T100 series 3. It is of a combined heat and power (CHP) design with the inclusion of a heat exchanger for the extraction of the thermal energy from the high temperature exhaust gas for the purpose of hot water

distribution for residential and industrial purposes. The MGT is rated at 100 kWe, with the CHP providing an additional 165 kW of thermal power.

The chemical absorption process of the CO_2 capture plant with the MEA is an already available technology [132], which can be used to capture the CO_2 from the exhaust flue gas exiting a fossil fuel power generation plant (micro gas turbine in this case). The capture plant comes in various configurations based on the desired performance and operation of the system. Major changes that affect the operation of the CO_2 capture plant are the external dimensions of the columns and the internal configurations of the packing material used in the columns.

Integrating both these systems produces a low greenhouse gas mitigation technology, although there is an energy cost associated with this process due to the high energy demand of the CO_2 capture plant.

The objectives of these experiments are;

1. Determine the operational characteristics of the MGT at decreasing power loads from the baseload.
2. Investigate the effect of S-EGR via CO_2 injection on the performance and emissions of the MGT, whilst operating at various power loads.
3. Examine the effect of increased CO_2 concentration in the flue gas being treated in a two-absorber capture plant.

3.2. System Layout and Operation

In the UKCCSRC PACT (UK Carbon Capture and Storage Research Centre/Pilot-scale Advanced Capture Technology) facility, there are two MGT's available for experimental use, the turbec T100 series 1 and the turbec T1000 series 3. The T100 series 3 as shown in Figure 3.1 is employed in this experimental study, as the Series 1 is an old device and as such incapable of attaining certain performance thresholds required in this analysis, which could lead to inaccurate results.

Both MGTs are located in the main hub building at PACT, Sheffield. The exhaust from the MGTs are directed outside the facility, with the option of being redirected to the CO_2 capture plant located at the rear of the facility. The CO_2 capture plant is surrounded by a two feet concrete wall to resist the flow of the mixture of amine and water leakage from the system flowing out of the confined capture plant area. The control room for the CO_2 capture plant is located next to the plant, as well as the tanks containing the water used to refill the water wash column.

Figure 3.1: Photograph of the Turbec T100 Series 3.

The MGT contains three key components – a compressor, a combustion chamber and a turbine as shown in Figure 3.2. The compressor and turbine are connected on a single shaft which has the benefit of optimizing maintenance, accessibility, as well as accounting for low emissions and high efficiency [133]. The simple design of the T100 is aimed at achieving the best possible maximum maintenance free unit [131].

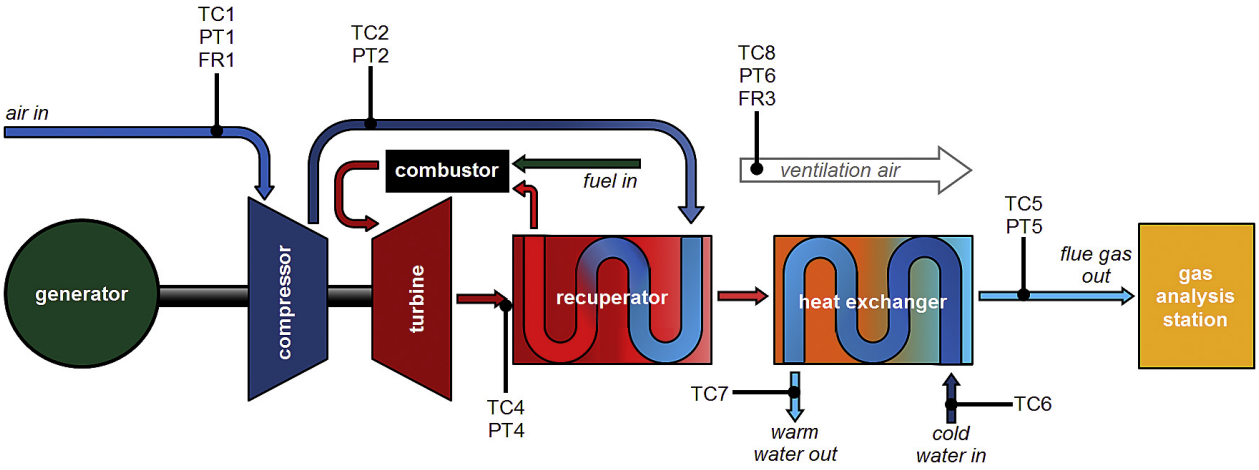

Figure 3.2: Schematic of the instrumentation locations in the MGT [134].

Installed in the MGT are thermocouples, pressure transducers and flowrate measurement devices which are highlighted as TC, PT and FR in the schematic in Figure 3.2.

Starting the MGT is simply the push of a button on the local control panel. The MGT is controlled by an automatic control panel in the PMC (Power Module Controller), and in the case of a system failure, the system automatically shuts down and registers the fault in the PMC. A normal start-up procedure will bring the T100 MGT from a cold start to 80% load in 10 minutes and 100 % load in 20 minutes. During the start-up, electrical power is used from the grid to operate the generator and after the combustor is ignited using the compressed air, the generator speeds up and the power generation process commenced [119]. It should be noted that the T100 has the capability of being restarted within 5 minutes upon an unexpected shutdown or interruption due to the flame instability. To shut down the MGT, the stop button located on the local control panel is pressed.

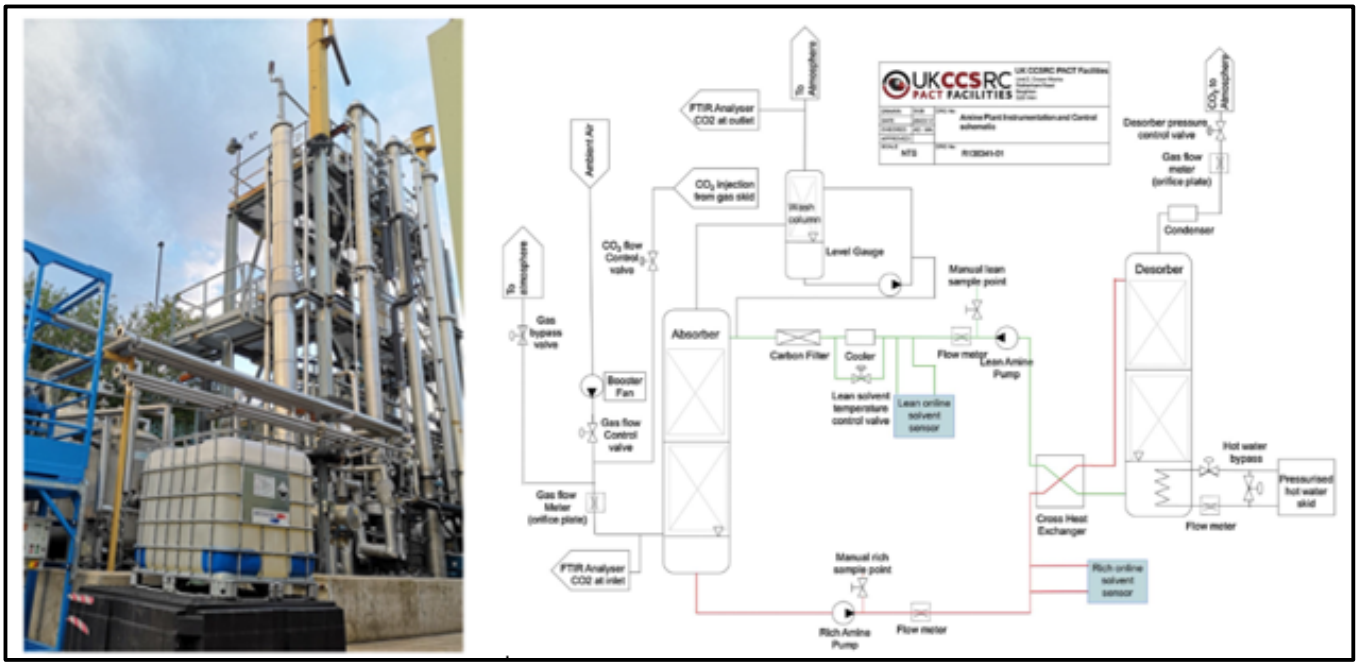

Figure 3.3: Photograph of the capture plant with the sampling points highlighted [123].

Installed on the CO_2 capture plant are thermocouples on the columns as well as flowmeters and pressure transducers. The capture plant at PACT is shown in Figure 3.3. The CO_2 capture plant can be operated with the flue gas obtained from either a biomass burner, a gas turbine or a gas mixing skid which can create synthetic flue gas from air, N_2 and CO_2, located in cryogenic tanks stored on-site in the PACT facility.

The plant utilizes pressurized hot water at a temperature of approximately 124 °C to regenerate rich solvent. A bypass valve allows the flow of pressurized hot water to the reboiler to be adjusted using a PID controller. The total solvent inventory of the plant is approximately 600 litres, the majority of which resides in the reboiler during the operation [135]. The composition of the flue gas into the absorber inlet is checked via FTIR (Fourier Transform Infra-red) spectroscopy, with a second FTIR located at the absorber outlet. The differences in the CO_2 composition from both FTIR's are implemented in determining the CO_2 capture efficiency. The flue gas at the absorber inlet is usually unsaturated, thus leading to water loss at the absorber outlet. To counter this, there is a manual water top-up on the plant operating days [135].

The flowrate is the solvent and this is controlled via valves located after the rich and lean solvent pump. To measure the solvent flowrate, a Coriolis flow meter is used [136]. The changes in the solvent flowrate can lead to a plant shutdown, as this correlates with the solvent level in the columns. To prevent this, large increments in the solvent flowrate have to be implemented. The temperature of the absorber inlet is maintained at 40 °C using a PID-controlled cooler and a bypass valve connected to the PLC (Programmable Logic Controller).

The temperature profile along the height of the columns are determined from the differential pressure in the packed beds [136]. The temperature profile is an important parameter in the CO_2 absorption process as changes in the process parameters, such as the flue gas flowrate, solvent flowrate and flue gas composition, will impact the performance of the plant. The dynamic behaviour of this system can be best monitored by observing the temperature profile in the absorber column [136].

3.3. Data collection and monitoring

The MGT is operated from a remote unit, called the RMC (Remote Monitoring and Control). This system monitors the continuous operation of the MGT as well as troubleshooting via LabView. A range of parameters are monitored in LabView, such as the temperatures, pressures and flowrates, which are shown in Table 3.1. The data provided in the table highlight a detailed component performance of the system.

With the use of a National Instruments data acquisition system, electrical signals from each device is received and transferred to the LabVIEW software. The LabVIEW software processes the signal data from the data acquisition system and automatically records the data measurements every second.

The CO_2 capture plant is operated from a control room in which the performance of the plant is monitored at different locations via the temperatures, pressures and flowrate measurements across the system. Along the columns, there are thermocouples installed, as well as pressure transducers and flow meters installed at the bottom of the columns, these are all connected to the control system highlighting the changes in these

parameters during plant operation. Other important parameters which are investigated are the CO_2 loadings in the amine during plant operation. This is obtained through manual sampling faucets which are highlighted in Figure 3.3. These sampling points are basically small taps located on the columns with the ability to extract the solvent. A small amount of solvent is usually extracted from the columns at two locations, the first is located after the absorber column (rich loading sampling point) and the other before the absorber column (lean loading sampling point). The samples obtained from the columns were taken immediately the system attained steady state operation. With changes in flue gas CO_2 concentration, the parameters in the capture plant are automatically re-adjusted until steady state operation is attained again.

Chemical analysis of these samples is used to determine the CO_2 loadings in the solvent. The device used is a Mettler Toledo Automatic Titrator. This process is carried out in the control room adjacent to the CO_2 capture plant in the PACT facility. In addition to the manual sampling analysis, rich and lean solvent sensors were installed to gather real-time measurements of CO_2 loading.

Table 3.1

Parameters monitored on LabView [131]

LabView	Parameter	Unit
Thermocouples		
TC1	System air inlet temperature	°C
TC2	Compressed air temperature	°C
TC4	Flue gas diffusion zone temperature	°C
TC5	Flue gas outlet temperature	°C
TC6	Cold water temperature	°C
TC7	Hot water temperature	°C
TC8	Ventilation air outlet temperature	°C
Pressure Transducers		
PT1	System air inlet pressure	bar g
PT2	Compressed air pressure	bar g

PT4	Flue gas diffusion zone pressure	bar g
PT5	Flue gas outlet pressure	bar g
PT6	Ventilation air outlet pressure	bar g
Flowmeters		
FR1	System air inlet flowrate	kg/min
FR3	Ventilation air outlet flowrate	kg/min

The implementation of the CO_2 injection in this research requires the incorporation of a system called the SCADA (Supervisory Control and Data Acquisition). This software, which is also installed in the control room, is used to log the measured flowrate of the CO_2 which is injected into the MGT. This parameter is only measured via SCADA, as the data required is from the skid and not from the gas turbine systems.

3.4. Gas Analysers

To sample the exhaust flue gas exiting the MGT and determine its composition, a Gasmet DX4000 gas analyzer, as shown in Figure 3.4, is used. The operating principle of the device is FTIR spectroscopy. This measures all the infrared-absorbing gases in the sample simultaneously, by scanning and analysing the entire infrared spectrum [137].

Each molecular structure of a gaseous compound has a unique combination of atoms and thus allows for a unique infrared spectrum (The infrared spectrum is a plot of the infrared radiation-related quantities as a function of the wavelength). Thus, all molecules can be identified by their unique absorption spectrum because each molecule absorbs infrared radiation at its characteristic frequency, with the exception of diatomic elements such as oxygen (O_2) and noble gases. Since the absorbance of each gaseous specie varies, the Gasmet FTIR is able to simultaneously measure up to 50 different gas species, with response time of < 120 seconds, depending on gas flow [137].

This method of analysis allows for both quantitative and qualitative data of the gaseous compounds investigated and as such, the species present as well as their concentration can be determined instantaneously. The device is operated through the Calcmet software

[137] in the operating computer in the control room. This software records the FTIR spectra and composition of the sampled gas. The Calcmet contains a library of infrared spectrums for different gas species, and from this library, relevant expected gas species are scanned and determined. Calcmet provides a flexible and easy to use interface, capable of making challenging measurements in a single software [137].

The Gasmet FTIR works by simultaneously scanning the entire infrared spectrum of the gaseous compound and the Calcmet software calculates the concentration of each gas in the sample based on its characteristic absorption, and thus creating an absorption spectrum for the sample. This makes it possible to add new compounds into the software without having to change the hardware [137]. As the recorded spectra cannot be amended, the recorded spectrum data is traceable in the library, making it easier to be re-analyzed, when scanning new gaseous compounds.

The Gasmet DX4000 FTIR analyser was supplied and configured by Quantitech. The system was delivered with a sampling system and heated sample lines so that hot, wet and even corrosive gases could be measured [137]. The sample cell can be heated to up to 180°C. This ensures the gas samples remain in the gaseous phase and inhibit condensation from the water-soluble gas species. The benefits of implementing the DX4000 system in the PACT facility are the flexibility and portability of the device. This ensures the ability of specifying different measurement parameters for various research programs. The portability of the device is advantageous due to its quick relocation and deployment on industrial sites [137].

To prepare the Gasmet FTIR for gas analysis, the instrument must be calibrated by purging of the instrument with Nitrogen (N_2) for approximately 30 minutes. As Nitrogen is a diatomic molecule, it does not absorb infrared radiation. Once purged, the instrument displays the background spectrum, which is checked with previous readings to ensure accuracy. Once competed a zero-check is initiated, where the readings are checked to see if they are at or near zero. The Gasmet FTIR operates with an accuracy of ± 0.2% [137], and as such, the background and zero-check values are expected to be within ± 0.2% of the previous readings, or a second background and zero-check is carried out.

Another diatomic molecule not monitored in this system is oxygen (O_2). As O_2 is an important gas in the flue gas analysis, therefore a Servomex analyzer is included in the flue gas analysis as shown in Figure 3.4. The Servomex Servoflex MiniMP 5200 gas analyzer implemented in the MGT, is used to measure the oxygen and carbon dioxide (O_2 and CO_2) concentration in the flue gas through advanced paramagnetic and infrared sensing technologies [138]. In the MGT, the Servomex is connected in two places; the flue gas duct and the ventilation duct from the turbine (when operating CO_2 injection experiments).
The servomex requires calibration before use, which requires connecting a calibration gas supply to the sample gas inlet and allowing the gas to pass through [138]. This is followed by pressing the calibration button on the MultiPurpose. The Servomex has an intrinsic error (accuracy) of ±0.1% and ±2.0% for O2 and CO2 reading, respectively [138].

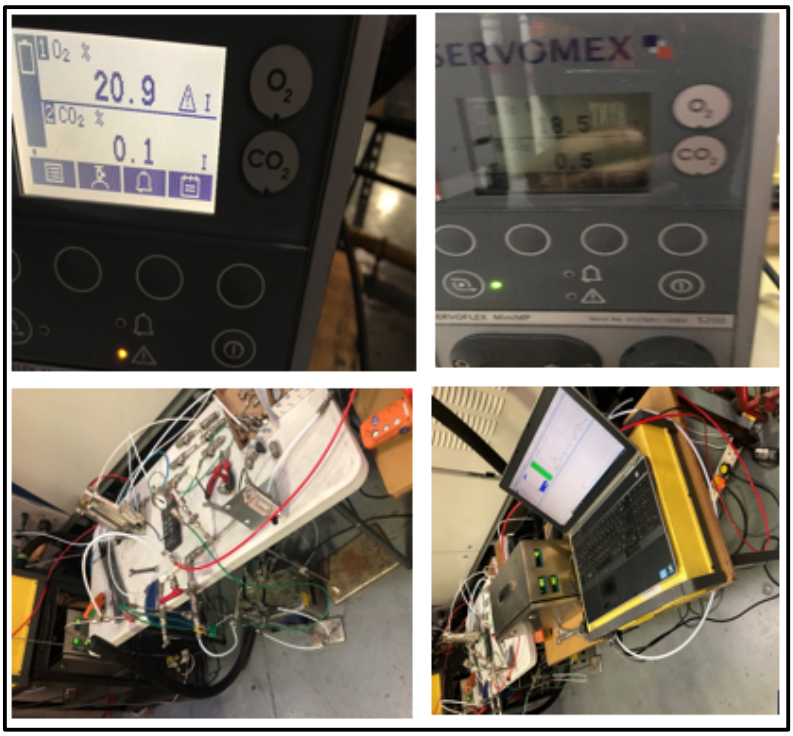

Figure 3.4: Servomex and Gasmet gas analysers connceted to the MGT

The MiniMP 5200 analyzer utilizes a paramagnetic transducer for the O_2 level and an infrared transducer for the CO_2 level. The paramagnetic transducer works on the principle that oxygen is a paramagnetic gas and thus is affected by a magnetic field. This

device therefore generates a strong magnetic field and the O_2 in the sample is attracted to the strongest part of the magnetic field. The magnetic field is within two glass spheres on a rotating suspension, filled with N_2 and separated by a fixed mirror. When light is reflected off the mirror into photocells, the O_2 in the sample gas displaces the rotating spheres, due to O_2 being attracted to the magnetic field. The higher the O_2 concentration, the higher the displacement. The photocells detect the change caused by this movement and thus generate a signal linked to a feedback system. This passes current through a wire to the rotating suspension and causes a motor effect to maintain the suspension in its original position. The current measured is directly proportional to the O_2 concentration and thus can be converted to an O_2 measurement.

To measure the CO_2, the non-dispersive infra-red (NDIR) sensor is assessed. The infra-red light is radiated at a constant frequency, via a measuring filter covering the infra-red sensor that blocks all frequencies outside the CO_2 range. The infra-red is passed through a sample gas containing CO_2, where the species absorbs the infra-red at specific wavelength bands. This infra-red travel through the cells to an infra-red detector, which provides a gas concentration measurement, by measuring the difference in absorbance. The infra-red absorption in a gas at constant pressure corresponds to the concentration of CO_2 in the sample.

3.5. CO_2 Injection System

The CO_2 injection system comprises of a series of pipework connected from the CO_2 skid, to the MGT inlet. The CO_2 being injected is stored on-site in an external cryogenic tank located at the back of the facility, provided by BOC. From these tanks, the CO_2 is passed through a trim heater and evaporator to maintain the temperature at approximately 10°C. The CO_2 is then passed through the gas mixing oxy-rig skid, which monitors and controls the flowrate and pressure of CO_2 being injected into the compressor inlet through the pipework shown in Figure 3.5. To do this, Coriolis mass flowmeters are installed and the pressure values are inspected regularly to determine CO_2 leakage during MGT operation.

The temperature variation of CO_2 entering the compressor inlet is also measured using a thermocouple shown in Figure 3.5.

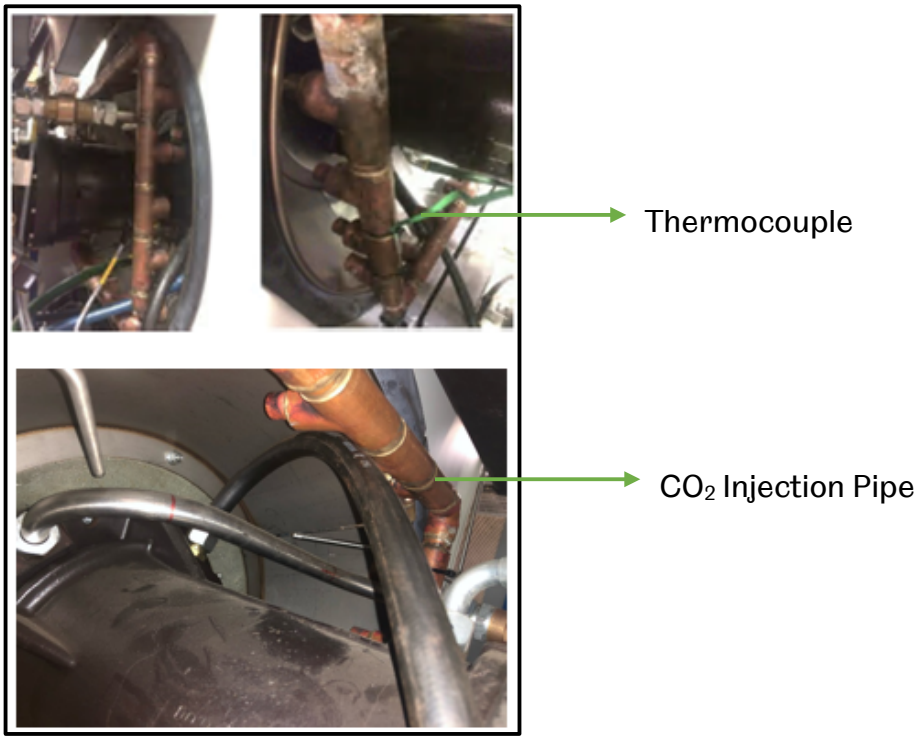

Figure 3.5: CO_2 Injection pipework and instrumentation

There are two supply lines which supply the CO_2 through the skid into the compressor inlet. Both lines are connected to the SCADA (Supervisory Control and Data Acquisition) system in the control room for monitoring and data acquisition, whereas the control of CO_2 is at the HMI panel by the oxy-rig skid. Using tow supply lines ensures a uniform distribution of CO_2 and thus a homogenous mixing with the combustion air. The CO_2 distribution system to the MGT from the gas mixing skid was designed for experiments conducted by Bellas et al., [139]. It should be noted that the two CO_2 supply lines are each designed to deliver a maximum flowrate of 150 kg/hr, thus allowing a maximum CO_2 flowrate of 300 kg/hr into the compressor inlet of the MGT.

3.6. MGT Performance Results

The experimental set-up of the MGT for CO_2 injection was carried out by the technical members of staff at the UKCCSRC PACT facility in Sheffield. The performance results obtained from the experimental campaign was shown in Table 3.2. The results shown in Table 3.2 show the performance results from the MGT as published by Bellas et al., [139]. The results highlight the change in output parameters for different operating conditions of the MGT. This gives a clear depiction of the performance of the MGT.

Table 3.2

MGT Performance Results [139]

Flow Description		Air Inlet		Comp Outlet		Turbine Outlet		CO_2 Inlet	
Electrical Output (kWe)	**T (°C)**	**P (bara)**	**F(kg/s)**	**T (°C)**	**P (bara)**	**T (°C)**	**P (bara)**	**T (°C)**	**F(kg/hr)**
100	17.3	1.0	0.8	200.7	4.2	645.0	1.0	14.5	0
100	15.2	1.0	0.8	197.0	4.2	645.0	1.0	14.6	100
100	14.6	1.0	0.8	197.0	4.2	645.0	1.0	14.6	200
100	16.4	1.0	0.8	194.9	4.3	645.0	1.0	16.4	300
90	20.5	1.0	0.7	196.3	4.1	645.0	1.0	17.7	0
90	15.6	1.0	0.7	186.8	4.0	645.0	1.0	14.6	150
90	13.8	1.0	0.7	181.7	4.0	645.0	1.0	14.0	250
80	20.2	1.0	0.7	185.0	3.8	645.0	1.0	17.5	0
80	15.2	1.0	0.7	175.6	3.7	645.0	1.0	14.3	150
80	14.9	1.0	0.7	170.6	3.8	645.0	1.0	15.1	300
70	20.1	1.0	0.6	174.9	3.6	645.0	1.0	17.4	0
70	15.4	1.0	0.7	166.6	3.5	645.0	1.0	14.5	150
70	17.9	1.0	0.6	168.7	3.6	645.0	1.0	17.4	300
60	19.7	1.0	0.6	164.2	3.4	645.0	1.0	17.1	0
60	15.2	1.0	0.6	156.5	3.3	645.0	1.0	14.5	150
60	15.5	1.0	0.6	155.6	3.3	645.0	1.0	15.7	300

As shown in Table 3.2, the electrical output of the MGT is decreased from 100 kWe to 60 kWe, whilst the flowrate of the CO_2 at the compressor inlet was increased from 0 kg/hr to 300 kg/hr when possible (250kg/hr at 90 kWe). It should be noted that not all the CO_2 flowrates implemented in the experimental campaign are considered in Table 3.2. For a detailed overview of results for all CO_2 flowrates, the data can be obtained from Bellas et al., [139].

The performance results were used to correspond with the data obtained from the modelling of the MGT carried out in Chapter 4 to further validate the accuracy of the model developed. Also, some sustained parameters which are highlighted in Table 3.2 such as the Turbine Outlet temperature and pressure and the air inlet pressure, were implemented in the model to provide a real-life operating scenario in the operation of the MGT.

3.7. Chapter Conclusions

In this Chapter, a detailed evaluation is carried out on the experimental methodology and set-up of the MGT and CO_2 capture plant available at PACT, Sheffield. The instruments used for data measurements and their functionalities are higlighted, as well as the corresponding applications installed at PACT, used for data storage and analysis. The parameters being investigated in these experiments provide a baseline for the modelling carried out in this thesis and thus help validate the process modelling. Further modifications which were carried out in PACT for CO_2 injection in the MGT are investigated, as well as the system put in place to deliver the CO_2 into the compressor inlet. The performance results obtained from the CO_2 injection experimental campaign is also detailed in the Chapter, with the MGT operating at various electrical power outputs with increasing CO_2 injection flowrates. The temperature, pressure and mass flowrates are investigated, as these parameters, allow for comprehensive analysis of the system to determine the performance and operation of the MGT, when CO_2 injection is implemented.

4. MGT modelling methodology

This chapter focuses on the process modelling of the micro gas turbine and the modifications made for selective CO_2 injection into the compressor inlet of the MGT. This involved the use of characteristic maps which were modified to account for the changes in operational parameters with various CO_2 flowrates into the compressor. The process modelling software used was Aspen Plus V10. This software was used due to the broad power generation and CCS packages being offered.

4.1. Process Modelling

Process modelling is a tool used for research and development. Process modelling provides information on how operational tests carried out will affect the performance of a system. It involves the use of computational models to predict the performance of the system in real case scenarios. This chapter presents the conceptual designs and assumptions used to develop a thermodynamic model of the MGT and the modifications carried out on the models for CO_2 injection into the compressor air intake. High accuracy and reliability of the results obtained are vital for this research, hence the comparison of results with the available manufacturer's data, the experimental results from Chapter 3 and other results from the literature using a similar system. The aim of the modelling is to provide an easier and less costly method of analysing the performance of the MGT when S-EGR with CO_2 is implemented. This involved the increase in CO_2 content in the working fluid at the compressor inlet by the injection of CO_2 into the compressor inlet at various injection flowrates.

The process modelling tool used in this project was chosen from a range of softwares available. The various process modelling software's vary in their use in small-scale systems to large–scale systems. The software available for potential use in this project were Chemcad, Speedup, gPROMS and Aspen. Aspen Technology, Inc is a process software used in petroleum and chemical companies, as well as engineering and construction firms

in the oil and gas industry, to ensure afro-mentioned companies achieve their goals in safety, profitability and productivity without compromising safety or reliability [140]. There are two Aspen Tech variations capable of process modelling and design. These are namely; Aspen Plus and Aspen HYSYS. They both offer a similar drag and drop service, where the model representing each component of the system is selected from a model palette and placed on the flowsheet. Both software requires a selection of the available in-built thermodynamic property packages, to take into account non-idealities in the vapour and liquid mixtures [141]. This ensures the correct prediction of the pressure and temperatures across the system. An understanding of the chemistry is also required to select the appropriate model based on the thermodynamic property package implemented.

Both simulation tools are frequently used for process modelling research in energy systems, because of its custom modelling ability. This aids in the development of research hypothesis, as novel thermodynamic assumptions can be implemented in the system flowsheet Both AspenTech simulation tools are very similar, however, the main differences in both software are the models for heat transfer, mass transfer and kinetics, as well as the equations of states implemented in the software. Also, Aspen Plus is a software used comprehensively in the chemical industry for optimizing batch and continuous processes during plant operation whilst Aspen Hysys is a software used comprehensively in the energy industry for optimizing upstream, midstream and refining processes, with the aim of sustaining profits [140]. Both software offers integrated tools for costing, energy management, safety analysis and equipment design within the work flowsheet, as well as real-time optimization modelling. However, in this project, modelling the MGT involves optimizing a continuous process and as such, Aspen Plus is used.

In this study, a flowsheet model of a MGT is developed and then validated using experimental data. To develop the flowsheet in Aspen Plus, the models are placed on the main flowsheet and connected using the material streams. This shows the direction of fluid flow in the system. Also, a work stream is used to connect the two pressure changers (compressor and turbine), which generate the work in the system which is transferred to the shaft.

4.1.1. Modelling Strategy

The process modelling strategy employed in this work is illustrated using the flowchart shown in Figure 4.1. The strategy highlights the steps taken from the inputs of variables into the process modelling platform to the results obtained as well as the validation of the results obtained.

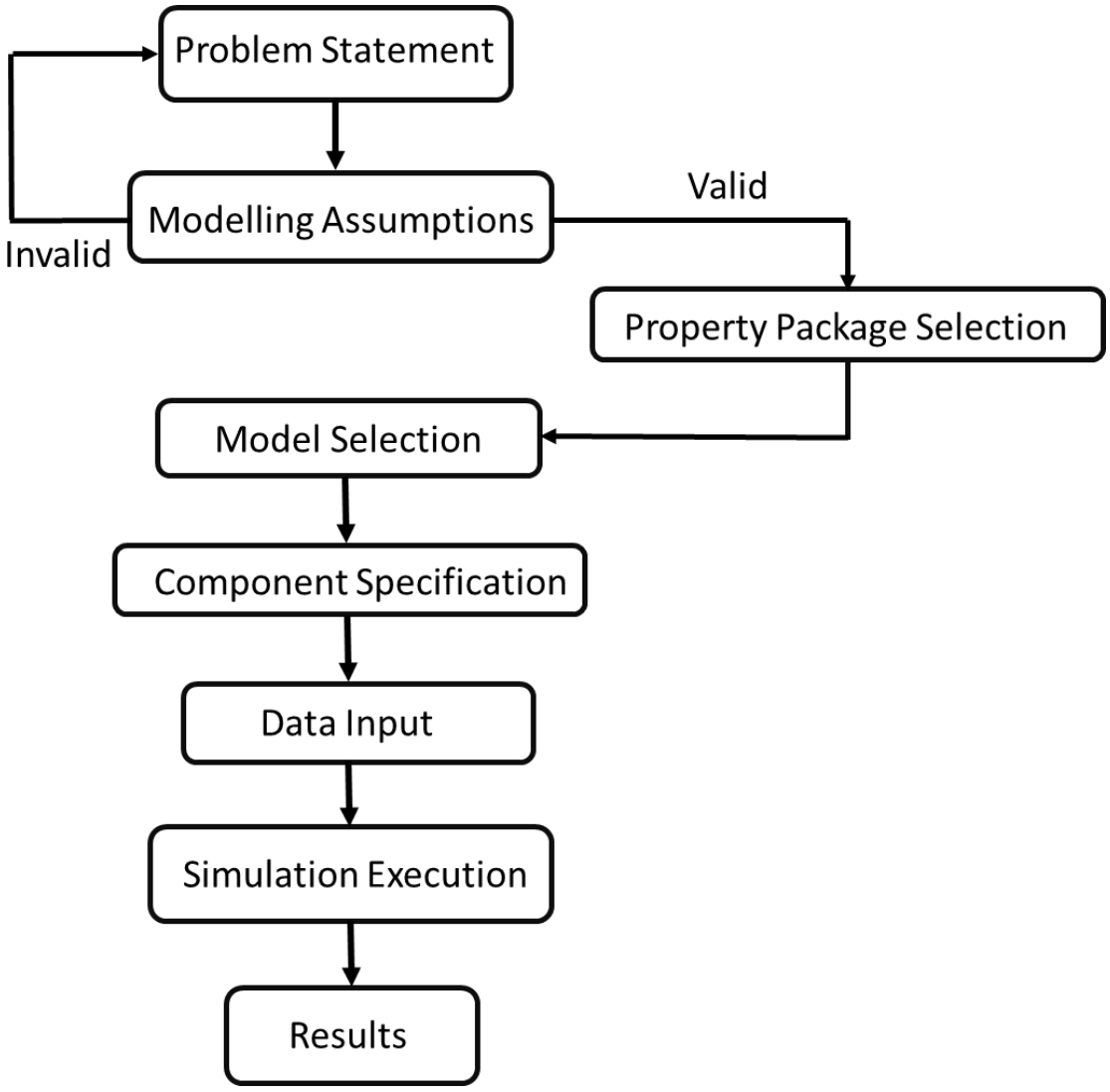

Figure 4.1: Flowchart highlighting the modelling strategy employed.

The problem statement highlights the objectives and goals to be achieved in the process modelling and simulation. This helps identify the operating conditions and the parameters to be used in the simulation. The first step is to make assumptions on the degree of freedom of the system based on the chemistry of the process. The degree of freedom is important as it highlights the independent and dependent variables used in describing the system being modelled. If the assumptions are considered invalid, then the problem statement needs to be re-visited to verify that all the variables being used have been carefully considered. If the assumptions are valid, then the property packages to be implemented are selected. The property method being used in this modelling is the Peng-Robinson method.

The next step is the selection of the models to be used in the process. Before the models implemented are selected from the model palette, the reacting species in the models are specified. This is important, as a mismatch of species and this can lead to failure in the execution of the simulation. Furthermore, the thermodynamic packages used will help determine the thermodynamic and transport properties of the system as well as the reaction kinetics. The models are selected based on their function.

The last step is to input data, such as the required power output of the system, the efficiencies of the components and the compositions of the fuel and the air. The inputs for the process are the parameters needed to achieve the desired operating conditions and output of the system. The number of input variables are determined by the boundary conditions of the process and the acceptable degree of freedom of the system. The degree of freedom of the model represents the operational flexibility of the overall system.

After a successful connection of the models using heat and work streams, there is a mass and energy transfer across the system. The complete interconnection of the models provides the process flow diagram (process flowsheet). This flowsheet model with the required inputs are then executed. The simulation runs the process under the assumptions stated earlier and using the thermodynamic packages to produce the results.

The base case results produced are validated against experimental data when possible which is provided from a similar set-up as the process modelling flowsheet and using a similar mode of operations of the components and inputs. An accurate model will usually produce good agreement with the experimental data.

4.2. Process Description

The MGT used in this project is a Turbec T100 Series 3 MGT [131]. The system is readily available at the PACT facilities.

The MGT used is mainly powered by natural gas but further modifications can be carried out on the MGT to accommodate different combustion fuels and different compositions of the air. Further modifications can be carried out on the MGT to investigate CO_2 injection and steam injection.

The MGT produces electrical power but it can also be used in processes where the hot exhaust gases are used directly for heating or to generate thermal power production only. In this study, the thermal power and its effect on the MGT are ignored. The MGT is a combined heat and power gas turbine with a recuperator and a counter-current gas/water heat exchanger, used to improve the electrical efficiency. The electrical power generated can go up to 100kWe. The overall electrical efficiency of the system is approximately 30% [131], without the use of the counter-current gas/water heat exchanger. Within this study, the power output generated is varied to provide an extensive examination into the performance of the MGT.

The composition of the air used in the process modelling as shown in Table 4.1 are obtained from literature with similar MGT configuration [81], while the natural gas composition as shown in Table 4.2 is obtained from the national grid. This gas composition is usually based on a laboratory analysis (gas chromatography) of the gas sample which is taken before being injected into the fuel supply pipeline [54, 81].

Table 4.1

Composition of the air in molar percentage [81].

Component	Composition (%)
N_2	77.3
O_2	20.7
Ar	0.9
CO_2	0.1
H_2O	1

Table 4.2

Composition of the natural gas in molar percentage.

Component	Composition (%)
CH_4	90.6
C_2H_6	5.1
C_3H_8	1.3
C_4H_{10}	0.4
CO_2	1.4
N_2	1.1
Lower Heating Value (LHV), MJ/kg	42

4.2.1. MGT Process Modelling

The flowsheet modelling of the MGT was carried out in the Aspen Plus V10. The main components (models) in the flowsheet were the compressor, turbine, generator, combustor, fuel inlet, air inlet and recuperator as shown in Figure 4.2. To model the combustor, a Gibbs reactor is used, which models the combustion using stoichiometric reactions of the components of the fuel being implemented as depicted in **Appendix A1.** The blue arrows indicate the flow of heat and the red arrows indicate the flow of fuel and air into the MGT. The stream results are also highlighted on the work flowsheet, showing

the main parameters such as temperature, pressure and mass flowrate being measured. Other parameters, such as the electrical efficiency, are calculated in an excel flowsheet.

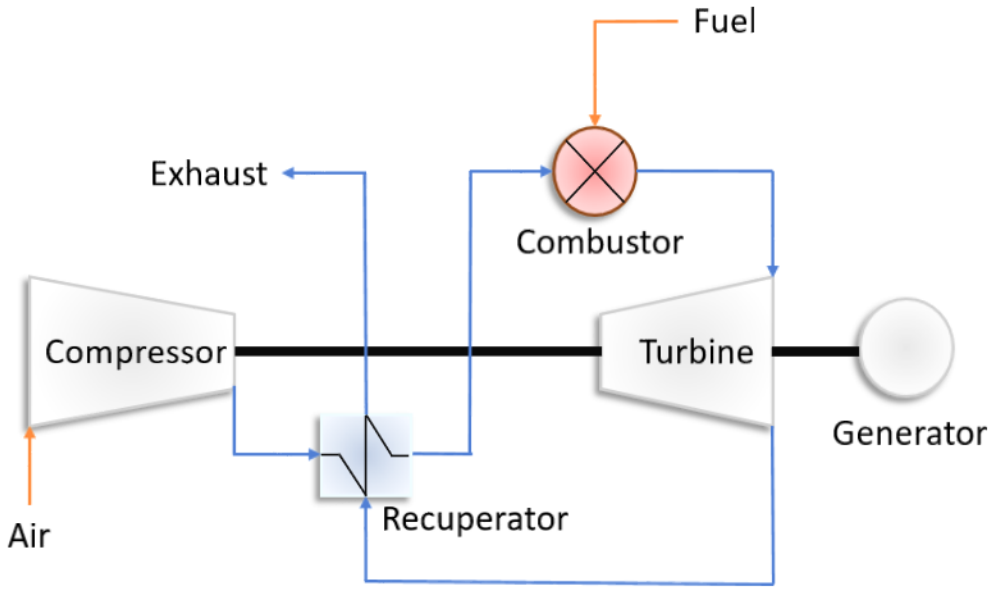

Figure 4.2: Flowsheet of the MGT.

The MGT flowsheet model works based on a material and energy balance across the components of the MGT. The flowsheet monitors major and minor species that play a role in the reaction kinetics occurring inside the MGT.

In modelling the MGT, the isentropic efficiency and performance curves of the compressor and turbine are specified and implemented as well as the turbine outlet temperature (TOT). This makes the modelling much easier and much more accurate as the actual MGT in PACT, Sheffield operates with a constant TOT of 645 °C (918.15 K). The system then calculates the other parameters, such as the air and fuel flowrates, the electrical efficiency and the other inlet and outlet temperatures within the system. Also, additional details such as the mechanical efficiencies, electrical losses in the generator as well as the heat exchanger minimum approach temperature which could not be estimated were adjusted to match the manufacturers' data as closely as possible [81, 82].

The air and fuel compositions used in this study did not change for different operating conditions and as such, the LHV is constant. Although, the flowrate of the fuel changes

with varying power output due to the change in heat input into the system. Hence, the fuel consumption in kW will change according to the following equation [130]:

$$Fuel\ consumption = \dot{m}_f * LHV \tag{4.1}$$

Where;

$\dot{m}_f$ = mass flow rate of the fuel in kg/s.

LHV = Lower Heating Value of the fuel in KJ/kg.

To further improve the modelling, the performance of the main components (compressor and turbine) in the MGT was determined using characteristic maps. The design (base case) and off-design operational conditions in this project were carried out using compressor and turbine maps. The characteristic maps give a detailed steady-state thermodynamic model of the MGT Turbec T100 [81].

4.2.2. Characteristic Maps

The characteristic map or performance curve are a set of data supplied by a gas turbine manufacturer for a specific gas turbine, to determine its performance at specified operating conditions [37]. This is because different gas turbines vary in design, and as such, the characteristic map is unique to a specific gas turbine system.

These maps can be used to determine the load output of a gas turbine at any given operating condition, such as the temperature and shaft speed. Small discrepancies can occur in the data when compared to the values obtained from the manufacturer's data and this usually tends to be an indication of engine problems that have occurred in the operation of the MGT [37].

Also, the discrepancies can be due to other conditions, such as change in ambient temperatures and degradation of the components due to continuous use of the MGT, as well as auxiliaries such as buffer air pumps and lubrication oil pumps which are hard to account for and usually not included in the MGT model [103, 134].

The characteristic maps indicate the performance of the system in terms of the mass flow rate, pressure ratio (or head) and isentropic efficiency (or polytropic efficiency) at

various rotational speed levels of the system [81]. For this study using Aspen, the mass flowrate and the head are the parameters used to define the characteristic maps. Also, the polytropic efficiency and mass flowrate can be used. The maps help provide accurate analysis on these parameters with respect to each other. In general, these maps can be used to determine the engine full load output at a given ambient temperature and a given rotational speed [37]. For different speeds, the characteristic map shape and hence the behaviour changes. At different rotational speeds, there is a different operating point which is highlighted out on the map. At this point, the operational characteristic of the component (compressor or turbine) can be defined accurately and hence the performance of the component based on further modifications on the component can be easily predicted.

For confidential reasons, the axes labels are not shown and the maps are presented in terms of non-dimensional and correctional parameters. This also assists in simplifying the variables required to specify the operating conditions of the system [54]. To determine the characteristic map/performance curve of the gas turbine system at a certain operating condition, requires a complex combination of variables to determine its operating point. As such, the use of non-dimensional and correctional parameters aid in simplifying these variables. Generic models of the characteristic maps are shown in Figure 4.3 and 4.4 for the compressor and turbine respectively.

The compressor maps are provided as the pressure ratio as a function of the mass flow rate and isentropic efficiency as a function of the mass flow rate as shown in Figure 4.3 [54]. The turbine characteristic maps are defined using a different arrangement of the axes labels. This is primarily because whereas the compression of air occurs in the compressor, the opposite process occurs in the turbine “expansion”. The turbine characteristic map is shown in Figure 4.4 [54] in non-dimensional and corrected parameters.

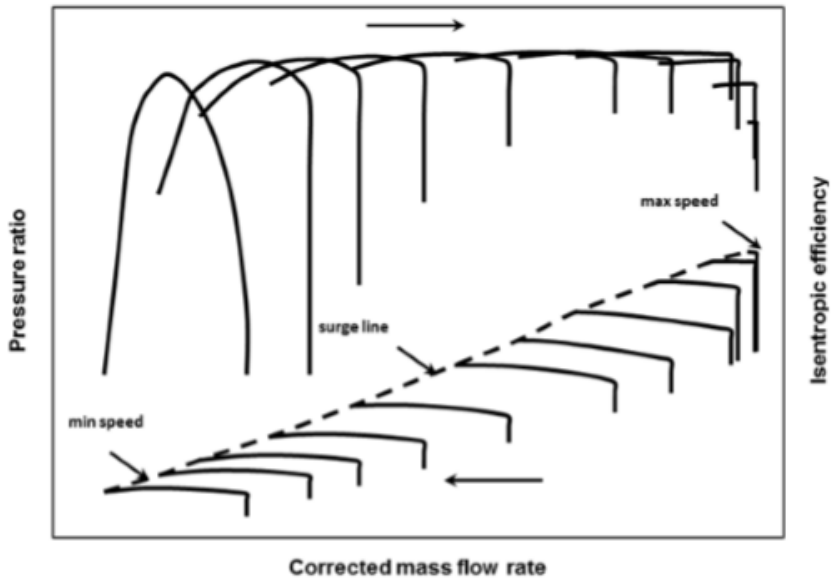

Figure 4.3: Compressor characteristic map [54].

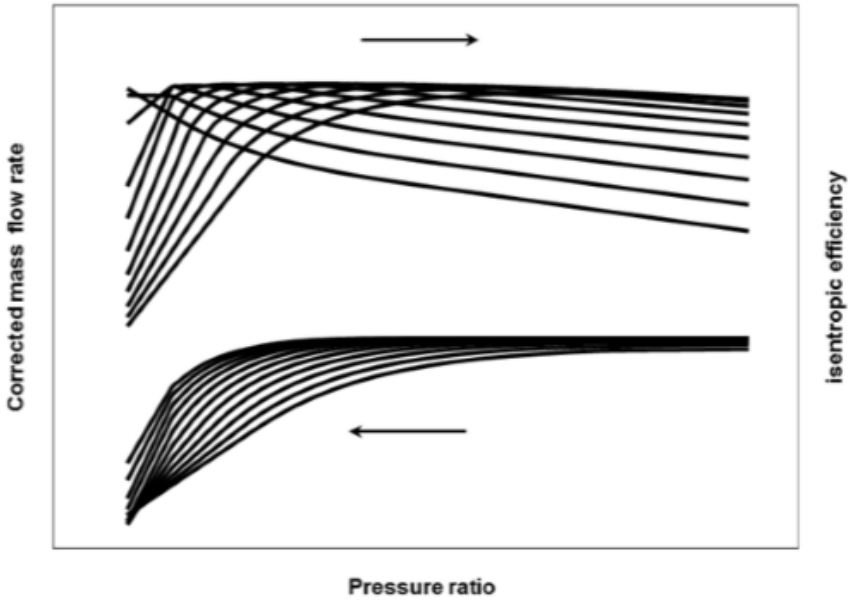

Figure 4.4: Turbine characteristic maps [54].

The characteristic maps used are provided by the manufacturer, Turbec S.p.A. The corrected parameters used in the maps are converted to normal parameters using the following equations provided in the literature [42, 46 and 81]. The corrected parameters to be normalized are the shaft speed and the mass flow rate.

The corrected parameters are normalized using reference conditions which are based on the manufacturer specification. The equations used are expressed as follows [84]:

$$N_{cr} = \frac{N}{\sqrt{T_{ref}}} \tag{4.2}$$

$$\dot{m}_{in,cr} = \frac{\dot{m}_{in}\sqrt{T_{ref}}}{P_{ref}} \tag{4.3}$$

Where *N* is the rotational speed, $\dot{m}_{in}$ is the mass flow rate of the fluid entering the component, *T* is the temperature of the fluid and *P* is the pressure. The subscript '*ref*' refers to the reference condition of the system and the subscript *'cr'* refers to the corrected parameters in the equations.

For process modelling in Aspen Plus, the pressure ratio will have to be expressed as head which is the required amount of internal energy of a fluid to exert pressure on its container while increasing its pressure from a lower pressure level (P_{in}) to a higher-pressure level (P_{out}).

The head is expressed as follows [84]:

$$H = \frac{\gamma}{\gamma - 1} zRT \left[\left(\frac{P_{out}}{P_{in}} \right)^{\frac{\gamma-1}{\gamma}} - 1 \right] \tag{4.4}$$

where *H* is the head, γ is the specific heat ratio, *z* is the compressibility factor, *R* is the universal gas constant, P_{in} is the pressure of the fluid entering the component and P_{out} is the pressure of the fluid leaving the component.

The reference values stated earlier in this chapter highlight the operating conditions used to develop the characteristic map. With a change in the air composition, ambient temperature and pressure, the map will change. These variations lead to the operating point of the MGT to move away from the design point on the curve. Further movements will lead to a phenomenon called surge. Surge is the operating point at which the maximum head and the minimum flow rate is reached for a given rotational speed of the compressor. On the compressor map, there are different surge points for different

rotational speeds, these points come together to form the surge line which is the region at which the compressor is no longer operational. The surge margin is expressed as follows [81, 84].

$$Surge\ margin = \left[\frac{PR_{at\ surge}}{PR_{operating\ point}} - 1\right] * 100 \tag{4.5}$$

where PR is the pressure ratio at a constant flow rate.

The way the map changes with respect to this modifications and manipulations of parameters will be investigated in this chapter. A study was carried out on the base case model of the MGT using the maps provided by the manufacturer after normalisation. The maps will be implemented into Aspen Plus and the data obtained will be analysed.

4.3. Base Case Model

The base case model is developed in steady-state at ISO conditions. The ISO conditions used are the international standard ISO 3977-2 which was prepared by Technical Committee TC 192, gas turbines [142]. The ISO conditions are tabulated in Table 4.3 [142]. At full load, the rotational speed of the shaft connecting the compressor and turbine is 70,000 rpm. The composition of the fuel as well as the composition of the air are shown in Tables 4.1 and 4.2. For the process modelling of the MGT at base case, some parameters are specified by the system such as the TOT at 645°C [81, 84]. This assists in reducing the number of assumptions to be made in modelling the system. The performance results of the MGT base case model at ISO conditions are tabulated in Table 4.4. The values obtained from the Aspen Plus flowsheet are compared to the manufacturer data.

Table 4.3

ISO conditions used in the MGT [142].

Parameter	Value
Pressure	101.3 kPa
Temperature	15°C
Relative Humidity	60%

Table 4.4

Performance evaluation of the MGT at ISO conditions.

Parameter	Manufacturer Data [134]	Modelling Results
Fuel Consumption (kW)	333	325.6
Electrical Power (kWe)	100	100
Electrical Efficiency (%)	30	30.7
Shaft Speed (rpm)	70,000	70,000
Pressure ratio	4.5	4.46
CO_2 in flue gas (mol%)	N/A	1.85
O_2 in flue gas (mol%)	N/A	17
Turbine Inlet Temperature(K)	1223.15	1210.25
Turbine Outlet Temperature(K)	923.15	918.15
Exhaust Temperature (K)	543.15	544.5
Exhaust gas flowrate (kg/s)	0.8	0.77

Table 4.5

Performance comparison of the MGT to literature.

Parameter	Manufacturer Data [134]	Ali et al., [84]	Nikpey et al., [103]	Majoumerd at al., [81]	Modelling Results
Fuel Consumption (kW)	333	331	322	321	325.6
Electrical Power (kWe)	100	100	100	100	100
Electrical Efficiency (%)	30	30.2	31.1	31	30.7
Shaft Speed (rpm)	70,000	70,000	69,740	69,675	70,000
Pressure ratio	4.5	4.5	4.4	4.4	4.46
CO_2 in flue gas (mol%)	-	1.6	-	1.6	1.85
O_2 in flue gas (mol%)	-	17.5	-	-	17
Turbine Inlet Temperature(K)	1223.15	1221.15	1220.15	1221.15	1210.25
Turbine Outlet Temperature(K)	923.15	918.15	923.15	923.15	918.15
Exhaust Temperature (K)	543.15	-	-	540.15	544.5
Exhaust gas flowrate (kg/s)	0.8	0.8	0.8	0.77	0.77
Software used	-	Aspen HYSYS	IPSEpro	IPSEpro	Aspen Plus

The modelling results shown were obtained after correcting the parameters in the characteristic map stated earlier and the implementation of the characteristic maps in Aspen Plus. As shown in Table 4.4, the values obtained are in good agreement with the manufacturer's data as they are within an acceptable range of < 4%. As explained earlier in Section 4.2, the discrepancies in the results can be due to changes in the MGT performance, as well as auxiliaries such as buffer air pumps and lubrication oil pumps which were not considered in this model [103, 134].

In Table 4.5, the performance parameters being investigated are compared to similar modelling work in the literature. The major differences observed are mainly due to the difference in software, and also different thermodynamic packages in the different software.

4.4. Chapter Conclusion

In this Chapter, a detailed investigation is carried out on the process modelling methodology implemented in modelling the MGT with characteristic maps. The model is developed from the Turbec T100 series 3 MGT available in PACT centre in Sheffield and the characteristic maps were provided by the manufacturer. The Base case model of the MGT was developed and compared to the manufacturer's data to validate the implementation of the characteristic map. Also, the base case modelling data was compared to other Turbec T100 modelling data from the literature.

There were observed similarity in the performance results, when the model is compared to the manufacturers data and the literature. However, the discrepancies observed were as a result of the differences in software used (literature) and auxiliaries in the MGT that were not considered in the modelling (manufactures data).

5. Modelling the effect of selective exhaust gas recirculation on micro gas turbines

This sub-chapter investigates the effect of map scaling on the process modelling of the MGT with S-EGR as well as the assumptions made to derive each scaling equation.

5.1. S-EGR CO_2 Injection

Work has been done regarding the effect of EGR (exhaust gas recirculation) on a MGT by Cameretti et al., [40], Nikpey et al., [82] and in S-EGR (selective exhaust gas recirculation) by Bellas et al., [139] and Ali et al., [84]. It was concluded by Ali et al., [84], that "the performance of the MGT for the S-EGR cycle can be better understood from the behaviour of the working fluid for an increased CO_2 content in the working fluid of the MGT". Hence, the study focuses on the impact of CO_2 injection at various flowrates into the compressor inlet on the performance of the MGT as a system. This methodology enabled easier modelling techniques to be implemented. To aid in this analysis, the characteristic maps are modified and scaled based on some thermodynamic assumptions highlighted. The scaling equations are derived from some thermodynamic first principles highlighted in Chapter 2.2 of the thesis. The results obtained are interpreted and discussed in this Chapter. The standard format for the turbomachinery map (characteristic map) is the Mach number similarity, hence all parameters in that map should have equivalent Mach numbers [143]. The Mach number is an important parameter and a change in Mach number can lead to a change in the aerodynamic behaviour of a component [37]. Hence, it is logical to express the component characteristic in terms of axial (M_x) and circumferential (M_θ) Mach numbers [144]. The axial Mach number is a measure of the amount of flow and the circumferential Mach number relates to the shaft speed.

The general equation for Mach number can be expressed as [37]:

$$M = \frac{v}{\sqrt{\gamma R T_s}} \tag{5.1}$$

where M is the Mach number, v is the velocity of the fluid, γ is the ratio of specific heats, R is the specific heat constant and T_s is the static temperature.

5.1.1. Scaling Methodology

Flowrate

The mass flowrate of the air entering the compressor is obtained from the conservation of mass equation [143], with the density term expressed in terms of static pressure, temperature, specific heat constant and heat capacity ratio. By re-arranging the equation, the mass flowrate can be expressed in terms of the axial Mach number as shown in the following equation [143, 144]:

$$\dot{m} = A \frac{P_s}{T_s} M_x \frac{\sqrt{\gamma}}{\sqrt{R}} \tag{5.2}$$

where A is the compressor annulus area, P_s is the static pressure, M_x is the axial Mach number and $\dot{m}$ is the mass flowrate of the fluid entering the compressor.

Assuming the axial Mach number, shaft area, static pressure and static temperature are constant then the ratio of the mass flowrate of a new fluid (with CO_2 injected) with a different heat capacity ratio and molecular weight can be expressed as follows:

$$\dot{m}_2 = \dot{m}_1 \sqrt{\frac{\gamma_2 R_1}{\gamma_1 R_2}} \tag{5.3}$$

Shaft Speed

Using the circumferential Mach number, the velocity term in Equation (5.1) can be expressed in shaft speed and diameter of the shaft as follows [37]:

$$M_\theta = \frac{2\pi D.N}{\sqrt{\gamma R T_s}} \tag{5.4}$$

where N is the shaft speed, D is the diameter. Assuming a constant area and static temperature as well as a constant circumferential Mach number, the ratio of shaft speeds when operating with a new fluid can be expressed as follows:

$$N_2 = N_1 \sqrt{\frac{\gamma_2 R_2}{\gamma_1 R_1}} \tag{5.5}$$

Pressure ratio

The power delivered per unit flow rate to the compressor (specific work) is given by [144]:

$$\frac{P}{\dot{m}} = \frac{c_p}{\eta_{isen}} T_s \left(1 + \frac{\gamma - 1}{2} M_x^2\right)\left(PR^{\frac{\gamma-1}{\gamma}} - 1\right) = M_x^2 \gamma R T_s \tag{5.6}$$

Re-arranging Equation (5.6), the compressor pressure ratio can be expressed as follows:

$$PR^{\frac{\gamma-1}{\gamma}} - 1 = \frac{M_x^2 \, \eta_{isen}(\gamma - 1)}{\left(1 + \frac{\gamma - 1}{2} M_x^2\right)} \tag{5.7}$$

The ratio of pressure ratios for PR_2 and PR_1 can be expressed as follows:

$$PR_2 = \left[1 + \frac{\eta_{isen(2)}(\gamma_2 - 1)\left(1 + \frac{\gamma_1 - 1}{2} M_x^2\right)}{\eta_{isen(1)}(\gamma_1 - 1)\left(1 + \frac{\gamma_2 - 1}{2} M_x^2\right)}\left(PR_1^{\frac{\gamma_1-1}{\gamma_1}} - 1\right)\right]^{\frac{\gamma_2}{\gamma_2-1}} \tag{5.8}$$

where *PR* is the pressure ratio, η_{isen} is the isentropic efficiency.

Efficiency

The polytropic and isentropic efficiencies of the components were assumed to be constant for varying CO_2 injection flowrates. This is due to the scaling rule being used excluding detailed loss models [144].

5.2. Matlab Implementation

The map modifications were carried out using Matlab R2018b. This was to shorten the computational time and provide ease in equation modification and map scaling compared to Microsoft Excel. The script was written as a function in which the initial characteristic maps for the Turbec T100 provided by the manufacturer were inserted. The script developed for the compressor and turbine characteristic maps are shown in **Appendix A2** and **Appendix A3.**

The equations used to determine the corrected parameters are as shown in Section 4.2, as well as the equations to calculate the specific heat constants and heat capacity ratios of the reacting components in the systems, are inserted into the Matlab script. The scaling equations described in Section 5.1.1 were written into a script. To obtain the new parameters at the defined operating conditions, a quadratic spline interpolation was carried out. This was preferred to the linear interpolation method because it produces more accurate results [145]. The new shaft speed, volumetric flowrate, head and polytropic efficiencies were calculated in Matlab by interpolating between the old speed and the operating parameter being extrapolated. The function used in this study saves the new characteristic maps generated as a new file with an arbitrary name. The data obtained for each operating curve from Matlab are then inputted into Aspen Plus for process modelling. The data transfer process between Aspen Plus and Matlab is shown in Figure 5.1.

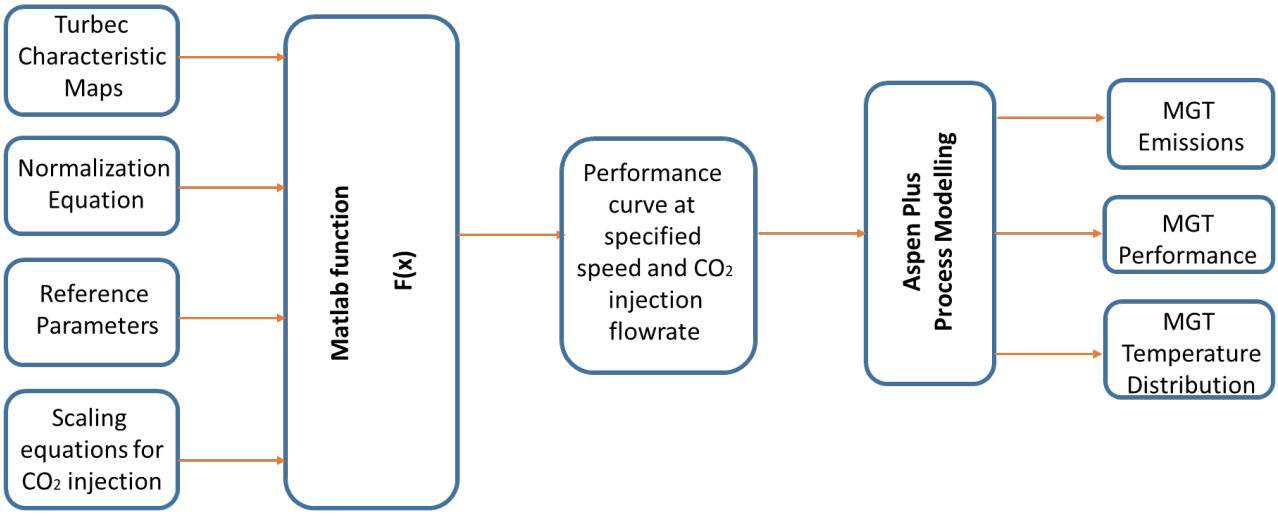

Figure 5.1: Schematic of the input and output parameters for both Matlab and Aspen Plus modelling.

In a real-life scenario, the MGT does not always operate at full load conditions, as the operational conditions deviate from the design point due to changes in parameters set by the user such as the power output and conditions uncontrolled by the user such as ambient conditions [103]. Thus, the study is further expanded by investigating the impact of CO_2 injection flowrates on varying power outputs in the MGT, to analyse the performance of the MGT at off-design operational conditions. The baseline rotational speeds at the varying power outputs are from previous experimental operation of the MGT performed by Bellas et al., [139] and highlighted in Table 5.1. Due to degradation of the MGT, the rotational speed at full load of MGT is lower than mentioned earlier from the manufacturer's data [134] in Table 4.4.

The decrease in rotational speed with decrease in power output is because the gas turbine is being used in mechanical drive applications, in which the generator converts the excess mechanical power from the gas turbine into electrical power and delivering the electrical power to the electric grid [146]. Other factors that will affect the system include changes in inlet temperature and pressure ratio, which have been kept constant throughout this work.

Table 5.1

Shaft speed at the different MGT power outputs [139].

Power Output (kWe)	100	90	80	70	60
Shaft Speed (rpm)	67500	66250	64100	62000	59500

With an increase in CO_2 injection flowrate, the rotational speed changes from the baseline speeds shown in Table 5.1, at different power outputs. The change in rotational speed is given according Equation (5.5). Using this new speed, the new map at the specified power output and CO_2 injection flowrate was generated. The shaft speeds used were extrapolated from the literature on experimental investigations with a similar MGT.

The performance curves vary for each CO_2 injection flowrate and power output. An example of a performance curve operating with no CO_2 injection at various power outputs is shown in Figure 5.2.

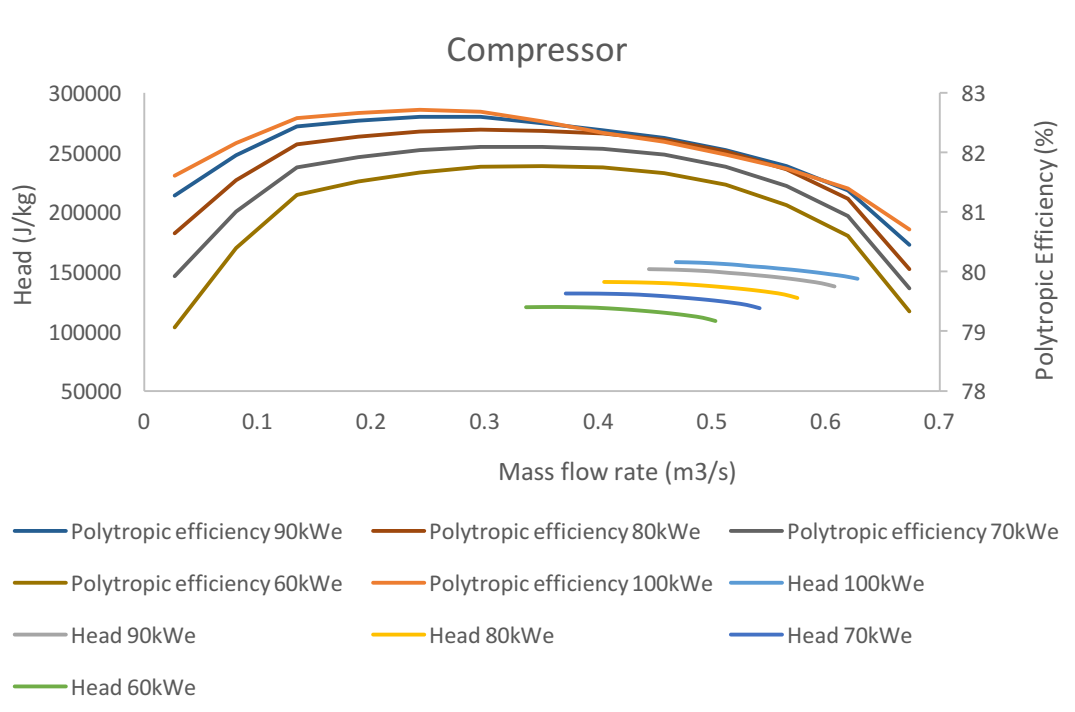

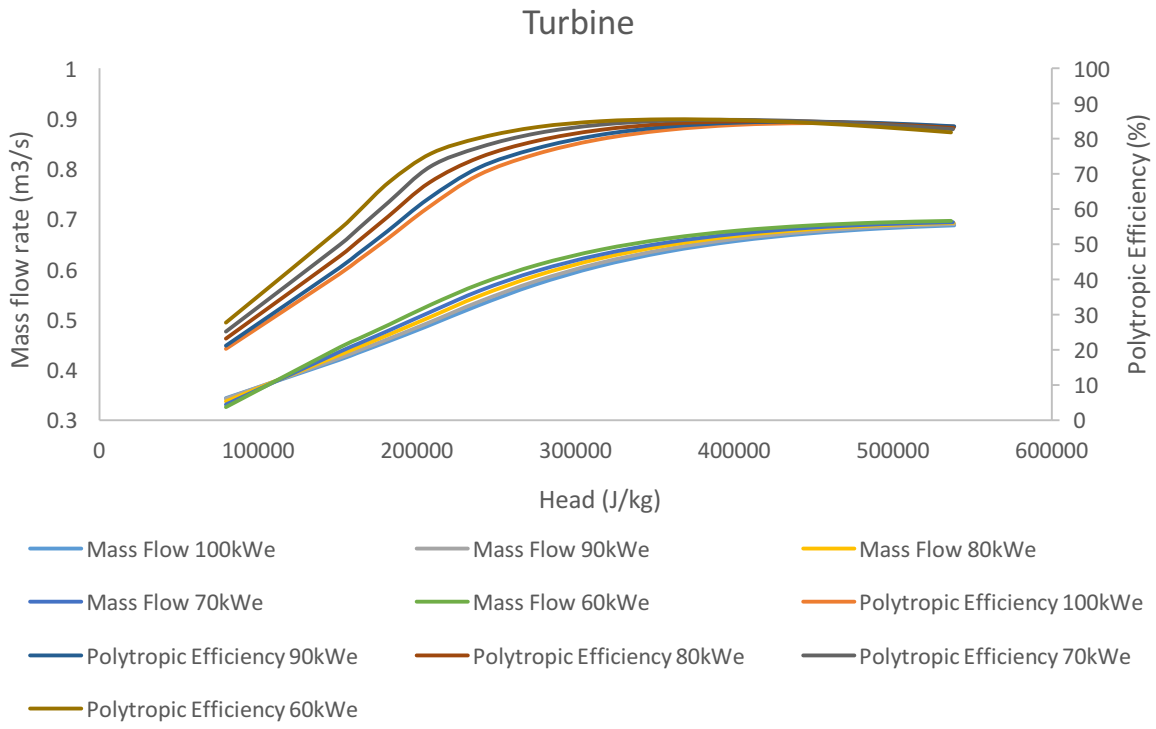

Figure 5.2: Compressor and Turbine Performance curves at various power outputs with no CO_2 Injection.

5.2.1. Results and Discussion

This chapter highlights the results obtained from the process modelling developed for S-EGR and the results are analysed and discussed. The impact of S-EGR on the MGT on the emissions, temperatures and overall performance of the system is investigated and the results are interpreted.

5.2.1.1. Impact of S-EGR on Emissions

The focus in this study is the effect of increasing the CO_2 injection flowrate in the compressor air intake on the performance of the MGT. With increases in the CO_2 flowrate at the compressor inlet, the flue gas composition changes, with a 433.7% increase and 9.9% decrease in CO_2 and O_2 concentrations, respectively, at 100kWe from natural gas to

300 kg/hr CO_2 injection flowrate. Also, there is an expected reduction in the O_2 concentration in the working fluid entering the combustion chamber with each increase in the CO_2 injection flowrate. This is due to the CO_2 displacing the oxygen in the air [85]. Reducing the power outputs further affects the CO_2 concentrations recorded in the flue gas. The CO_2 and O_2 concentrations recorded in the flue gas for each increaseCO_2 are presented in Figures 5.2 and 5.3.

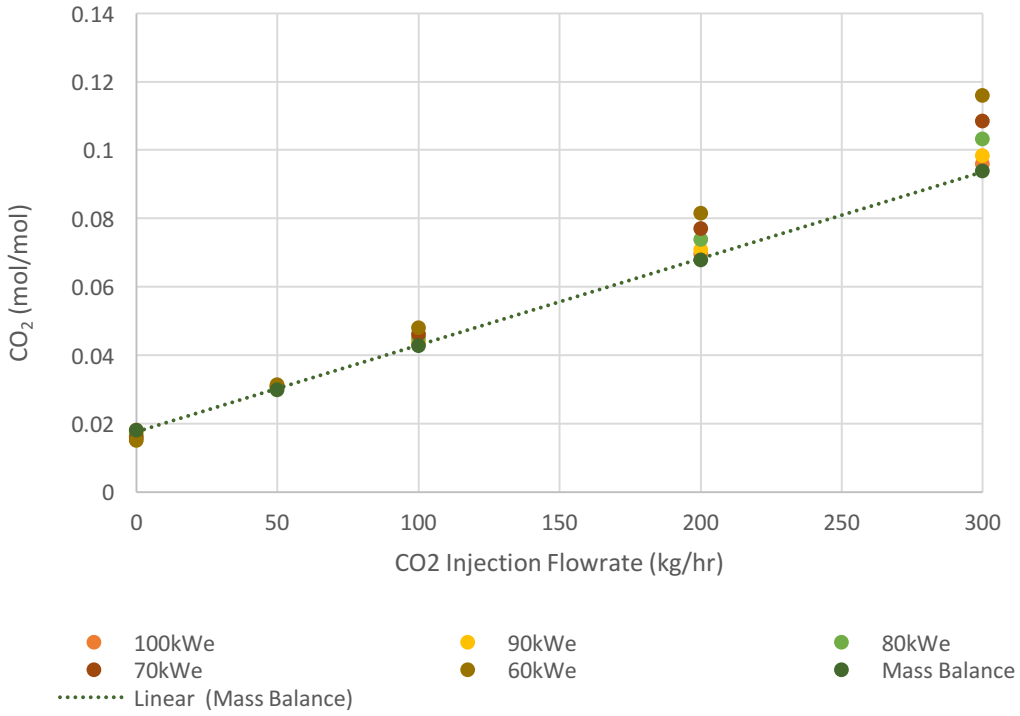

Figure 5.3: CO_2 concentrations in the flue gas for increasing CO_2 injection flowrates across varying power outputs.

As shown in Figure 5.3, with an increase in the CO_2 injection flowrates, the CO_2 concentration in the flue gas increases. The CO_2 at high injection flowrates displaces the oxygen in combustion, hence leading to poorer combustion characteristics, which leads to an increase in fuel consumption to enable the MGT maintain the specified power output at the CO_2 injection flowrate investigated [85]. At lower power outputs, the recorded CO_2 concentration in the flue gas is higher. This is as a result of the increase in

excess air and increase in AFR (air-fuel ratio) to enable complete combustion at off-design operational conditions. Also, the increase in CO_2 concentration in the exhaust when operating at lower power outputs can be attributed to the lower total mass flow rates at lower turbine rotational speeds for the lowest power outputs [85]. Due to the presence of more CO_2 in the combustion system and as CO_2 does not support combustion, there is a higher CO_2 concentration in the flue gas.

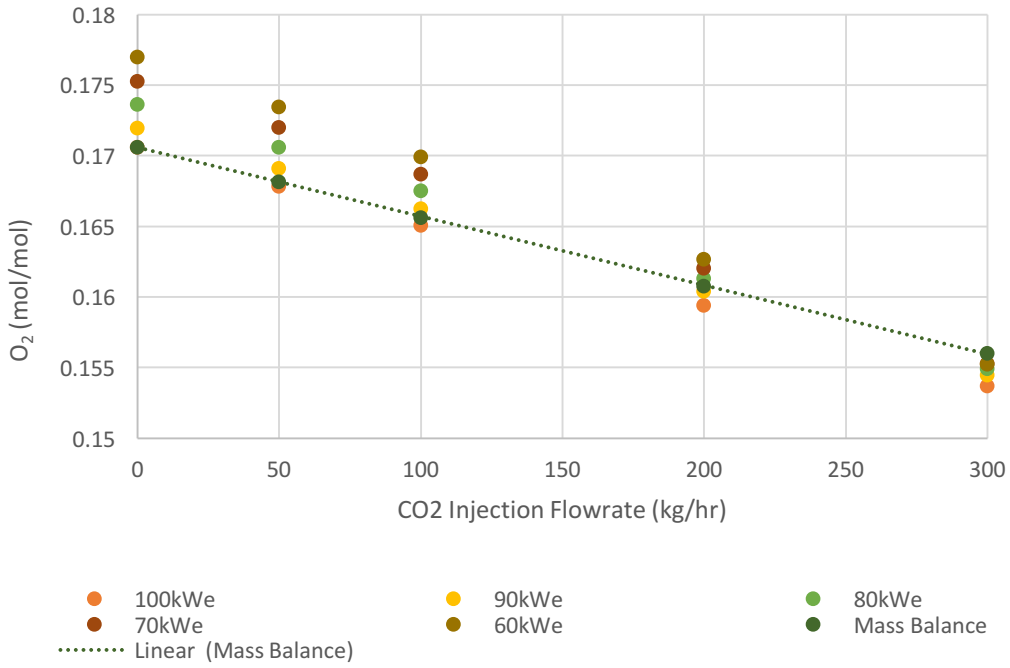

Figure 5.4: O_2 concentrations in the flue gas for increasing CO_2 injection flowrates across varying power outputs.

Figure 5.4 highlights the effect of CO_2 injection flowrates on the O_2 flue gas concentration. The oxygen level is an important parameter in combustion as lower oxygen levels in the combustor have been shown to lead to unstable flames [98]. As shown in Figure 5.4, the oxygen concentration reduces with increasing CO_2 injection flowrates as a result of the reduced O_2 concentration in the compressor air intake as CO_2 dilutes the working fluid. Also, at lower power outputs, the O_2 concentration is seen to increase due to the increase in excess air. Chemically, the presence of CO_2 in the working fluid inhibits the fuel oxidation process because of the competition for hydroxyl radicals [82, 147]. Also, an

increase in CO_2 injection flowrate reduces the flame speed and reaction rates in the combustion chamber. The required air oxygen concentration in the combustion chamber for stable combustion has been recommended by Bolland et al., [148] to be between 16-18 mol% and by Elkady et al., [98] to be 15 mol %. Above these values, the flame becomes unstable, which leads to poorer combustion [85].

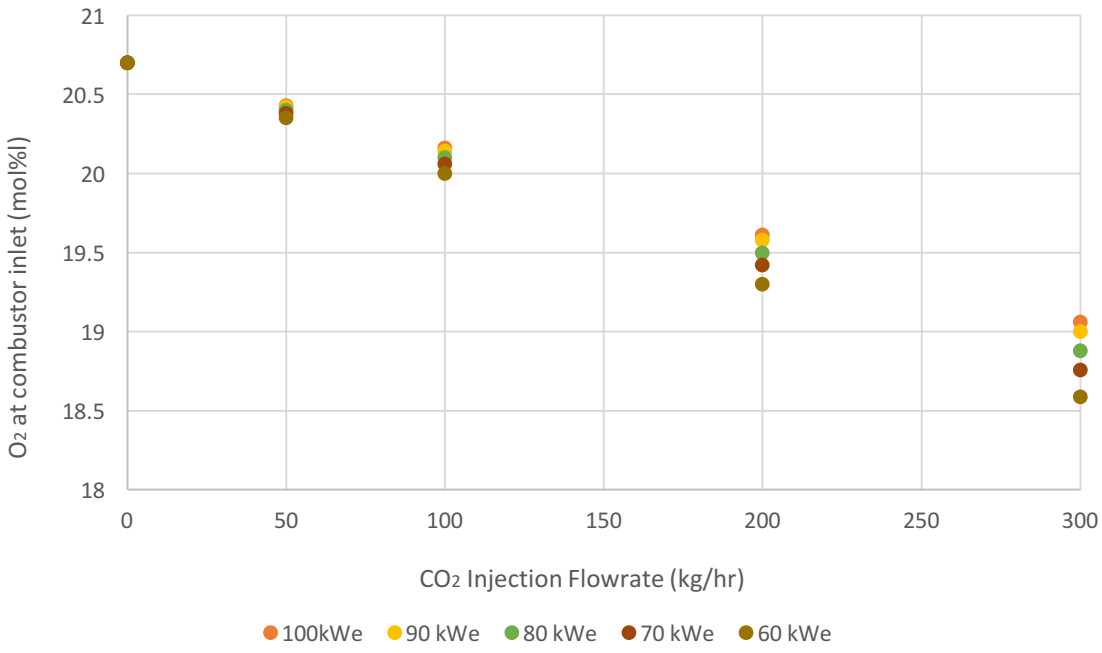

Figure 5.5: O_2 concentrations at the combustor inlet for increasing CO_2 injection flowrates across varying power outputs.

As shown in Figure 5.5, there is an observed similar trend between the O_2 concentration in the combustor inlet and the flue gas. The O_2 concentration at the combustor inlet is seen to reduce with an increase in CO_2 injection flowrate, with a steeper decrease occurring at lower power outputs. At 100 kWe, an increase in CO_2 injection flowrate from 0 to 300 kg/hr, produces a decrease in O_2 concentration from 20.7 mol% to 19.06 mol%, whereas at 60 kWe, an increase in CO_2 injection flowrate from 0 to 300 kg/hr, leads to a decrease in O_2 concentration from 20.7 mol% to 18.59 mol%. However, at a maximum CO_2 injection flowrate of 300 kg/hr at all power outputs monitored, the limiting O_2

concentrations in the working fluid required for complete combustion is never reached in the model.

A mass balance was carried out to determine the O_2 and CO_2 concentrations in the flue gas exiting the MGT at 100 KWe, with increasing CO_2 injection flowrates. This was compared to the 100 KWe scenario as shown in Figures 5.3 and 5.4. There is a strong correlation in the trends observed, which validates the Aspen model. However, the discrepancy in data/results between the analytical calculation and the model is due to the reaction chemistry occurring in the combustion chamber in the model which could not be accounted for analytically.

5.2.1.2. Impact of S-EGR on MGT temperature distribution

The increase in CO_2 injection flowrates plays an important role in the heat balance across the MGT. The TIT (turbine inlet temperature) and CDT (compressor discharge temperatures) vary accordingly as shown in Figures 5.6 and 5.7.

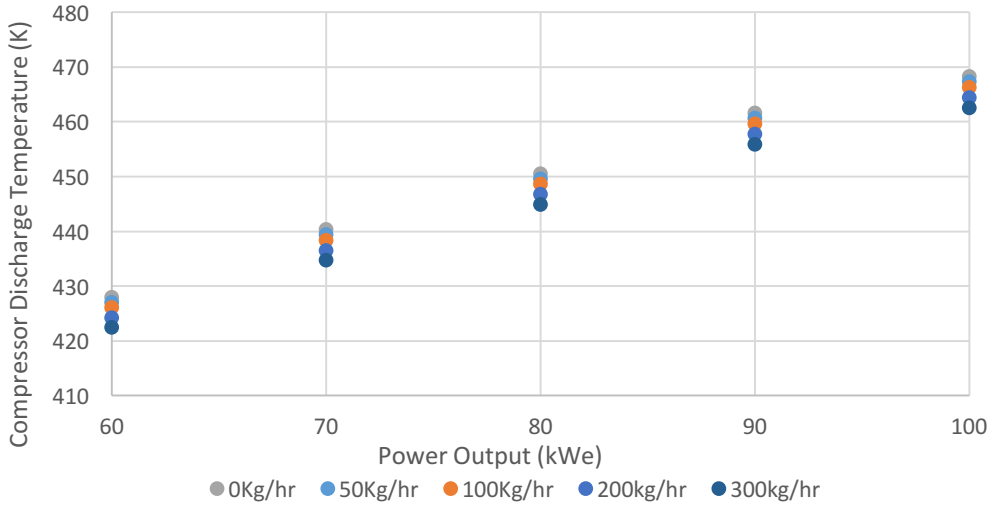

Figure 5.6: Compressor Discharge Temperatures for increasing CO_2 injection flowrates.

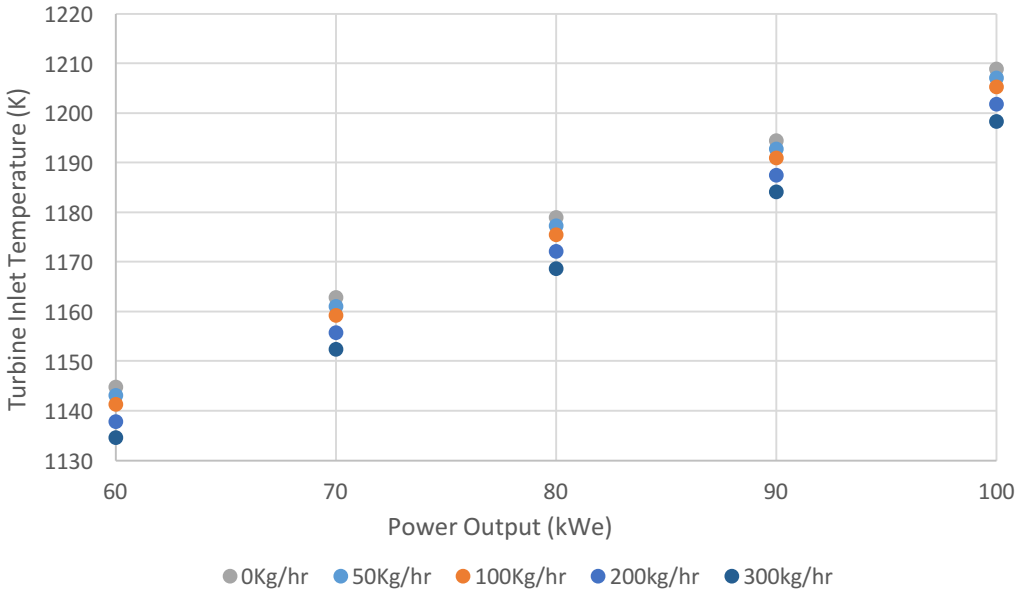

Figure 5.7: Turbine Inlet Temperatures for increasing CO_2 injection flowrates.

The impact on the turbine performance by CO_2 injection is dominated by the effect of CO_2 on the oxidizer temperature. This is due to CO_2 having a higher heat capacity than air and as such, it takes more energy to increase the temperature by the same amount, hence a similar energy input will produce lower compressor temperature outputs [85].

At a constant turbine outlet temperature of 918.15 K, the Figures 5.6 and 5.7 show that there is a decrease in compressor discharge temperature and turbine inlet temperature following an increase in the CO_2 injection flowrate at each power output. The CDT is strongly affected by the performance of the compressor which is influenced by the working fluid composition. As mentioned earlier in Section 5.2, CO_2 has a higher heat capacity than air and it is thus denser than air [84, 85]. As such, the required energy for compression is lower. Due to a specified power input in the system for an increase in the CO_2 injection flowrates, the outlet temperature is decreased. The TIT also decreases with an increase in the injection flowrate. This is due to the CO_2 displacing oxygen in the combustion chamber. By displacing the air intake in the compressor with CO_2, the heat capacity of the working fluid increases. Hence, the temperature increases in the combustion chamber decreases [134].

The decrease in temperature rise in the combustion chamber causes the power output to decrease [134] However, as the power output is fixed in the model, the heat input into the system is increased by increasing the fuel consumption which is caused by an increase in fuel flowrate [81]. When the power output is decreased, the fuel and air flowrates decrease [134] as well as fuel consumption as explained using Equation (4.1). The O_2 levels in the flue gas also increase with decreasing power outputs as less oxygen was used in combustion due to the lower fuel flowrates which lead to a lower temperature rise in the combustion chamber. Hence, a decrease in CDT and TIT is observed in Figures 5.6 and 5.7 for a decrease in power output.

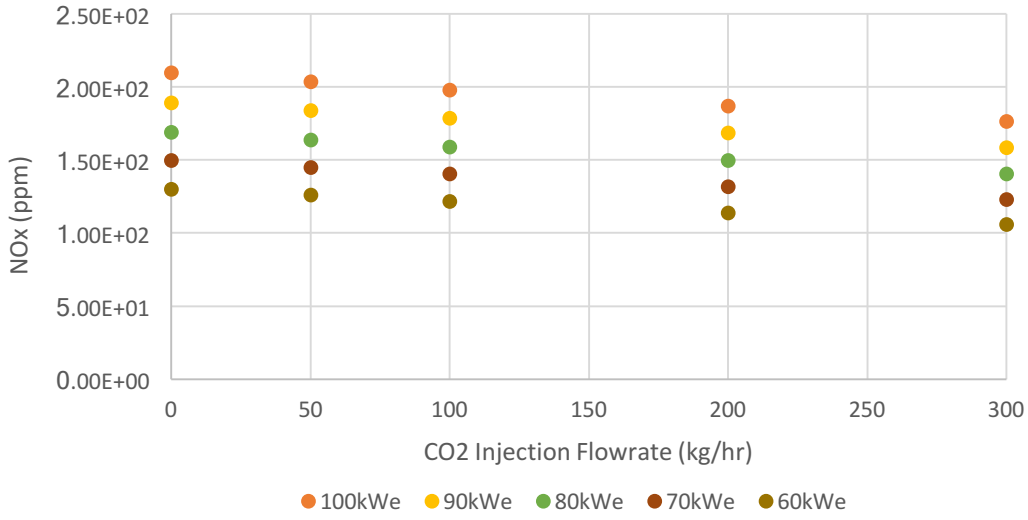

Figure 5.8: NO_x concentrations in the flue gas for increasing CO_2 injection flowrates across varying power outputs.

As shown in Figure 5.8, when operating at lower power outputs, the NO_x is observed to decrease. Also, with higher CO_2 injection flowrates, the NO_x is also observed to decrease. This occurs due to the reduction in CDT with decrease in power output and increase in CO_2 injection flowrate. This causes a reduction in the combustion temperature across the combustion chamber and thus lower production in thermal NO_x. This has been verified in the literature by researchers such as Best et al., [85] and Nguyen et al., [149]. It is shown that the combustion temperature is an important factor in the NO_x formation. With an increase in CO_2 concentration in the working fluid entering the compressor, the heat

capacity of the working fluid increases due to the high heat capacity of CO_2. This leads to an increased rate of heat radiation in the combustion chamber [85], thus causing a lower combustion temperature.

5.2.1.3. Impact of S-EGR on the MGT Performance

Performance parameters affected by the injection of CO_2 into the compressor inlet are investigated in this sub-section. The impact of the shaft speed, electrical efficiency and recuperator effectiveness with increasing injection flowrate at varying power outputs in the MGT are illustrated in Figure 5.9.

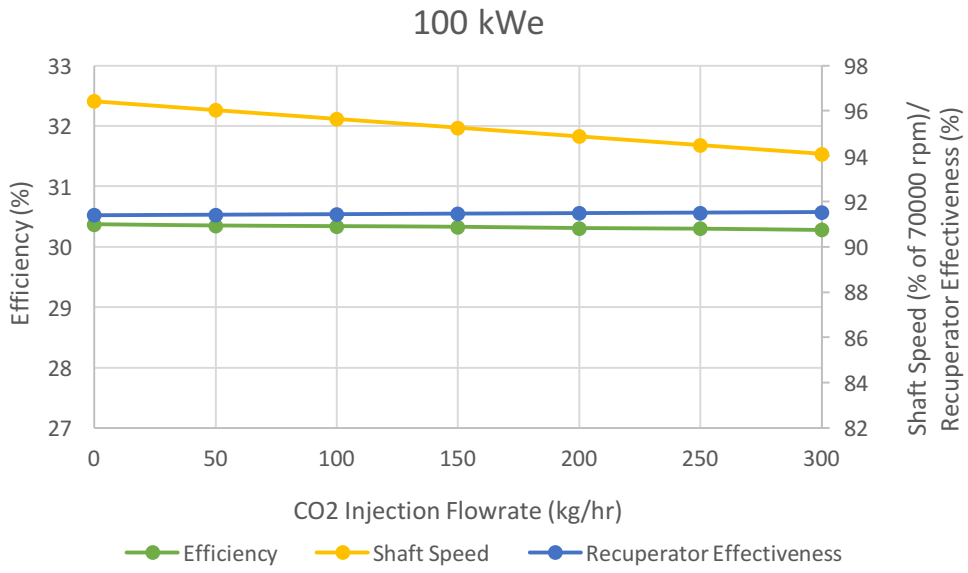

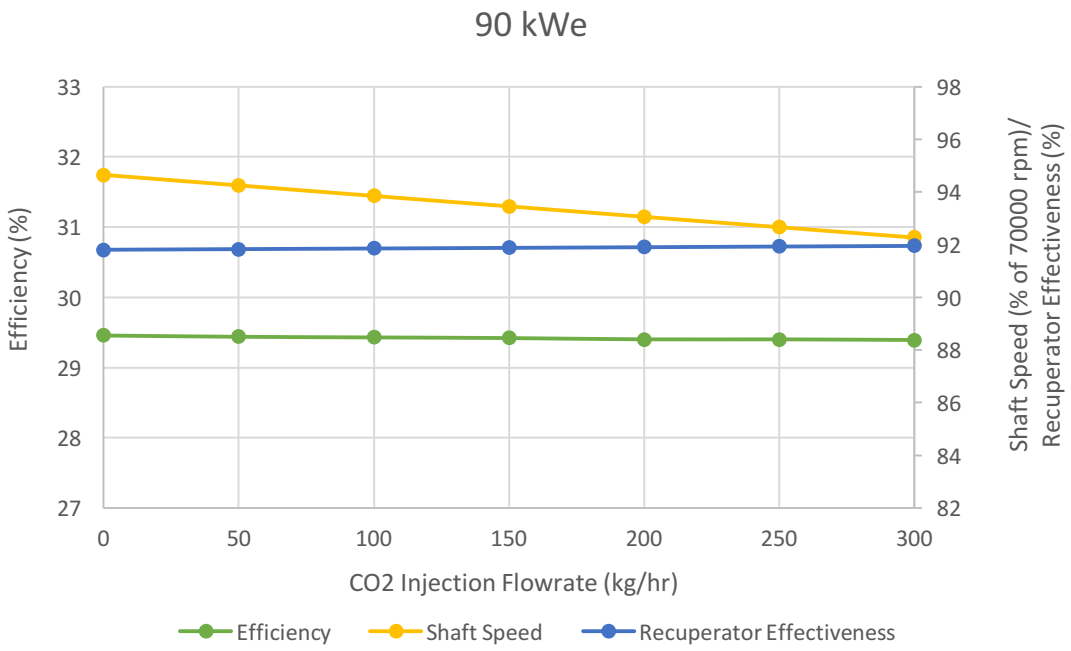
90 kWe
Efficiency (%)
Shaft Speed (% of 70000 rpm)/ Recuperator Effectiveness (%)
CO2 Injection Flowrate (kg/hr)
Efficiency
Shaft Speed
Recuperator Effectiveness


80 kWe
Efficiency (%)
Shaft Speed (% of 70000 rpm)/ Recuperator Effectiveness (%)
CO2 Injection Flowrate (kg/hr)
Efficiency
Shaft Speed
Recuperator Effectiveness

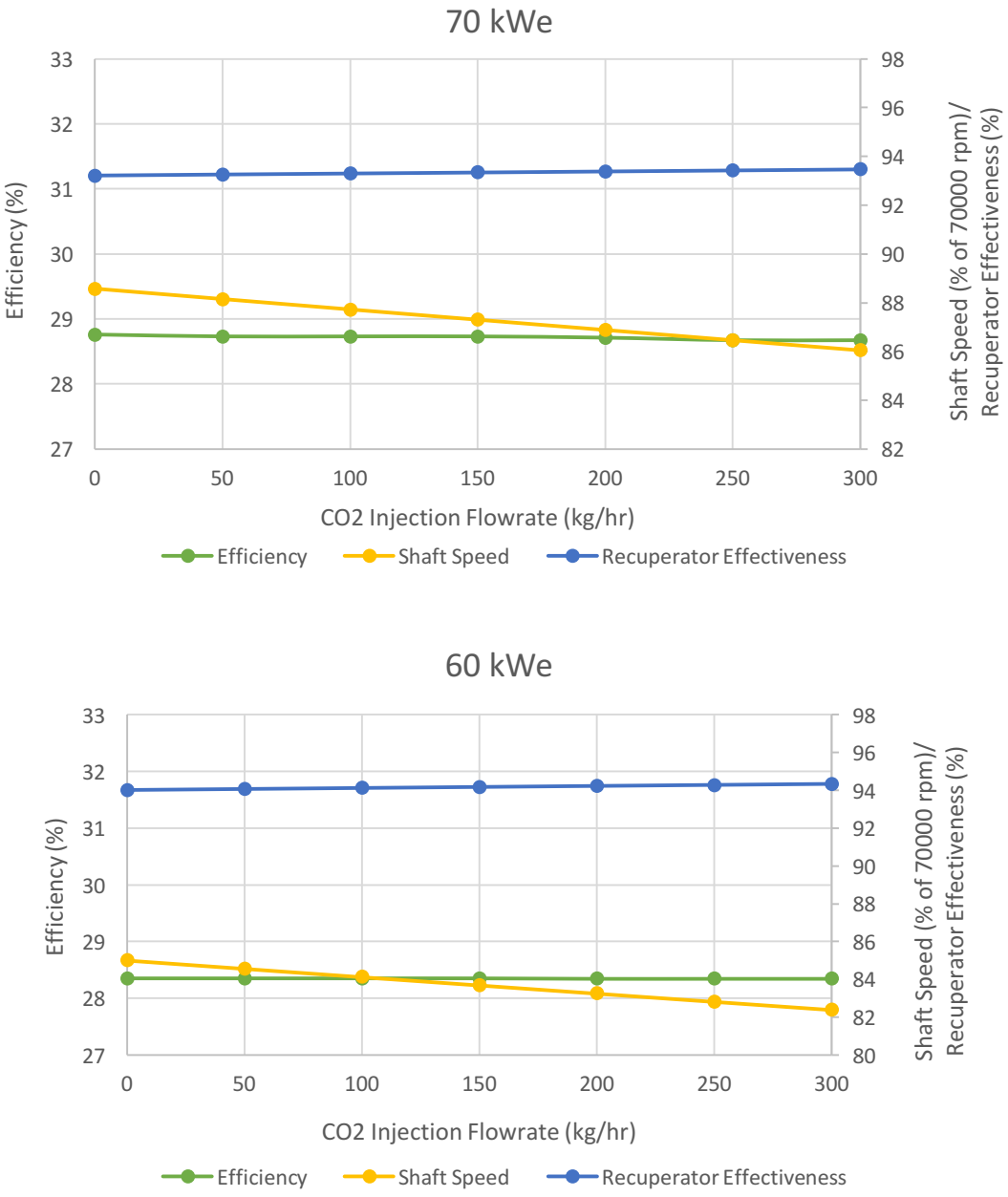

Figure 5.9: Impact of increasing CO_2 injection flowrates on system efficiency, recuperator effectiveness and turbine speed for varying power outputs.

At lower power outputs, the MGT was observed to operate at lower electrical efficiencies and lower rotational speeds. The decrease in power output leads to a decrease in fuel and air flowrate as well as rotational speed [134], which also causes the compressor pressure ratio and work done by the compressor to decrease. This leads to a decrease in the fuel

consumption and heat input. As the electrical efficiency is dependent on the heat input and power output as shown in Chapter 2, the electrical efficiency is seen to decrease at lower power outputs.

Also highlighted in Figure 5.9, the electrical efficiency and rotational speed is also seen to decrease with an increase in CO_2 injection flowrate. This is because of the heat capacity of the working fluid which increases with CO_2 injection flowrates. Hence, to maintain the same fuel consumption, the temperature increase in the combustion chamber has to decrease, which will reduce the power output of the MGT [134]. Consequently, to maintain a constant power output, the fuel consumption has to increase by increasing the fuel flowrate [54]. This then leads to a decrease in the electrical efficiency of the MGT. However, it should be noted that the drop in electrical efficiency is marginally smaller at a constant power output [81, 82 and 134]. Although, in a CCGT, the influence would be greater due to a higher air and fuel flowrate, fuel consumption and power outputs [85].

The shaft speed of the gas turbine also reduces with increasing CO_2 injection flowrates and it is also observed that at lower power outputs, the shaft speed reduces. The reason is as follows; the fuel flowrate increases with an increase in injection flowrates, which leads to an increase in the turbine inlet flow and pressure ratio across the turbine. Hence, creating the need for a higher power output. However, since the power output in the MGT is specified, the air intake mass flowrate reduces which is translated into the decrease in shaft speed. Operating at lower power outputs at a constant CO_2 injection flowrate, the compressor air intake mass flowrate and fuel flowrate are reduced and as such the shaft speed is lower. Similar trends have been observed experimentally by Majoumerd et al., [81] and Ali et al., [134], that highlight the decrease in shaft speed with a decrease in power output in a MGT as demonstrated in Table 5.1.

The recuperator effectiveness is observed to increase with increasing CO_2 injection flowrates and also slightly increase when operating at lower power outputs. As shown in the recuperator effectiveness equation, as shown in Chapter 2, the recuperator effectiveness is dependent on the temperature difference between the temperatures of the compressed air entering and exiting the recuperator to the combustion chamber and the TOT which is constant at a value of 918.15 K.

As the TOT is constant for all the simulations, the driving parameter is the CDT, which is the temperature of the compressed air entering the recuperator. The effectiveness increases at lower power outputs due to a decrease in the CDT. As the CDT decreases with a decrease in power output, the effectiveness increases to maintain a high temperature of air entering the combustion chamber. A similar trend is observed with an increase in the CO_2 injection flowrates. However, the drop in CDT is marginally smaller with an increase in CO_2 injection flowrates, which translates to a slight increase in recuperator effectiveness for an increase in CO_2 injection flowrates.

5.3. Chapter Conclusion

In this chapter, an accurate modelling of a MGT was performed, in which the characteristic maps were scaled to simulate the effect of varying CO_2 injection flowrates in a MGT at various power output. The MGT was modelled in accordance to the Turbec T100 available at PACT and the characteristic maps used were obtained from the manufacturer for that specific device. The scaling equations used were obtained from the literature and derived from first principle thermodynamic equations such as the 1-D compressible flow equations. The maps were implemented using Matlab into the models developed. Each CO_2 injection flowrate and each power output required a new map to be extracted from the original map using Matlab. This is due to the fact that an increase in CO_2 injection flowrates reduces the rotational speed of the turbine and also, operating at lower power outputs corresponds to a lower rotational speed of the turbine. This process made the modelling more relevant to the operating conditions of the MGT and also increased the reliability of the results obtained as the volumetric flowrate, head and polytropic efficiencies at the new operating point are changed from the design point due to change in working fluid composition as well as power output of the MGT.

CO_2 injection has a significant impact throughout the operation of the MGT, which are attributed to the change in the composition of the working fluid with increase in CO_2 injection flowrate into the compressor. This leads to an increase in density and heat

capacity of the working fluid, hence affecting the work done by the compressor and consequently, the expansion being carried out in the turbine. Hence, there are changes in emissions, temperatures across the system and overall performance of the MGT. The CO_2 injected into the compressor inlet is increased from 0 to 300 kg/hr, while operating at varying power outputs between 60kWe to 100kWe. For each parameter investigated, the trends are similar at all power outputs for varying CO_2 injection flowrates and at all CO_2 injection flowrates, the trends are similar for varying power outputs.

Regarding the emissions, the CO_2 concentration in the flue gas increases with increase in power output and CO_2 injection flowrate from 1.8 to 9.6 mol% while increasing the CO_2 injection flowrate from 0 to 300 kg/hr when operating at 100 kWe and also increases from 1.5 to 1.8 mol% between 60 to 100 kWe, with no CO_2 injection. However, the O_2 concentration in the flue gas reduces from 17 to 15.4 mol% between 0 to 300 kg/hr when operating at 100kWe and reduces from 17.7 to 17 mol% between 60 to 100kWe when operating at 0 kg/hr. The O_2 concentration in the combustor inlet also reduces with an increase in CO_2 injection flowrate from 20.7 to 19.06 mol% between 0 to 300kg/hr when operating at 100kWe. This leads to changes in the combustion characteristics such as flame speed and reaction rates of the species involved in combustion as explained earlier in Section 5.2. A decrease in O_2 concentration in the combustor inlet leads to unstable flames and consequently incomplete combustion. However, throughout the modelling, the O_2 concentration limit recommended by the literature was not reached.

The temperatures across the MGT vary according to the power output and CO_2 injection flowrate. In this study, the CDT and TIT were investigated and observed to reduce with an increase in CO_2 injection flowrate and increase with an increase in power output. There is an observed reduction of 1.2% in the CDT and 0.87% in the TIT when the CO_2 injection flowrate is increased from 0 to 300 kg/hr at 100kWe. Whereas, there is an increase of 9.4% in the CDT and 5.6% in the TIT when operating at higher power outputs from 60 to 100 kWe at 0kg/hr CO_2 injection flowrate. The results also highlight a decrease in rotational speed and electrical efficiency as well as an increase in recuperator effectiveness with an increase in the CO_2 injection flowrate. At lower power outputs, the

electrical efficiency and rotational speed of the turbine is seen to decrease whereas the recuperator effectiveness increases.

There is an observed decrease of 2.4% and 0.3% in both the rotational speed and electrical efficiencies, respectively, when increasing the CO_2 injection flowrates from 0 to 300 kg/hr at a power output of 100 kWe and a decrease of 6% and 12 % in both the rotational speed and electrical efficiencies, respectively, when decreasing the power outputs from 100 to 60 kWe when no CO_2 is injected. The recuperator effectiveness is observed to increase by 0.15% with an increase in CO_2 injection flowrate from 0 to 300 kg/hr at a power output of 100 kWe and increase by 2.9% when decreasing the power outputs from 100 to 60 kWe, with no CO_2 injection.

In this Chapter, the novelty includes the characteristic map scaling methodology and equations, developed for changes in working fluid composition and conditions in a simple gas turbine.

6. Modelling the effect of selective exhaust gas recirculation on a pilot scale amine-based CO_2 capture plant

In this chapter, an amine based absorption process model of a CO_2 capture plant is developed and analyzed. The process model involves the use of an equilibrium based thermodynamic property package in Aspen Plus. The CO_2 capture plant is a novel two absorber pilot plant that was recently installed in PACT, with the purpose of further reducing the reboiler duty involved in the CO_2 capture process. The model is validated against baseline experimental data, provided by from PACT, Sheffield and the model is further tested through a different flue gas composition in order to understand its performance over a range of varying operating conditions. A parametric study is then carried out on the performance of the capture plant at different concentrations of amine solution. The focus of this study, is the contribution of knowledge regarding the impact of two absorber columns in a CO_2 capture pilot plant on its performance. This study was carried out with the aim of reducing the "specific reboiler duty" in the amine regeneration process, by increasing the amine concentration and increasing the CO_2 concentration of the flue gas being treated.

6.1. Process Description

As discussed earlier in Chapter 2, post combustion capture is an already available technology, capable of being retrofitted with existing power plants. In this chapter, the effect of the increase in CO_2 concentration in the exhaust gas from a micro gas turbine modified with selective exhaust gas recirculation (S-EGR) on a CO_2 capture plant is modelled and investigated. The capture plant model validation is based on the experimental data obtained from a two-absorber pilot-scale capture plant available at the UKCCSRC PACT facility, in Sheffield. A further analysis of the pilot-scale capture plant is carried out in order to understand the process performance of the system at different solvent concentrations.

The modelling framework implemented in this chapter involves the use of Aspen Plus V10, which is a process modelling software developed by Aspentech. This platform was chosen due to its industrial acceptability as well as its ease in optimizing model designs for energy use and carbon loading [150]. The model was developed and validated with one set of experimental data. Previous research has been carried out on an amine capture plant, using Aspen Plus, such as research carried out by Arachchige et al., [151] that investigated the impact of the solvent properties, absorber pressure and packing height on the performance of an amine capture plant in combination with a 500 MW coal and gas fired power plant. Also, research carried out by Abu-Zahra et al., [152] performed a parametric study on a CO_2 capture plant with the flue gas obtained from a 600 MWe bituminous coal fired plant. In this study, the lean solvent loading monoethanolamine (MEA) weight percentage, CO_2 capture rate and stripper operating conditions are varied. The effect of these changes on the CO_2 capture plant is then investigated.

There are also detailed Aspen Plus modelling processes, which have been carried on CO_2 capture plants. Rezazadeh et al., [119], analysed a rate based model of the CO_2 capture plant, which employs 30 wt% MEA. The rate-based model used was the RateSEp, which is a rigorous framework developed for rate-based separations in Aspen Plus. The developed model was validated using experimental data obtained from the PACT pilot plant, when operating with one absorber and one stripper column. The rate-based Aspen Plus simulation for the CO_2 absorption and desorption has been expansively detailed by Zhang et al., [153], where the physical and chemical properties associated with the RateSep process is comprehensively analysed.

Other software packages, such as Aspen HYSYS, have also been used in the process modelling of the CO_2 capture plant. A study by Akram et al., [120], highlights the impact of various CO_2 concentrations in the exhaust flue gas, thus representing a range of exhaust gas recycle (EGR) ratios on a pilot-scale CO_2 capture plant with 30 wt% MEA. This study was performed with a modelling methodology, in which the Aspen HYSYS was the chosen software package implemented.

Most studies involving the modelling of the CO_2 capture plant are carried out under steady state conditions. However, to gain much more insight into the effect of the process

parameters that produce a dynamic response within the capture plant, a dynamic model is needed. This assists in the development of the control strategies for the flexible operation of the CO_2 capture plant [136]. A dynamic model of the PACT CO_2 capture plant has been developed in gCCS, a gPROMS software package by Bui et al. [136]. In this study, the researchers investigate the performance of the capture plant whilst undergoing partial load stripping, capture plant ramping and reboiler decoupling. Similar to other studies, experimental data was obtained and used to validate the model.

However, in this study, two absorbers and one stripper column are implemented. This new configuration in the PACT facility is shown in Figure 6.1. As shown in Figure 6.1, the capture plant consists of two absorbers, a stripper, cross heat exchanger, rich and lean amine pumps, a condenser, a direct contact cooler, a blower, a lean amine cooler and a reboiler.

In this model, the detailed rate-based model is not implemented because of the high complexities involved in the modelling process. Also, the model developed is a steady state model. Due to the increase in the components and liquid/gas flows across the system, a simple CO_2 capture plant model is suggested and executed in this study. The design specifications for the new CO_2 pilot plant is shown in Table 6.1.

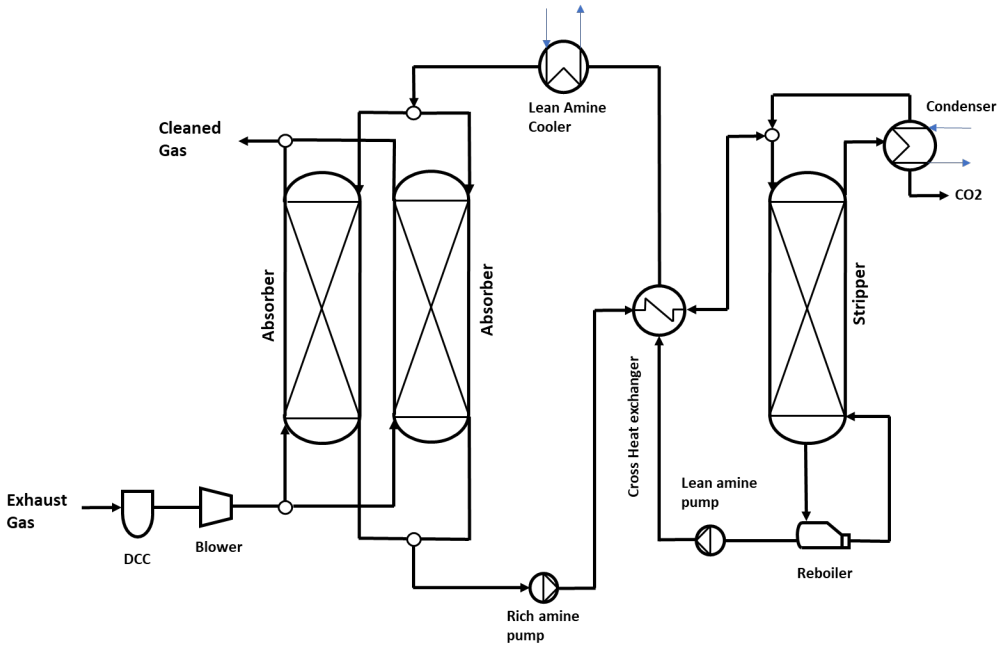

Figure 6.1: Schematic of the capture plant with two absorber columns.

Table 6.1

Pilot plant design specifications

Parameters	Specification
Number of columns	
Absorber	2
Stripper	1
Packing type	
Absorber	Flexipak 350X
Stripper	IMTP 25
Height of packing	
Absorber	6 m
Stripper	7.5 m
Diameter of packing	
Absorber	0.25 m
Stripper	0.3 m
Packing material	Metal
Pressure in absorber	Atmospheric pressure
Pressure in stripper	0.5 barg
Solvent flowrate	300 kg/hr
Solvent type	40 wt% MEA
Solvent temperature in absorber	40°C

The flue gas from the MGT passes through the direct contact cooler in which it is cooled in a counter current manner with water. This cooled flue gas is then passed through a blower to increase the pressure of the flue gas entering the absorber. The flue gas flows through a junction where it is split into two streams, with each stream flowing into the bottom of an absorber column. In each absorber column, it comes in contact with the lean amine flowing in a counter current direction. This strips the CO_2 from the flue gas to produce the rich amine solvent. The rich amine solvent from both absorber columns are coupled at another junction and sent to the rich amine pump, where the pressure is

increased to 3 bar and progressed to the cross heat exchanger. In the cross-heat exchanger, the temperature of the rich amine is increased through the heat exchange from the hot lean solvent from the reboiler. The rich CO_2 solvent is pumped to the stripper column for solvent regeneration and thereby releasing a high concentration CO_2 stream at the top of the stripper column. The lean solvent that has been stripped of CO_2 is pumped into the cross heat exchanger for the heat recovery and then further passed through an air cooler to further cool the amine before being re-used for the absorption process.

In the absorber column in PACT, the lean solvent flowrate is fixed at a constant value in order to control the liquid/gas (L/G) ratio in the column. However, the rich solvent flowrate varies in order to control the level in the stripper and absorber columns. This control mechanism is similar to the previous mechanism used in one of the absorber columns at PACT that was investigated by Rezazadeh et al., [119] and Akram et al., [120].

The absorption process is an exothermic reaction [154], as thermal energy is released in the reaction process between the amine and CO_2 in the flue gas. However, during the regeneration process in the stripper, thermal energy is added to the rich amine solution to release the CO_2.

The capture plant is operated at 40 wt% MEA as the solvent, and the exhaust flue gas is obtained from a 100 kWe micro gas turbine which is also located in the same PACT facility. However, to investigate the impact of a wider range of exhaust flue gas compositions, a gas mixing system can be used, which involves mixing gases from storage tanks, and this is available in the PACT facility. The process description, and the modelling and experimental data are described in this Chapter.

6.2. Experimental Data

In the literature, there are various experimental studies on pilot-scale CO_2 capture plants with MEA as the solvent, such as the studies by Akram et al., [120, 121]. However, most of the studies carried out involved the use of one absorber column for the absorption process, while operating at the baseline MEA concentration of 30wt%. The experimental

data recorded, as shown in Table 6.2, was obtained from a capture plant operating with two absorber columns at 40wt% MEA as the solvent, available at the UKCCSRC PACT Pilot-Plant, Beighon, Sheffield.

Table 6.2

Experimental data recorded from the CO_2 capture plant.

Parameters	**unit**	**Test 1**	**Test 2**	**Test 3**
Gas flowrate	m^3/hr	200	200	200
Solvent flowrate	Kg/hr	300	300	300
Gas inlet temperature	°C	32	29.6	36
CO_2 inlet concentration	Dry %v	5.18	5.18	5.19
CO_2 outlet concentration	Dry %v	0.6	0.4	0.57
Capture efficiency	%	88.9	92.7	89.3
Lean loading	mol/mol	0.275	0.218	0.272
Rich loading	mol/mol	0.495	0.48	0.503
Reboiler temperature	°C	115.8	116.2	117.3
PHW inlet temperature	°C	118.2	118.4	118.4
PHW outlet temperature	°C	116.7	117.1	117.1
PHW flowrate	m^3/hr	14.5	14.5	14.5
Rich outlet temperature	°C	77.5	82.6	84.4
Reboiler duty	kW	24.37	21.5	20.82
Specific reboiler duty	MJ/kg_{CO2}	5.06	4.14	4.33
Gas outlet temperature	°C	33.2	30.8	30.4
Captured CO_2 flowrate	kg/hr	17.3	18.2	17.3

The experimental tests were carried out on three different days and as such, the temperature of the flue gas varies. Although, the CO_2 concentration in the flue gas is constant on the three days, the absorption process is compromised (capture efficiency), and this leads to changes in the captured CO_2 concentration and conditions. Downstream

in the CO_2 capture plant, the reboiler temperature is also affected, as well as the reboiler duty. Thus, affecting the rich and lean loadings accordingly.

To accurate depict the operation of the PACT pilot plant in a process model, the model is developed with similar framework as in literature by Abu-Zahra et al., [152] and Zhang et al., [155]. The modelling framework that describes the reaction chemistry being employed in the columns are highlighted in Section 5.3.

6.3. Modelling Framework

The modelling of the pilot-scale capture plant is carried out using the Aspen Plus V10 process modelling package. The thermodynamic and transport properties were modelled using the Electrolyte NRTL (ELECNRTL) property method [152], to thermodynamically describe the CO_2-MEA-H_2O system. The ELECNRTL activity coefficient, describes the non-ideal activity and interactions between molecules and ions in the Aspen Plus model. The solubility of the aqueous amine solution is determined by both its physical solubility and chemical equilibrium for the aqueous phase reactions among the acid gas, water and amines [155].

The reactive absorption of the CO_2-MEA-H_2O system is usually complex when considering the equilibrium and kinetic reversible reactions taking place in each column. However, in this study, only equilibrium based reactions are implemented in the absorber and stripper columns.

The basic reaction chemistry for the aqueous MEA solution and CO_2 is represented by the following reversible reaction [156]:

$$MEA + CO_2 + H_2O \overset{K_j}{\leftrightarrow} MEACOO^- + H_3O^+ \tag{6.1}$$

where K_j is the chemical equilibrium constant of the reaction j.

The detailed equilibrium reactions included in this model are expressed according to Austgen et al., [157] and other literature [158]:

Water dissociation/ hydrolysis:

$$2H_2O \leftrightarrow H_3O^+ + OH^- \tag{6.2}$$

CO_2 hydrolysis:

$$CO_2 + 2H_2O \leftrightarrow H_3O^+ + HCO_3^- \tag{6.3}$$

Bicarbonate dissociation:

$$HCO_3^- + H_2O \leftrightarrow H_3O^+ + CO_3^{-2} \tag{6.4}$$

Amine protonation:

$$MEAH^+ + H_2O \leftrightarrow MEA + H_3O^+ \tag{6.5}$$

Carbamate dissociation/hydrolysis:

$$MEACOO^- + H_2O \leftrightarrow MEA + HCO_3^- \tag{6.6}$$

The components in the liquid and gaseous phases involved in the equilibrium reactions in the columns are calculated using the following rate [151]:

$$\ln K_j = A_j + \frac{B_j}{T} + C_j lnT + D_j T \tag{6.7}$$

Where *A*, *B*, *C* and *D* are reaction constants, and *T* is the reaction temperature.

In modelling the CO_2 capture plant, the following parameters are kept constant: the flowrate of the exhaust flue gas, the gas inlet temperature, the rich loading outlet temperature and the stripper pressure. Although this reduces the flexible operation of the capture plant, it directs the focus of the study towards the effect of the CO_2 concentration in the flue gas on the loadings, capture efficiency, specific reboiler duty and subsequently the temperatures along the columns. The parameters being investigated are then compared for different amine strengths, with the aim of highlighting the optimum performance characteristics of the capture plant

6.4. Model Validation

To validate the Aspen Plus model, one result from the experimental data from the pilot plant is used and the results are tabulated in Table 6.3. The deviation of a simulated result from the experimental one is calculated using the following equation [119]:

$$Deviaton(\%) = \frac{i_{experimental} - i_{simulation}}{i_{experimental}} X\ 100 \quad (6.8)$$

Where $i_{experimental}$ is the experimental value and $i_{simulation}$ is the simulated value.

Table 6.3

Experimental data for Test 1 vs the Modelling Results.

Parameters	unit	Test 1	Aspen
	Input		
Gas flowrate	m^3/hr	200	200
Gas inlet temperature	°C	32	32
CO_2 inlet concentration	Dry%v	5.18	5.18
Lean loading	mol/mol	0.275	0.275
Rich outlet temperature	°C	77.5	77.5
	Output		
Capture efficiency	%	88.9	92.2
Rich loading	mol/mol	0.495	0.477
PHW inlet temperature	°C	118.2	-
PHW outlet temperature	°C	116.7	-
PHW flowrate	m^3/hr	14.5	-
Captured CO_2 flowrate	kg/hr	17.3	14.68
Reboiler duty	kW	24.37	24.37
Specific reboiler duty	MJ/kg_{CO2}	5.06	5.975
Reboiler temperature	°C	115.8	116.8

The experimental data was used to validate the accuracy of the model. As shown in Table 6.3, the deviation between the experimental and modelling results for the output parameters are within a range of 0 – 18 percent. This is above the normal range suggested in the literature by researchers such as Rezazadeh et al., [119], that have published acceptable ranges of 0.15 – 5 percent. However, in this study, the major deviations occur in the parameters such as the specific reboiler duty and the CO_2 capture flowrate, which are dependent and inversely proportional to each other. With a decrease in the captured CO_2 flowrate, there is an increase in the specific reboiler duty. In the Aspen model, the captured CO_2 flowrate is lower than the experimental value and this is due to differences in the packing specifications in the absorber column, therefore the exact packing dimensions in the experimental work could not be replicated in the model due to the absence of the exact experimental packing specifications in the Aspen model and as such, approximate packing dimensions were implemented.

6.5. Variations in the CO_2 composition in the flue gas

In this study, the CO_2 concentration in the exhaust flue gas is increased from the experimental value of 5.18 dry %vol by increments of 1 mol%, starting from 6 dry mol% to 10 dry mol%. This is to simulate the effect of the S-EGR on the exhaust flue gas.

The parameters measured in this analysis are the L/G ratio, the reboiler duty, lean and rich loadings, and the CO_2 capture efficiency. A further analysis on the temperature profiles of both the absorber and stripper columns are carried out.

With an increase in the CO_2 concentration in the flue gas, the solvent flowrate and L/G ratio is observed to increase as shown in Figure 6.2. Contrary to the experimental set-up, in the model, the lean solvent flowrate is not maintained at a constant value, however, the flue gas flowrate is maintained at a constant value of 200 m^3/hr for all the scenarios. The lean solvent flowrate is left to vary with an increase in the CO_2 concentration in the flue gas, and as such the L/G ratio also varies. As the CO_2 concentration in the flue gas increases, the required amount of solvent to capture the CO_2 in the absorber column is increased in order to maintain a high CO_2 capture efficiency, hence increasing the solvent

flowrate. With a constant flue gas flowrate, the L/G ratio is also observed to increase. This follows similar studies by Akram et al., [120].

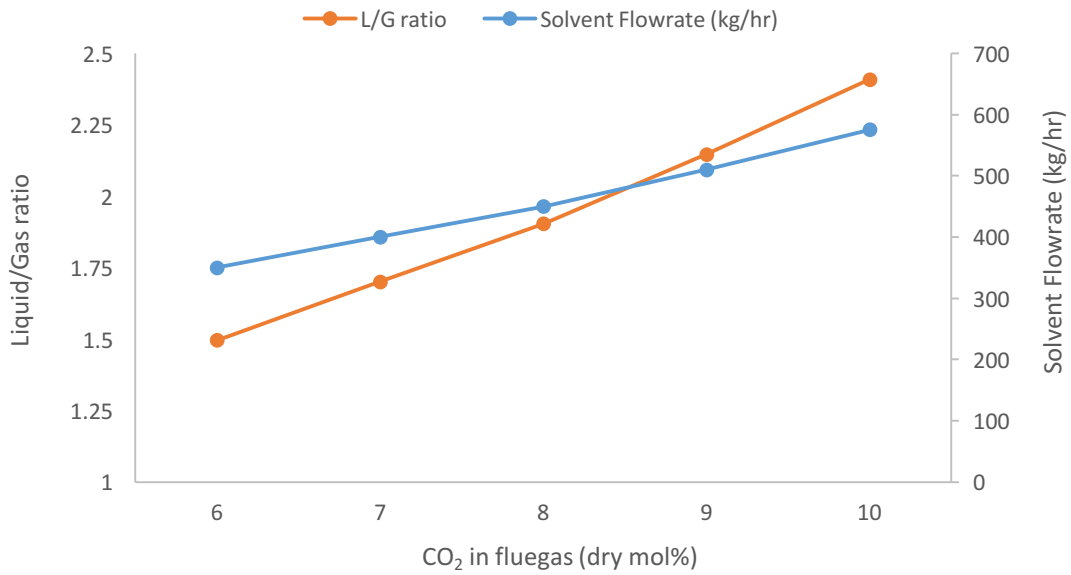

Figure 6.2: L/G ratio and lean solvent flowrate for varying CO_2 concentration in the flue gas.

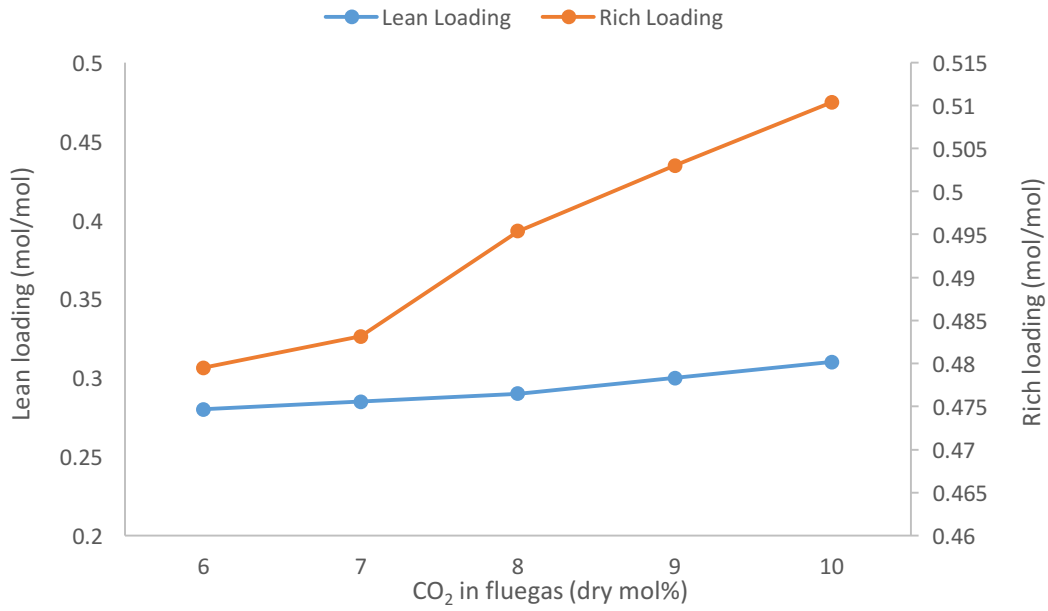

Figure 6.3: Lean loading and rich loading for varying CO_2 concentration in the flue gas.

With an increase in CO_2 concentrations in the flue gas, both the lean and rich loadings are observed to increase, with the lean loading increasing slightly and the rich loading increasing substantially and this shown in Figure 6.3. Experimental studies with one absorber column have reported a similar trend such as that observed by Akram et al., [120]. As the CO_2 concentration in the flue gas increases, the mass of CO_2 transferred between the liquid and gaseous phase increases. As the contact area (column size) is constant, a larger amount of CO_2 is transferred due to the increased driving force in the column [120]. This leads to an increase in the rich loading exiting the bottom of the absorber column. As shown in Figure 6.3, there is a tiny increase in rich loading, when the CO_2 concentration in the flue gas increases from 6 to 7 mol% CO_2. This is attributed to the differences in magnitude of the CO_2 partial pressure in the column. As such, there is a small increase in CO_2 absorption in the column at 7 mol%, leading to a small increase in rich loading.

As observed in Figure 6.2, the solvent flowrate increases with an increase in the CO_2 concentration in the flue gas. At higher solvent flowrates, the lean loading of the solvent also increases, as this reduces the energy required to regenerate the solvent [84, 159]. The decrease in regeneration energy is highlighted by the decrease in the specific reboiler duty as shown in Figure 6.4.

As shown in Figure 6.4, the specific reboiler duty and CO_2 capture efficiency decrease with an increase in the CO_2 concentration in the flue gas. The decrease in specific reboiler duty is due to the higher partial pressure of the CO_2, which increases the driving force in the column and increasing loadings, thus favouring the CO_2 capture reaction [62]. The CO_2 efficiency is observed to also reduce, due to the increase in lean loading. Other Aspen simulation studies such as Arachchige et al., [151], have performed research, in which the lean loading was varied in a CCS plant coupled to both a 500MW gas and coal fired power plant. It was observed that with an increase in the lean loading, the capacity of the solvent for CO_2 absorption decreases, thus, leading to a decrease in CO_2 capture efficiency.

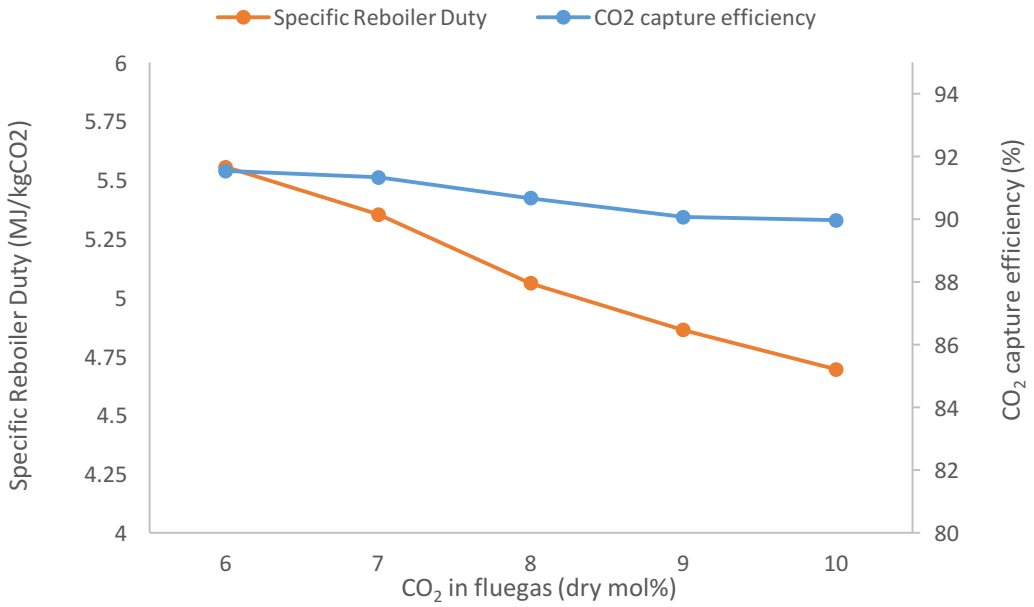

Figure 6.4: CO_2 capture efficiency and specific reboiler duty for varying CO_2 concentration in the flue gas.

As mentioned earlier in Section 6.1., the reactions in the absorber columns are exothermic reactions and thus heat is given out and the temperature increases as the flue gas travels from the bottom to the top of the column as shown in Figure 6.5. This leads to a temperature bulge, showing the highest reaction point in the absorber column [120]. Whereas the reactions in the stripper columns are endothermic reactions, because the regeneration reactions require heat from the reboiler, thus leading to a decrease in the temperature as the heat travels from the bottom to the top of the column as shown in Figure 6.6.

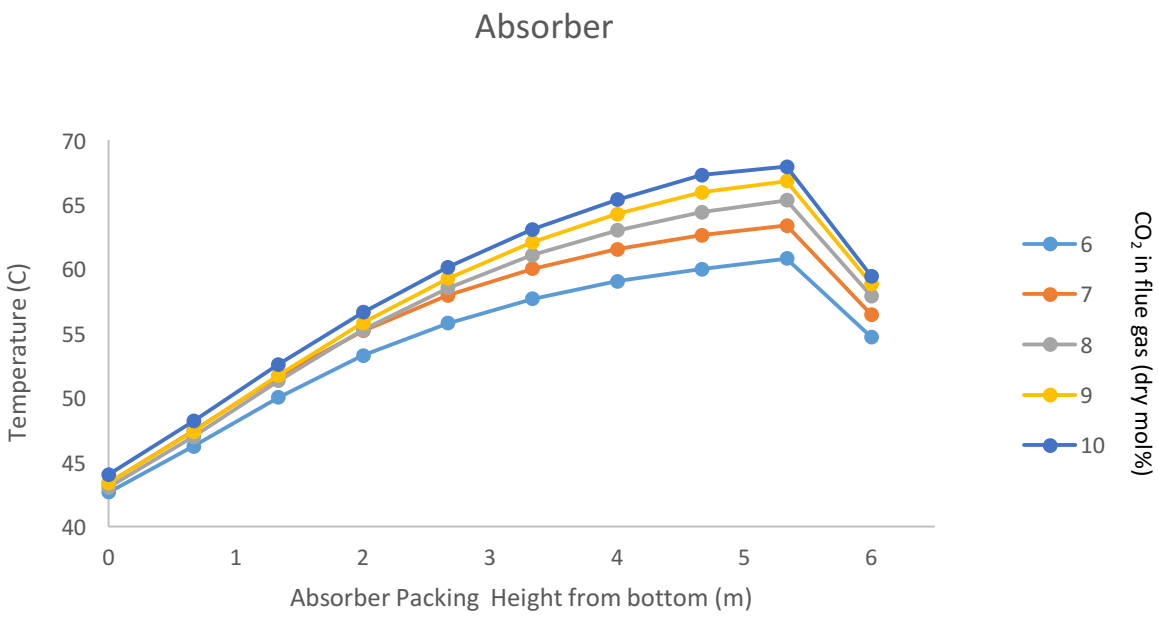

Figure 6.5: Temperature profile for the absorber column.

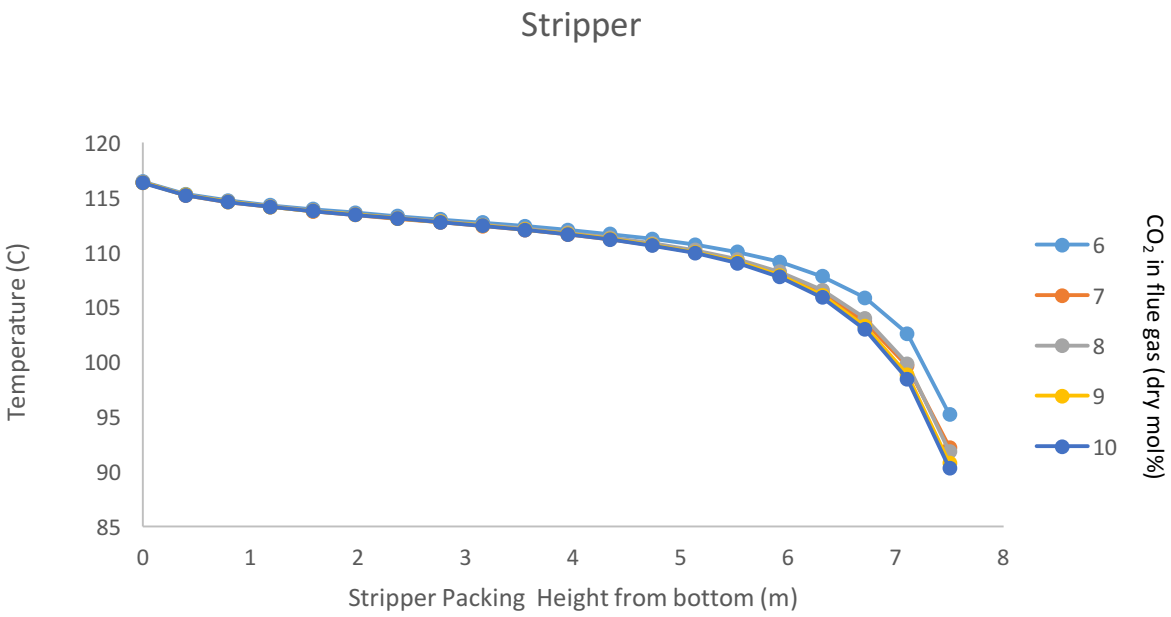

Figure 6.6 Temperature profile for the stripper profile.

Figure 6.5 shows the temperature bulge occurring towards the top of the absorber. This indicates that most of the CO_2 is absorbed at the top of the column, where it comes in

contact with the lean solvent. Thus, the maximum driving force for the mass transfer occurs at the top of the column.

With an increase in CO_2 concentration in the flue gas, the temperature profile in the absorber is observed to follow a steeper trend with an increase in the bulge temperature. This is because the higher CO_2 content flue gas reacts with more solvent due to the higher lean solvent flowrate, thus leading to a faster exothermic amine-CO_2 reaction and an increase in temperature in the columns. However, in the stripper column, with an increase in CO_2 concentration in the flue gas, the temperature profile is less steep. With an increase in CO_2 content in the flue gas, the specific reboiler duty reduces as shown in Figure 6.4, thus reducing the thermal energy required for regeneration. With the reduction in thermal energy, there is less heat from the reboiler to the stripper and thus lower temperature endothermic reactions occurring in the column.

6.6. Variation in the amine strength (40 wt% vs 30 wt%)

In this study, the MEA concentration is reduced from 40 wt% to 30 wt%. This reduces the absorption capacity of the amine, but it leads to other changes in the performance parameters. The standard MEA concentration that serves as the benchmark for evaluating post-combustion capture is 30 wt% [160, 161]. However, in a two-absorber column pilot plant, there is less knowledge on the impact of the amine strength on the performance of the system. In general, higher MEA concentrations promote CO_2 absorption and CO_2 solubility [162].

The effect of the amine strength on the rich and lean loadings, CO_2 capture efficiency and specific reboiler duty is investigated. To extensively research the impact of the amine strength, the study encompasses both 40 wt% MEA and 30 wt% MEA at different CO_2 concentrations in the flue gas.

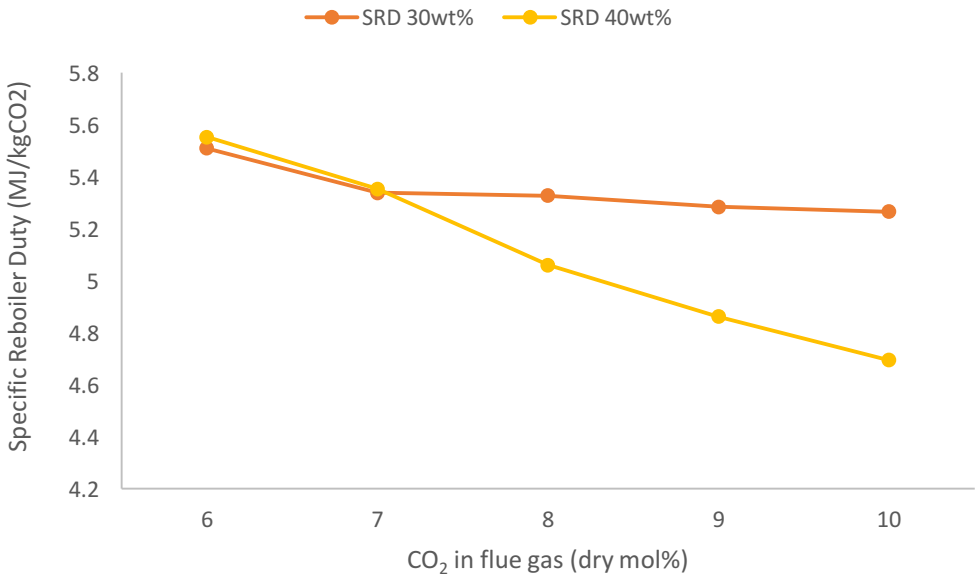

Figure 6.7: Specific reboiler duty for different amine strengths for varying CO_2 concentration in the flue gas.

It should be noted that increasing the amine strength in the capture plant will have pronounced corrosive effects [152]. Previous studies have suggested the inclusion of corrosion inhibitors will assist in reducing this effect [163].

The specific reboiler duty reduces with an increase in the MEA concentration as shown in Figure 6.7. At low CO_2 concentration in the flue gas, both 30 wt% and 40 wt% MEA have similar values and at higher CO_2 concentration in the flue gas, the 40 wt% MEA reduces at a faster rate compared to the 30 wt% MEA. Thus, indicating lower values for specific reboiler duty at different flue gas CO_2 concentrations compared to the 30 wt% MEA. This is because high MEA concentration promotes CO_2 absorption performance, as well as improving the CO_2 reaction rate within the column, thus leading to a reduction in the required regeneration energy [126]. Other researchers have published a similar outcome with an increase in the MEA concentration in the capture plant, see for example Agbonghae et al., [164].

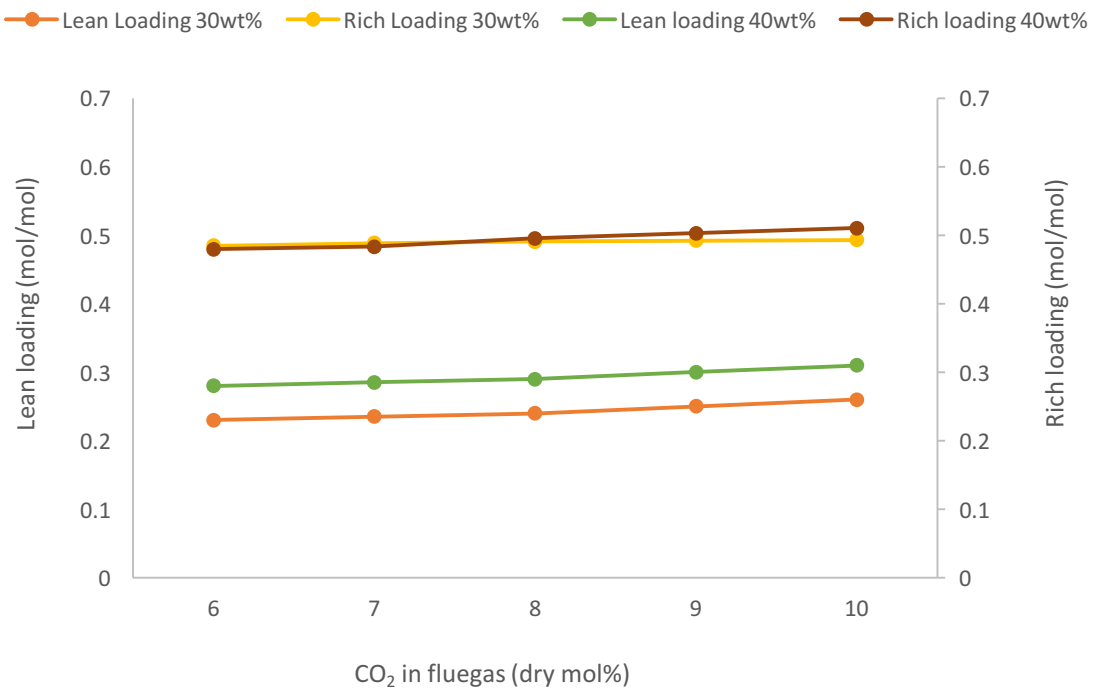

Figure 6.8: Lean and rich loadings for different amine strengths for varying CO_2 concentration in the flue gas.

As shown in Figure 6.8, an increase in the CO_2 concentration in the flue gas causes an increase in the lean and rich loadings and at both 30 and 40 wt% MEA concentrations, a similar trend is observed. At 40 wt% MEA, the lean loading is higher than at 30 wt% for all flue gas CO_2 concentrations. However, the rich loading is initially lower at 40 wt% at low flue gas CO_2 concentrations, but increases at a faster rate compared to 30 wt% MEA for an increasing CO_2 concentration in the flue gas.

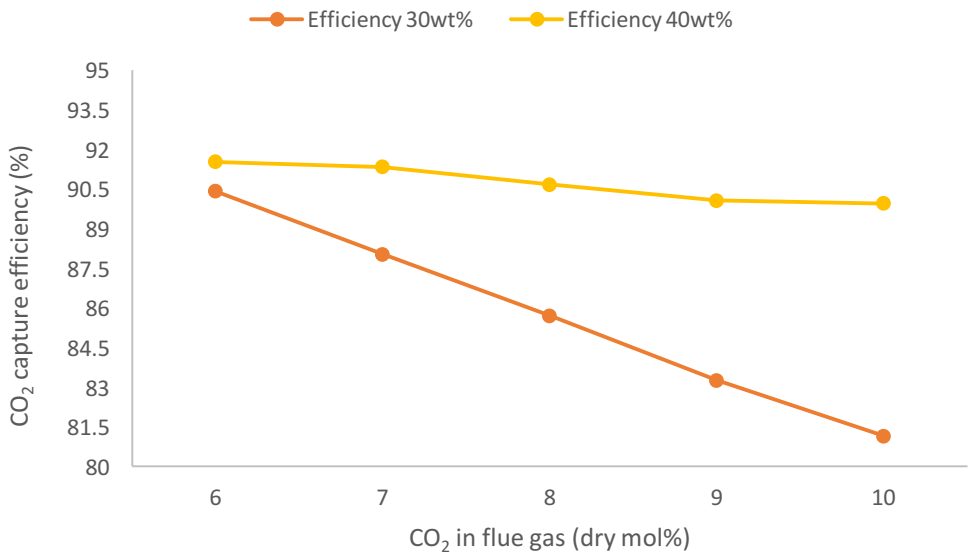

Figure 6.9: CO_2 capture efficiency for different amine strengths for varying CO_2 concentration in the flue gas.

In Figure 6.9, the CO_2 capture efficiency reduces with an increase in the CO_2 concentration in the flue gas. It is also observed to be higher when operating with 40wt% compared to 30 wt% MEA. At higher MEA concentrations, the lean loading is observed to be high, which should reduce its absorption capacity, lean solvent flowrate and CO_2 capture efficiency. However, due to the implementation of a similar solvent flowrate for both MEA concentrations, the CO_2 capture efficiency increases. This is as a result of the increased CO_2 solubility and improved absorption process associated with the higher amine strength.

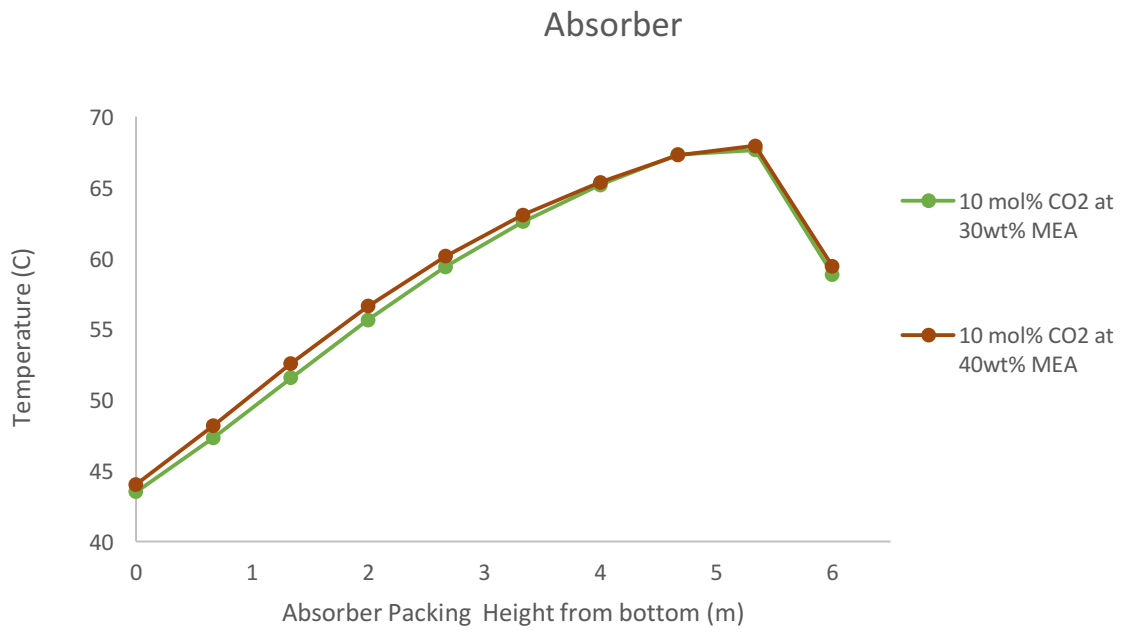

Figure 6.10: Temperature profile for the absorber column at 10 mol% CO_2 at both 30 and 40 wt% MEA.

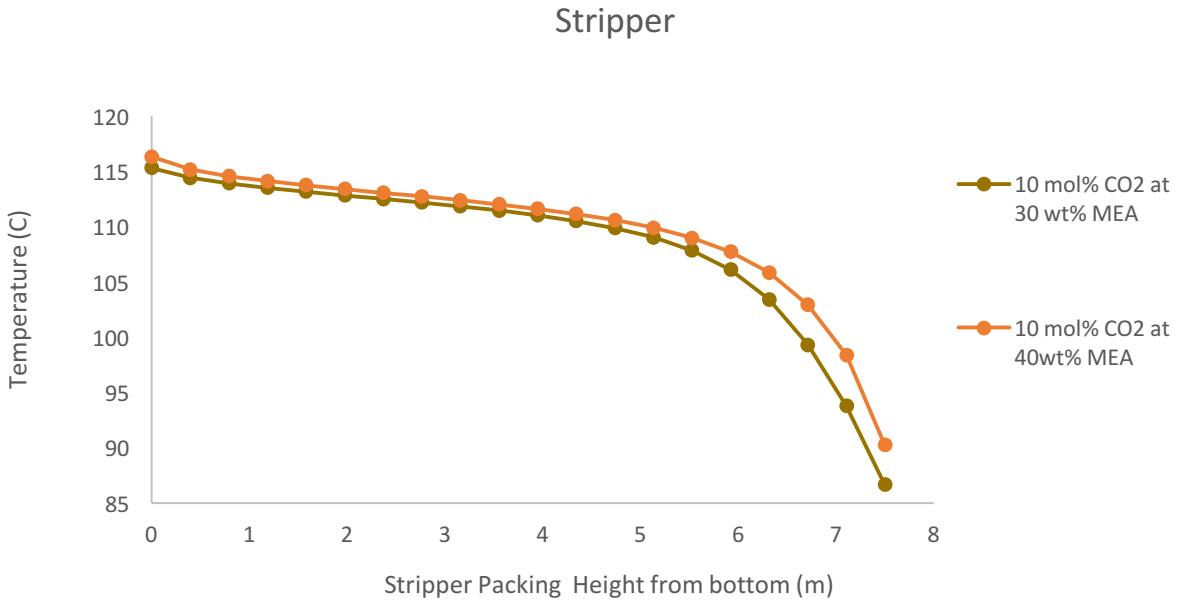

Figure 6.11: Temperature profile for the stripper column at 10 mol% CO_2 at both 30 and 40 wt% MEA.

At both 40 wt% and 30 wt% MEA concentrations, the temperature profiles of both the absorber and stripper columns follow a similar trend, and this is due to similar reactions

occurring in the columns. However, as shown in Figure 6.10, the temperatures along the column at 30 wt% MEA is lower compared to 40wt% MEA. This indicates a slightly lower temperature bulge at a lower amine concentration, and this is as a result of the reduced mass transfer and a lower driving force in the column.

In Figure 6.11, a similar pattern is observed. The temperatures along the column are lower at 30 wt% MEA compared to 40 wt% MEA. This is because of the lower rich loading entering the top of the column, thus less temperature is required for the regeneration process.

6.7. Chapter Conclusion

In this Chapter, a two absorber CO_2 capture plant operated with MEA as the solvent is modelled. The model is validated against a set of experimental data from a new two absorber CO_2 capture plant available at the UKCCSRC PACT in Sheffield. The model validation with the experimental data was carried out with 40 wt% MEA as the solvent. The process modelling software implemented in this study is Aspen Plus v10, which is available from AspenTech. The thermodynamic reactions, as well as the process description of the model are detailed in this Chapter.

There are two studies performed in this Chapter, the first study involves the variation of the CO_2 composition in the flue gas whilst operating at 40 wt% MEA. It was observed that with an increase in CO_2 concentration in the flue gas comes an increase in the solvent flowrate and thus the L/G ratio. This also causes an increase in the CO_2 loading (both rich and lean) in the absorber columns. This is due to the increased driving force in the column as a result of the high CO_2 mass transfer between the liquid and gas phase in the column. However, the CO_2 capture efficiency decreases due to the decrease in the CO_2 absorption capacity by the lean solvent. Also, the specific reboiler duty decreases as a result of the high CO_2 partial pressure due to the increased driving force in the absorber column.

The temperature across the absorber and stripper columns are observed to increase and decrease, respectively, with an increase in CO_2 concentration in the flue gas. This causes a higher temperature bulge in the absorber column. The temperature bulge is not

necessarily beneficial for the absorption process as the rate of absorption reduces at higher temperatures. Thus, creating a scenario in which the mass transfer and driving force are higher in the absorber column, whereas the absorption rate is reduced due to the high bulge temperature.

The second study involves a comparative analysis between 30 wt% and 40 wt % MEA in the CO_2 capture plant. Operating with a high concentration of MEA solvent generally improves the CO_2 solubility of the amine as well as the absorption process. This causes an increase in the CO_2 capture efficiency when operating with higher amine concentrations, and thus the lean loading and rich loading are also increased. However, the specific reboiler duty is reduced when operating with higher amine concentrations. This is due to the CO_2 absorption performance and reduced required regeneration energy. The temperature profiles in both the absorber and stripper columns follow a similar trend at a high MEA concentration, although the values are observed to be higher at a higher MEA concentration. This is mainly due to the increased CO_2 mass transfer in the columns and the reduced specific reboiler duty, thus increasing the temperature bulge in the absorber column and less steep curve in the stripper column.

From both studies, it can be concluded that the performance of the CO_2 capture plant is increased with an increase in CO_2 concentration in the flue gas as depicted by a decrease in specific reboiler duty. Also, increase in amine strength further reduces this energy consumption, indicating better performance. However, with amines being corrosive, further increase in amine strength might not be suitable. To develop a proper understanding on the performance of this system, a techno-economic analysis is required.

The novelty in this Chapter includes; the process modelling a two-absorber pilot-scale CO_2 capture plant with various CO_2 concentrations in the flue gas and increasing amine concentrations.

7. Techno-economic analysis on EGR and fuel flexibility via increasing the CO_2 concentration in the fuel on a commercial scale CCGT with Carbon Capture

Previous chapters in the thesis investigate the impact of S-EGR (Selective Exhaust Gas Recirculation) in a micro gas turbine as well as the effect of operating a pilot carbon capture plant with varying CO_2 concentration in the flue gas, which results from the injection of CO_2 into the compressor of the micro gas turbine. To perform an economic analysis on the effect of EGR in a gas turbine, a commercially large-scale gas turbine is implemented. This ensures an accurate correlation of economic data with less assumptions.

In this chapter, an economic analysis is carried out on the effect of EGR on a commercial scale combined cycle gas turbine (CCGT), and the effect of the flue gas compositions from the gas turbine on a carbon capture plant. Different fuels were tested to investigate the flexibility of the model in a growing natural gas trading economy.

7.1. Study description

In this chapter, a commercial scale combined cycle gas turbine (CCGT) was modelled and integrated with a carbon capture plant operating with 30 wt% monoethanolamine (MEA) to remove the CO_2 present in the exhaust gas stream. The CCGT model was validated with a 2013 U.S DOE/NETL (United States Department of Energy/National Energy Technology Laboratory) [165] report using a similar power plant. The power plant is a natural gas 650 MWe combined cycle power plant located in Greenfield, Midwestern, Indiana, USA. However, the capture plant was modelled based on the hydrodynamic parameters of the capture plant and hence expected discrepancies were observed between both results. Subsequently, various fuel compositions were introduced to investigate the effect of increasing the CO_2 content in the fuel on the performance of the CCGT integrated with an amine capture plant (ACP).

A further study involving EGR was analysed, using a modified CCGT configuration with an exhaust gas recycle stream which is condensed before being introduced back into the compressor. Using a similar schematic for the commercial-scale ACP as in the first study, the EGR was integrated with the capture plant to remove the increased amount of CO_2 in the exhaust stream leaving the heat recovery steam generator (HRSG). The EGR model was validated with the EGR modified power plant in the 2013 DOE/NETL report [165], at an EGR ratio of 35%. Further EGR ratios up to 50% could have been investigated, however, according to the 2013 DOE/NETL report [165], major redesign and improvements on some of the components, such as the combustion chamber, would have to be carried out to ensure flame stability and complete combustion taking place. This is a non-feasible modification, thus, further increasing the EGR was not considered in this chapter.

Finally, the economic viability of increasing the CO_2 content in the air via EGR and also increasing the CO_2 content in the fuel via fuel flexibility is investigated. The methodology and data used in the economic analysis was obtained from the "Quality Guidelines for Energy System Studies" [166] and the "Cost Estimation Methodology for NETL assessments of power plant performance" [167].

Other energy-efficiency methodologies such as the NPV analysis, is built on the assumption that "the variance of the present value of future benefits and costs is zero" [168]. Whereas, the essential element overlaying the DOE cost methodology is the ability to accurately predict future energy prices, as this analysis favours a "certainty model" [168].

Similar work has been performed by researchers such as Diego et al., [94], using the same scaling methodology, where a CCGT is modelled and integrated into a CO_2 capture plant. Also, other studies carried out by researchers, such as Diaz-Herrera et al., [169], have used the scaling methodology for the economic assessment of novel configurations of a combined cycle gas turbine and CO_2 capture plant. A study involving a similar configuration has been performed by Omehia et al., [170], where a CCGT was analysed to investigate varying fuel compositions. However, this study was expanded to investigate the effect of EGR on fuel flexibility.

In this chapter, the software used in the process modelling is gCCS. Microsoft Excel is also used to analyse the data obtained from the model and perform a techno-economic assessment on the system. Using the aforementioned methodology, the cost of electricity (COE) and cost of CO_2 avoided (COA) are used to carry out a comparative economic analysis on the fuel flexibility via increasing the CO_2 concentration in the fuel of a CCGT stand-alone and a CCGT with 35% EGR, when a CO_2 capture plant is integrated.

In this study, the maximum CO_2 content of 10 mol% was chosen to ensure complete combustion in combustion chamber model. This has been validated in research carried out by Nikpey et al. [101] on a MGT with varying increase in CO_2 content in the fuel. This study concluded that combustor flameout occurs when operating at higher than 10mol% CO_2 in the fuel at full load operating conditions.

The fuel flexibility economic study involves investigating fives cases; (i) CCGT without an ACP, (ii) CCGT with an ACP, (iii) CCGT with an ACP and 5% CO_2 content fuel, (iv) CCGT with an ACP and 7.5% CO_2 content fuel, and (v) CCGT with an ACP and 10% CO_2 content fuel.

The EGR economic study involves investigating four cases which include; (i) CCGT at 35% EGR ratio with an amine capture plant (ACP), (ii) CCGT at 35% EGR ratio with an ACP and 5% CO_2 content fuel, (iii) CCGT at 35% EGR ratio with an ACP and 7.5% CO_2 content fuel, and (iv) CCGT at 35% EGR ratio with an ACP and 10% CO_2 content fuel. As stated earlier in this Section, it was considered unnecessary to investigate beyond 35% EGR ratios.

7.2. Modelling Methodology

The modelling studies in this chapter are realized using the gCCS v1.1.0 process modelling software. A software package developed by PSE for the purpose of modelling power generation systems as well as CO_2 capture systems [171].

The CCGT was created gradually by first building the simple gas turbine section, then connecting the exhaust source to the HRSG (Heat Recovery Stem Generators) which comprise of three economizers, four super-heaters and three evaporators. The heat released from the HRSG is sent to the steam turbines (LP/IP/HP) to increase the overall

efficiency of the system. The low temperature exhaust is then sent to the ACP to strip the CO_2 contained in the exhaust flue gas. Figure 7.1 shows the flowsheet for the CCGT modelled in this study.

Table 7.1

Base case fuel and air compositions and properties [165].

Natural gas	
Inlet temperature (°C)	*38*
Composition (mol %)	
CH_4	*93.1*
C_2H_6	*3.2*
C_3H_8	*0.7*
nC_4H_{10}	*0.4*
CO_2	*1*
N_2	*1.6*
LHV (MJ/kg)	*47.2*
Air	
Inlet temperature (°C)	*15*
Composition (mol %)	
N_2	*77.32*
O_2	*20.74*
H_2O	*0.99*
CO_2	*0.03*
Ar	*0.92*

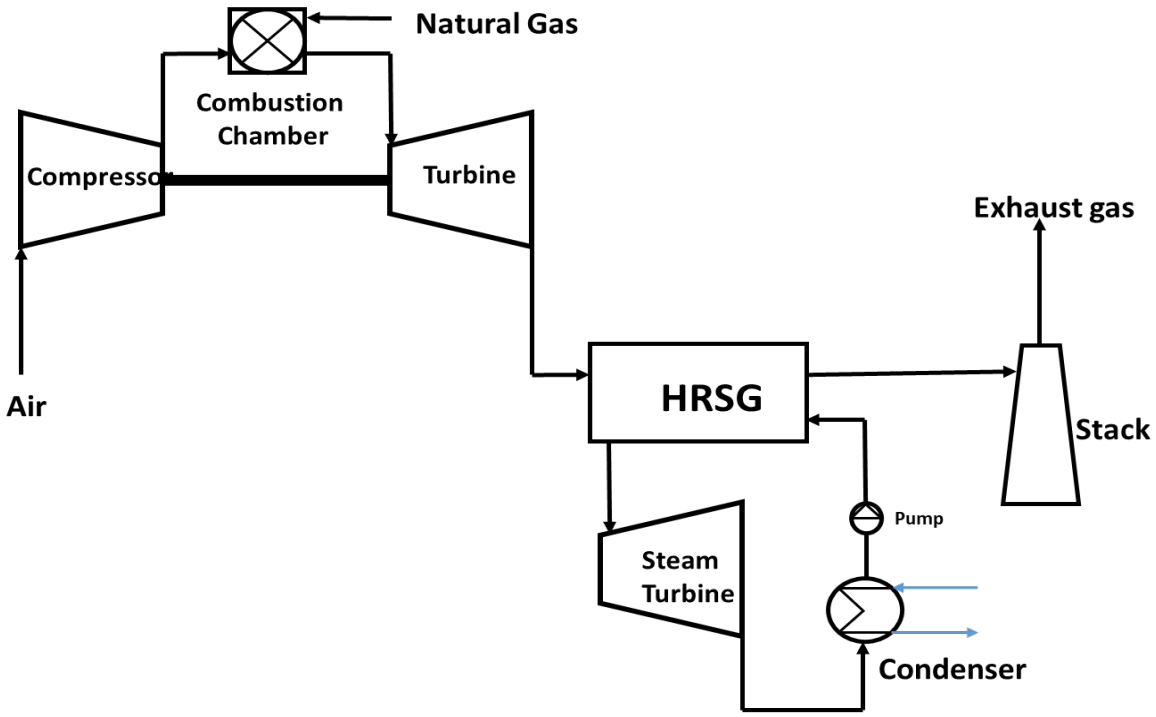

Figure 7.1: CCGT Flowsheet.

The input specifications of the air and natural gas for the CCGT in the reference case can be found in Table 7.1. The model of the CCGT was developed following the DOE/NETL report flowsheet as a guideline, hence adapting similar fuel and air compositions.

The commercial-scale CCGT power plant design comprises of two state-of-the-art (SOA) commercial GE 7FA.05 gas turbines, coupled with two triple pressure level single reheat type HRSG and a condensing steam turbine with an evaporative cooling tower [165]. The pressure drop in the combustion chamber was assumed to be 5% as suggested by Diego et al., [94]. The CCGT power plant is capable of producing a gross power output of 650.42 Mwe, with 420.82 Mwe from the gas turbines alone. For the different fuels simulated in this chapter, the power output of the gas turbine was kept constant, whilst the gross power output varied depending on the impact of the different fuel compositions on the system. The HRSG comprises of High-Pressure (HP), Intermediate-Pressure (IP) and Low-Pressure (LP) steam drums, and superheaters, reheater and economiser sections. The steam turbine is configured with HP, IP and LP steam turbine sections with isentropic

efficiencies of 88.3%, 92.4%, and 90.7%, respectively, and a condenser operating at 5000 Pa. These values were obtained from the validation of the CCGT with the 2013 DOE/NETL report [165]. Theses isentropic efficiencies and condenser operating pressure ensured similar results were obtained from the DOE/NETL report and the Aspen model.

The HRSG was initially configured in a calibration mode. In this mode of operation, the outlet pressure, temperature and heat transfer coefficient of the economizers, superheaters and evaporators are specified from the DOE/NETL 2013 report [165]. The mode of operation for each component is later changed to the operational mode, using the heat transfer area calculated in the calibration mode. Following similar steps for the HRSG, the steam turbine was modelled. Each turbine was configured in its calibration mode, where the inlet and outlet conditions of the turbine was specified according to the 2013 DOE/NETL report [165], and using the inputs, the isentropic efficiencies and Stodola's constant was obtained.

The models being developed in this chapter are used to evaluate the performance of the CCGT and ACP in different conditions. To allow the monitoring of the steam turbines in off-design conditions, the Stodola constant and isentropic efficiency was implemented [172]. This is because of the non-linear behavioural characteristics of parameters such as the efficiency, pressure ratio and rotational speed of the steam drums and off-design conditions [173]. Consequently, to provide a more accurate estimation of the steam turbine behaviour, with changes in mass flow and pressure, the Stodola ellipse equation has to be applied [172, 173].

To capture the CO_2 from the exhaust gas, a chemical absorption CO_2 capture plant with MEA was implemented. The flowsheet for the capture plant is shown in Figure 7.2. The capture plant was built to operate with 30 wt% MEA. The MEA was used in this analysis because of its high popularity within amines, due to its high-reaction rate with CO_2 and low cost [174]. The concentration used is considered to provide the optimum operating conditions for the capture plant as it has been established as the benchmark concentration [175, 176]. Although, researchers such as Feron et al., [177], have suggested other novel absorption liquids to be used in the chemical absorption process with better performance than the benchmark standard. As a result of the little knowledge and

information on these other liquids, the use of the benchmark concentration of 30wt% MEA was maintained in this chapter.

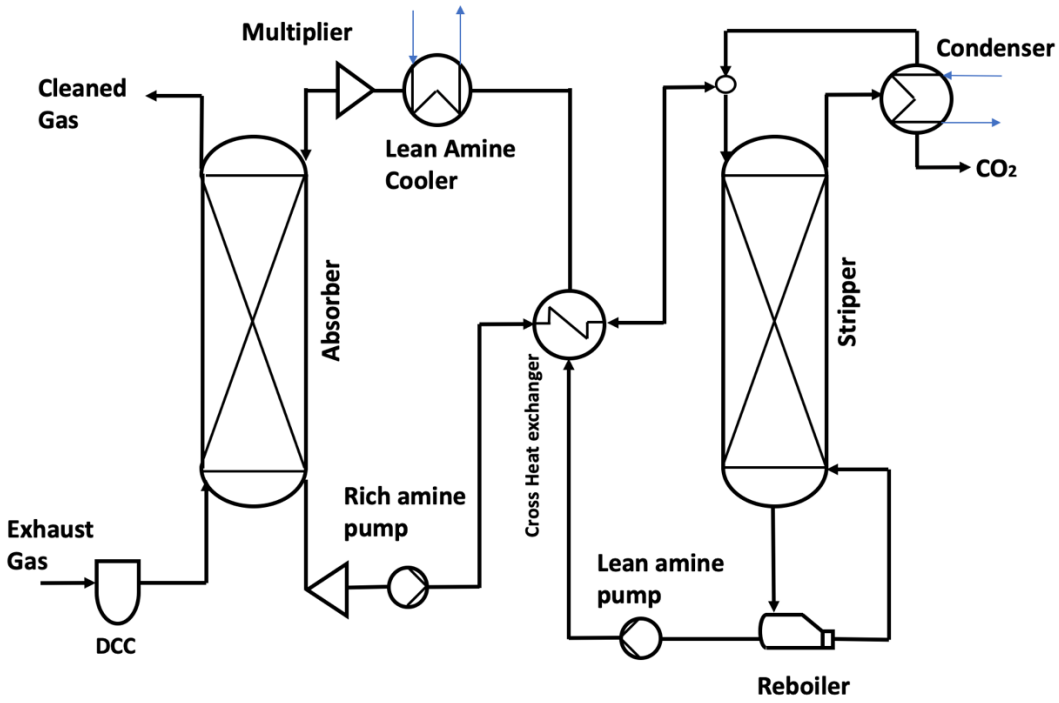

Figure 7.2: Amine capture plant flowsheet.

The exhaust gas from the CCGT flows into a DCC that reduces the temperature of the exhaust flue gas in order to achieve effective absorption [178]. Although the flue gas temperature is not detrimental to the CO_2 capture level of the absorber column [179], reducing the temperature of the flue gas entering the absorber column, reduces the blower's electric energy demand [180]. The blower then increases the pressure of the flue gas entering the absorber column to compensate for the pressure drop/losses in the absorber column [178]. At the entrance of the absorber, the temperature of the exhaust gas is controlled at 40°C [86, 93 and 94]. In the absorber column, the flue gas flows upwards and the MEA solvent flows in a counter-current direction (downwards), resulting in absorption of the CO_2 in the flue gas by the solvent [119]. The solvent, now rich in CO_2 flows to the stripper for the desorption process. In the stripper, the downward

flowing rich solvent is stripped of its CO_2 by the high temperature steam generated in the reboiler [118].

The pumps in the capture plant are specified to operate at an efficiency of 75%. The rich and lean amine pump generate a maximum pressure of 3 bar for the base case with natural gas [93, 118]. In modelling the base case capture plant, a capture efficiency of 90% whilst operating with 30wt% MEA was implemented because of its common adaptation in amine-based capture systems in literature [118]. The lean solvent loading was set to 0.2 mol CO_2/mol MEA [119]. In the stripper section, the temperature in the reboiler was set to a value of 120°C and the pressure in the reboiler was set to a value of 1.8 bara [86, 94]. According to the literature, at temperatures higher than 120°C, solvent degradation often occurs [45].

Although chemical absorption via MEA has shown to be a promising technology, the main disadvantage involved in the process application is the thermal energy requirement for stripping the CO_2 from the solvent [181]. To provide the reboiler with high temperature heat to supplement with the amine regeneration process, some hot steam from the steam turbine is required. To supply this hot steam, a fraction of the steam entering the LP turbine is extracted after leaving the IP steam turbine section and redirected to the reboiler. Researchers, such as Luo et al., [182], have suggested a similar set-up for the steam draw off from the IP/LP turbine crossover. The saturated steam exiting the reboiler is sent back into the steam cycle via the condenser [94]. Removing a fraction of the steam from the LP turbine leads to a reduction in the power generated by the steam turbines, furthermore reducing the overall net plant efficiency when the CO_2 capture plant is retrofitted into the system. The lean solvent (stripped of CO_2) leaves the reboiler and flows into the cross heat exchanger as shown in Figure 7.2 for the heat recovery [120, 183]. The cross heat exchanger uses the heat obtained from the lean solvent to pre-heat the rich solvent entering the stripper column, hence, reducing the solvent regeneration heat requirement in the reboiler [183].

The lean solvent is further passed through a lean amine cooler to further cool it before being fed into the absorber column. This is because the absorption process is favoured

by low temperature [183], hence the temperature of the lean amine is designed to match the temperature of the flue gas entering the absorber.

As mentioned earlier in this Chapter, the CO_2 capture plant was developed based on the hydrodynamic parameters (effective inter-facial area available for the mass transfer, pressure drop, liquid hold-up and gas and liquid mass transfer coefficients) [184], as well as some operational parameters (solvent concentration and lean solvent loading). In generating the model, the optimum heights and diameters of the absorber and stripper columns were determined using these parameters at a chosen solvent and packing type [118].

The packing type is essential in providing increased time for solvent-gas (liquid-gas) interaction throughout the CO_2 absorption process [174]. The packing type used in this process model was the structured packing Mellapak 250 Y, characterised by its specific surface area of $250m^2/m^3$ and a 45° angle of orientation to the vertical axis [185, 186]. This packing type was chosen because of its high efficiency and low pressure drop. Using the Billet and Schultes correlation [187], the mass transfer coefficients used to calculate the hydrodynamic parameters are calculated.

For an optimized design of the system, a two absorber and one stripper column design was implemented. This design was generated based on the column cost and the heat requirement associated with the capture system [188]. Therefore, the minimum number of columns required to obtain a balance between high capital and operating cost and a low heat requirement in the system was implemented. Using two absorber columns also provide greater operational flexibility when operating with flexible fuel scenarios [162]. Furthermore, researchers such as Olaleye et al., [189], have suggested using more than one absorber column could improve the turndown ratio in processing large volumes of flue gas from the power plant. To reduce computational complexities as well as time when modelling the two absorber columns for the CO_2 capture plant, a multiplier is used as shown in the flowsheet in Figure 7.2. This halves the flow parameters into the absorber column and doubles these flow parameters at the absorber exit, hence depicting a two-absorber absorption process.

The operating region of the packed columns is determined by the maximum pressure drop tolerated in the column and the maximum flooding velocity of the column [86, 118]. When the column reaches this flooding point, there is a noticed pressure drop increase. This is as a result of the increase in flue gas flowrate, which restricts the downward flow of the solvent [188]. At this point, the wetted packing surface area is reduced, thus affecting the operation of the columns [188]. At higher flue gas flowrates entering the absorber, the columns become more liable to extend past the flooding point and becoming inoperable.

From the literature, it was observed that operating at 80% flooding ratio provided the best performance of the columns [86, 93 and 94]. The prediction of the flooding ratio is principal in the determination of the absorber and column diameters [190]. The determined diameter of the absorber and stripper columns are 16.32m and 8.90 m, respectively, for the CCGT with CO_2 capture plant scenario for different fuel compositions. However, as two CCGT configurations are investigated, the diameter of the absorber and stripper columns are 14m and 9.0m, respectively, for the CCGT at 35% EGR with a CO_2 capture plant scenario.

With increase in packing height, there is an increase in mass transfer area, which improves the absorption of CO_2 [159]. However, from the literature, at heights higher than 18m, the increase in efficiency of the capture plant is negligible and the high cost associated with tall absorbers in not economically feasible [159]. By adjusting the height of the absorber and stripper columns manually, the CO_2 capture efficiency and specific reboiler duty change respectively. For the base case scenario, the height of the absorber and stripper columns were adjusted until a CO_2 capture efficiency of 90% was achieved in the absorber column and a reduction in specific reboiler duty of less than 1% was observed in the stripper section, which was considered negligible. The determined packing height of the absorber column was 17.10 m and for the stripper column it was 30.27 m. However, the heights of the absorber and stripper columns are 19.5 and 30.1m, respectively, for the CCGT at 35% EGR with a CO_2 capture plant scenario.

Table 7.2

Main assumptions for the base case CO_2 capture plant [165].

Assumptions	
CO_2 capture efficiency (%)	*90*
Column packing type	*Mellapak250 Y*
MEA concentration in the solvent (wt%)	*30*
Number of Absorbers	*2*
Number of Strippers	*1*
Solvent lean loading (mol CO_2 /mol MEA)	*0.2*
Flue gas temperature at absorber inlet (°C)	*40*
Flue gas pressure at absorber inlet (bara)	*1.13*
Cross heat exchanger pressure drop (bara)	*0.1*
Cross heat exchanger hot outlet approach (°C)	*10*
Rich amine pump pressure (bara)	*3*
Lean amine pump pressure (bara)	*3*
Pump efficiency (%)	*75*
Stripper condenser pressure (bara)	*1.62*
Reboiler temperature (°C)	*120*
Reboiler pressure (bara)	*1.8*

The ACP was modelled to operate with optimum performance. To do this, some assumptions were adapted in the model as shown in Table 7.2. For all scenarios modelled, the flowrate of CO_2 being emitted from the top of the absorber was kept constant. This was to ensure consistent analysis in the chapter, whereby the power plants are expected to produce constant low CO_2 emission gases. However, this leads to drastic changes in the performance of the capture plant.

To reduce the high thermal energy requirement of the CO_2 capture plant, the CO_2 concentrations in the flue gas in increased by recycling a fraction of the exhaust gas to the compressor inlet, in the process of EGR [45].

EGR increases the economic viability of the CO_2 capture process by increasing the CO_2 concentration of the flue gas entering the absorber column and reducing the flowrate of the flue gas entering the CO_2 capture plant [72]. This also allows for a decrease in cost for the CO_2 capture plant as the volumetric flowrate of the flue gas is decreased [191]. With the introduction of EG R in the CCGT, the gas turbine power output reduces slightly from 420.82 MWe to 418.56 MWe, due to an increase in the temperature of the gas entering the compressor inlet [93]. This causes an increase in work done by the compressor and a slight decrease in mass flowrate at the compressor suction [45].

As mentioned earlier in this Chapter, the limiting ratio in the EGR is controlled by combustion-related effects such as flame stability [191]. This is because increasing the EGR ratio reduces the level of oxygen available in the air for combustion, although a decrease in the oxygen level in the CCGT has the potential to reduce the oxidative degradation of the amine in the CO_2 capture plant [94]. For this reason, publications such as Diego et al., [93, 94] and Adams et al., [87], have suggested the use of maximum EGR ratios of 35 - 40%. In this study, 35% of the exhaust gas was recycled into the inlet of the compressor via a condenser and a blower (fan) as shown in Figure 7.3. This was following the suggestion in the 2013 DOE/NETL report [165]. The function of the condenser and blower is to boost the pressure of the recycle stream to match the inlet pressure of the air in the compressor inlet.

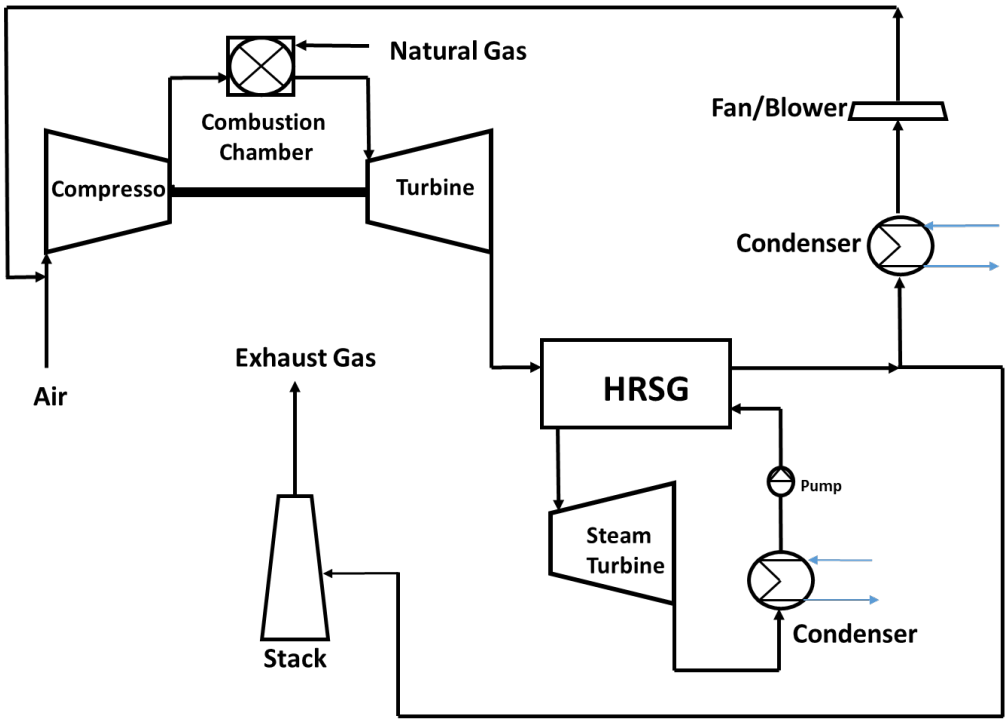

Figure 7.3: CCGT with EGR flowsheet.

7.3. Economics methodology

Using the economic methodology flow diagram as shown in Figure 7.4, the economic analysis process is carried out in this study. Using the plant from the 2013 DOE/NETL report as the reference plant, as well as the economic assumptions in Table 7.3 and scaling parameters in Table 7.4, the TPC is determined as well as the operating cost of the plant. This parameter is then utilized in estimating the COE and COA for different operating plant scenarios (different fuel compositions). The economic study in this chapter makes use of the capital Scaling Methodology [166], explained earlier.

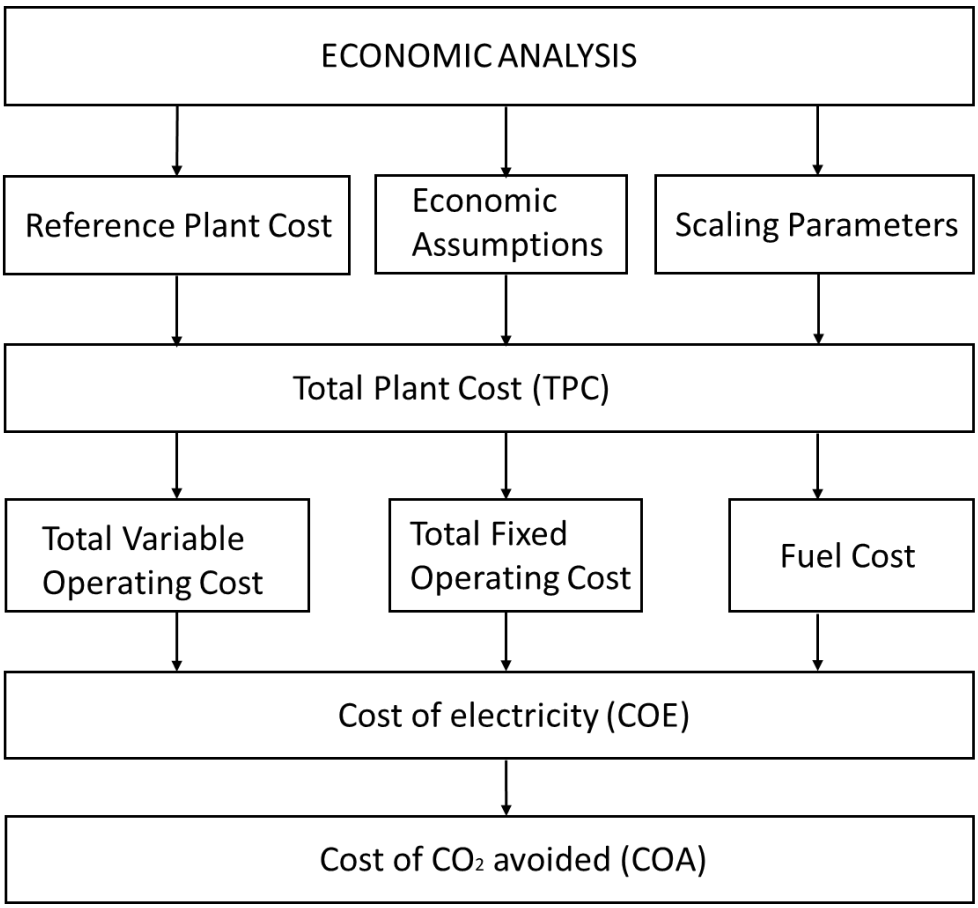

Figure 7.4: Flow diagram of the economic methodology.

The capital costs for the reference CCGT and ACP are obtained from the data reported in the DOE/NETL report [165]. Using these values, the capital cost for the fuel flexibility model and the EGR model including the ACP are scaled. The location of the reference plant is the US Gulf Coast, the reference year of the study is 2011 and the currency being used in the analysis is the United States Dollar (USD).

In general, the most implemented characteristic used in defining different power plants is the cost of electricity (COE). Moreover, considering the power plants retrofitting with CCS, the evaluation in this study includes the estimation of carbon management cost with the cost of CO_2 avoided (COA) [93]. The COE is determined by [165]:

$$COE = \frac{(CCF)(TOC) + OC_{FIX} + (OC_{VAR}) + FC}{(CF)(MWh)} \quad (7.1)$$

where CCF is the capital charge factor, TOC is the total overnight cost, OC_{FIX} is the sum of fixed annual operating costs, CF is the capacity factor, OC_{VAR}, is the sum of the variable annual operating cost, FC is the fuel cost for one operating year and MWh is the annual net megawatt-hours of power generated at 100% capacity.

The cost of CO_2 avoided is determined by [165]:

$$COA = \frac{(COE_{CCS} - COE_{ref})}{(Emission_{ref} - Emissions_{CCS})} \tag{7.2}$$

Where COE_{CCS} and COE_{ref} are the cost of electricity with and without CO_2 capture, respectively. $Emissions_{ref}$ and $Emissions_{CCS}$ are the CO_2 emission rate with and without CO_2 capture, respectively.

Table 7.3

Economic assumptions employed [93, 165].

Parameters	Value	Unit
Capacity factor	85	%
Capital charge factor with CCS	11.1	%
Total as spent cost factor	107.8	%
CO_2 transport and storage cost over 100km	10	\$/tonne CO_2
Plant Operational period	30	Years
Cost year	2018	-
Labour rate	39.70	\$/hour
Labour per shift	6.3	-
Shifts per day	3	-

The economic assumptions employed, as shown in Table 7.3, were determined from the 2013 DOE/NETL report [165] as well as the literature where a similar system was modelled.

7.3.1. Capital Cost

The key assumption in the process is the constant CCGT and CO_2 capture plant when operating with different fuel compositions. However, with EGR modifications to the CCGT, the CO_2 capture plant is re-sized. The main parameter in calculating the COE is the TOC (Total Overnight Cost), which is calculated form the TPC (Total Plant Cost). Estimation of the capital cost for each major component is derived from the 2013 DOE/NETL report [165] as the reference case as follows:

$$SC = RC \left[\frac{SP}{RP}\right]^{n} \tag{7.3}$$

where SP is the scaling parameter, RP is the reference parameter, RC is the reference cost, SC is the scaled cost and n is the scaling exponent. In addition, all costs are adjusted to 2018 USD by utilising the Chemical Engineering Plant Cost Indices (CEPCI).

The reference capital cost of the plant are obtained from the reference plant in the DOE/NETL report [165]. Using the scaled cost equation as shown in Equation (7.3) [94, 166], the estimated scaled cost of the modelled plant is derived. The scaling parameters and exponents for each plant component used are shown in Table 7.4. For both the CCGT and 35% EGR scenarios, the same scaling exponents were implemented when required. This was to ensure an unbiased comparative analysis on the operation of the system.

Table 7.4

Scaling parameters used in the estimation of capital costs in this work [166].

Plant Component	Scaling parameter	Scaling Exponent
Feed water System and Miscellaneous	Feed water flowrate (HP only)	0.72
CO_2 removal	CO_2 flowrate at absorber inlet	0.61
Exhaust Gas Recycle	Exhaust gas flowrate	1.47
CO_2 compression	CO_2 flowrate	0.77
HRSG, Ducting and Stack	HRSG Duty	0.7
Steam Turbine System	Steam Turbine Power	0.8
Cooling Water System	Cooling tower duty	0.71
Instrumentation and Control	Net Auxiliary Power	0.6
Improvements to Site	Gross Total	0.47
Accessory Electric Plant	Net Auxiliary Power	0.6
Buildings and Structures	Gross Total	0.34

The scaling parameters are derived from the operational data within the gCCS model whereas the reference parameters are obtained from the 2013 DOE/NETL report [165]. Adding up the scaled costs for each plant component gives the total plant cost (TPC).

Table 7.5

Other costs employed for estimating the Total Overnight Cost (TOC) [165].

Cost component	Estimate Basis
A. Equipment cost	As shown in Table 7.4
B. TPC	Sum of Scaled Cost in table 7.4
C. Total preproduction cost	
	6 Month of all labour cost
	1 month maintenance materials at 100% CF
	1 month non-fuel consumables at 100% CF
	0.25 of 1 months fuel at 100% CF
	Miscellaneous (0.02 of TPC)
D. Total Working & Inventory capital	
	60 day supply of consumables at 100% CF
	0.005 of TPC (spare parts)
E. Initial cost for catalysts & chemicals	$1,383,000
F. Land	$300,000
G. Other owners cost	15% of TPC
H. Financing cost	2.7% TPC
Total Overnight Cost (TOC)	Sum of A, B, C, D, E, F, G, H

In calculating the TOC, the TPC is considered as well as other costs which are shown in Table 7.5. The other costs mostly constitute constants, such as land and estimates from the TPC. The basis of the estimations used in determining these costs are also highlighted in Table 7.5.

7.3.2. Operating Cost

As shown in Equations (7.1) and (7.2), the COE is calculated from the TOC, OC_{FIX} and OC_{VAR}, and the COA is calculated from the COE. In calculating the OC_{FIX} and OC_{VAR}. However, there are other operating and maintenance (O & M) costs to be considered which are tabulated in Table 7.6. The estimation method is further explained in [167]. Using the estimation method highlighted in Table 7.6, the O & M cost were calculated for the system.

Table 7.6

Estimation method for O &M and labour costs [167].

Operating and Maintenance Cost (O & M)	
Cost	**Estimate Basis**
Variable Operating Cost (OC_{VAR})	Maintenance material cost (1.3% TPC CF)
	Non-fuel consumables (1.5 Maintenance material cost – 1.3% TPC CF)
Fixed Operating Cost (OC_{FIX})	Property taxes and Insurance (0.02 TPC)
	Operating labour rate ($347772/yr)
	Operating Labour Burden (0.3 Operating Labour Rate)
	Operators per shift (6.3)
	Number of shifts (4)
	Annual Operating Labour Cost (Operating labour rate x Operating Labour Burden x Operators per shift x Number of shifts)
	Maintenance Labour Cost (2/3 Maintenance Labour Cost)
	Admin and Support Labour (0.25 Sum of other labour cost)
Fuel Cost (FC)	5.81 $/GJ HHV

7.4. Base case Analysis

The base case model of the CCGT was validated against the data obtained from the CCGT in the 2013 DOE/NETL report [165]. As shown in Table 7.7, with similar input data, there appears to be a correlation in most of the output data extracted.

Table 7.7

Inputs and base case results for the stand alone CCGT and with CO_2 capture.

CCGT	**2013 DOE/NETL [165]**	**gCCS Model**
	Input	
Natural Gas flowrate (kg/s)	23.38	23.38
Gas turbine Power (MWe)	420.82	420.82
	Output	
Air flowrate (kg/s)	*1006.34*	*1006.32*
Steam turbine Power (MWe)	*229.61*	*229.59*
Total Gross Power Output (MWe)	*650.42*	*650.41*
Power plant auxiliaries (MWe)	*16.53*	*15.81*
Total Net Power Output (MWe)	*633.89*	*634.60*
Net power plant efficiency (%)	*57.4*	*57.51*
CCGT with CO_2 capture plant	**2013 DOE/NETL [153]**	**gCCS Model**
Steam turbine Power (MWe)	*185.50*	*176.06*
Total Gross Power Output (MWe)	*606.32*	*596.88*
Power plant auxiliaries (MWe)	*53.5*	*49.95*
Total Net Power Output (MWe)	*552.82*	*546.92*
Net power plant efficiency (%)	*50.1*	*49.56*

As shown in Table 7.7, there is agreement in the results extracted from the gCCS model when compared to the 2013 DOE/NETL report [165]. Although there are a few expected

discrepancies in the output data such as the plant auxiliary power. However, the values reported in Table 7.7 are all within a 5% of the DOE/NETL reference report.

When coupling the CCGT to the CO_2 capture plant, there is an observed decrease in steam turbine power and total power output (gross and net), thereby reducing the net power plant efficiency, as shown in Table 7.7. There is also a notable increase in power plant auxiliary power. The decrease in steam turbine power is due to the extraction of steam from the IP/LP crossover from the steam turbine section. The reduction in steam turbine power causes the total power output to decrease. Regarding the increase in auxiliary power, this occurs due to the inclusion of more components in the system for the CO_2 capture, such as the CO_2 auxiliary pumps and the CO_2 compression turbine. This leads to an increase in energy requirement and hence an increase in auxiliary power.

As expected, the results highlight that coupling the CCGT with the CO_2 capture plant leads to major deviations in the results when compared to the 2013 DOE/NETL report. This is because the CO_2 capture plant modeled in gCCS are not similar in dimensions and performance to the CO_2 capture plant in the DOE/NETL report [165] and other publications using a similar system. It is also important to note that the 2013 DOE/NETL uses an advanced solvent process which is different from the solvent used in the CO_2 capture plant gCCS model. This reduces the regeneration energy requirements in the reboiler, hence an expected difference in performance in CO_2 capture [93].

As highlighted in Table 7.7, the steam turbine power and total power output is lower in the gCCS model when compared to the 2013 DOE/NETL report. This is because of the reduced energy requirements in the reboiler in the DOE/NETL report, hence there is less steam required and less steam drawn off from the steam turbine section to the reboiler. Also, the dimensions of the columns in the gCCS model was intentionally increased to account for an increase in mass transfer and packing area in the columns, which is necessary when operating with higher CO_2 content in the flue gas with an acceptable CO_2 capture performance such as a low reboiler duty and high capture efficiency. This leads to an increase in the steam drawn off from the steam turbine section. Hence, a lower steam turbine power output.

7.5. CCGT Fuel Flexibility

As mentioned earlier in this Chapter, the focus of this study is the performance of a CCGT coupled to a CO_2 capture plant when operating with high CO_2 content fuels (fuel flexibility). The compositions of the various fuels investigated are tabulated in Table 7.8, with the concentration of CO_2 in the fuel always expressed in molar percentage. The CO_2 content in the fuel is increased from 1 mol% (natural gas CO_2 content in DOE/NETL report [165]) to a maximum of 10 mol%. As mentioned earlier in Section 7.1, the maximum CO_2 concentration investigated in the CCGT is 10 mol%. This study provided insight into the limitations in operating a CCGT and capture plant, with various amount of permissible CO_2 in the fuel.

Table 7.8

Fuel compositions for the different fuels used in the fuel flexibility study.

	Natural Gas	**5% CO_2**	**7.5% CO_2**	**10% CO_2**
Methane (mol %)	93.1	89.3	86.9	84.6
Ethane (mol %)	3.2	3.1	3	2.9
Propane (mol %)	0.7	0.7	0.7	0.6
Butane (mol %)	0.4	0.4	0.4	0.4
Nitrogen (mol %)	1.6	1.5	1.5	1.5
Carbon dioxide (mol %)	1	5	7.5	10
Lower Heating value (MJ/kg)	47.20	42.60	40.00	37.60

7.5.1. Technical Study

The performance of the CCGT with the CO_2 capture plant is analyzed, with a strong focus on the power output and efficiency of the system.

Table 7.9

Results with the use of various fuel compositions in the CCGT with CO_2 capture.

Parameters	**Natural Gas**	**5% CO_2**	**7.5% CO_2**	**10% CO_2**
Fuel flowrate (kg/s)	23.38	25.88	27.55	29.32
Gas turbine power output (MWe)	420.82	420.82	420.82	420.82
Steam turbine power output (MWe)	176.06	174.43	173.45	172.49
Total gross power output (MWe)	596.88	595.25	594.27	593.30
Auxiliary power (MWe)	49.95	50.45	50.73	50.99
Total net power plant output (MWe)	546.92	544.80	543.54	542.32
Net power plant efficiency [LHV] (%)	49.56	49.42	49.32	49.20
Turbine Inlet temperature (°C)	1271	1268	1267	1265
Turbine Outlet temperature (°C)	606.63	605.37	604.53	603.65
Flue gas temperature (°C)	93.19	87.76	84.56s	84.51
CO_2 capture rate (%)	90	90.4	90.6	90.8
O_2 concentration in flue gas (mol %)	12.37	12.36	12.33	12.3
CO_2 concentration in flue gas (mol %)	3.91	4.06	4.15	4.26
Flue gas flowrate (kg/s)	1029.7	1032.2	1033.89	1035.66
Solvent rich loading (mol CO_2 /mol MEA)	0.471	0.472	0.473	0.474

As shown in Table 7.8, with an increase in CO_2 content in the fuel, the lower heating value (LHV) reduces. This is because the heating value of CO_2 is zero [192], hence the CO_2 inhibits the combustion reaction. This leads to a reduction in the fuel LHV.

As mentioned earlier in Section 7.2, the gas turbine power output was maintained at a constant value of 420.82 MWe. As a result, using a higher CO_2 content fuel leads to an increased consumption in natural gas in order to produce the same amount of power output [192]. This is because the fuel consumption is a function of the fuel flowrate and heating value. Hence, the fuel flowrate increases with an increase in CO_2 content in the fuel as shown in Table 7.9. As a result, the flue gas flowrate also increases. With higher CO_2 content fuels, the turbine temperatures, Turbine Outlet Temperature (TOT) and Turbine Inlet Temperature (TIT) noticeably reduce. This occurs due to the reduction in the air-fuel ratio. Hence, there is an expected increase in excess air in the combustion chamber. However, in the model, the excess air remains constant for an increase in CO_2 content in the fuel, thus causing a decrease in the temperature of the gas exiting the combustion, which is the TIT and thereby reducing the TOT.

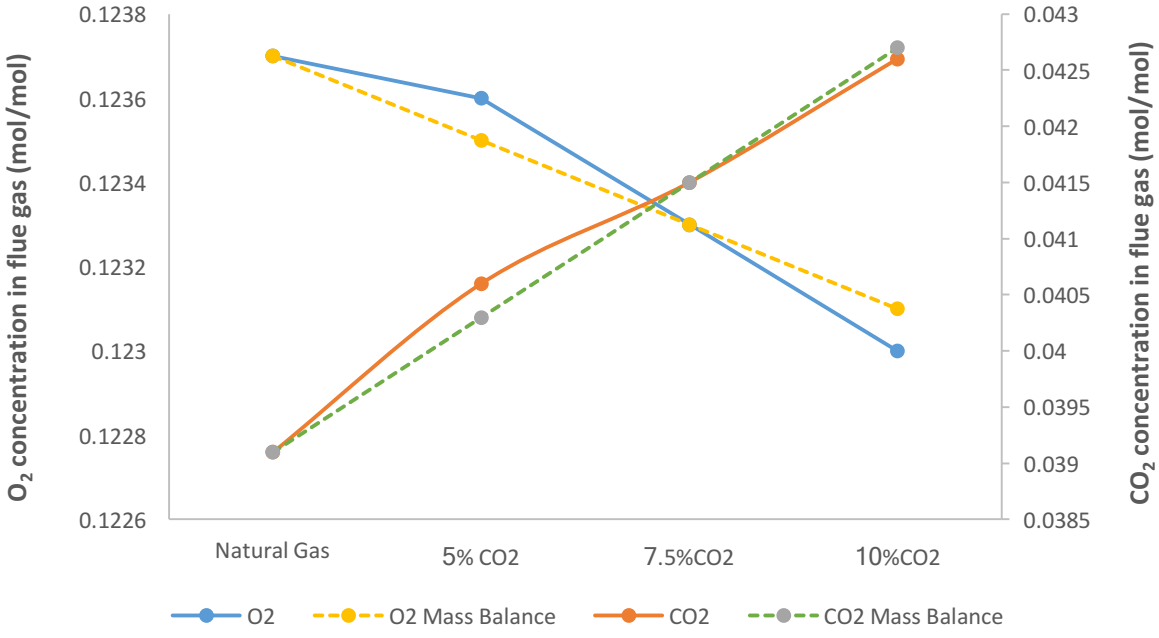

Figure 7.5: Relationship between the O_2 and CO_2 in the CCGT flue gas.

The different fuel compositions simulated create a downstream effect on the composition of the exhaust flue gas leaving the HRSG and entering the CO_2 capture plant. As shown in Figure 7.5, the O_2 in the flue gas decreases as the CO_2 increases. This is because of the increased CO_2 content in the combustion chamber, therefore, some CO_2 flows straight through the turbines. A mass balance was carried out to determine the O_2 and CO_2 concentrations in the CCGT flue gas and this was compared to the concentrations obtained from the gCCS model. As seen in Figure 7.5, they both follow similar trends, hence validating the reliability of the model.

When the CO_2 capture plant is coupled to the CCGT, the steam turbine power output reduces noticeably. This is due to the steam drawn off (as mentioned earlier in Section 7.2) from the steam turbine section to the reboiler for solvent regeneration. As shown in Table 7.9, when operating with higher CO_2 content fuels, the steam turbine power output reduces even further. As mentioned earlier in this Section, higher CO_2 content fuels leads to decrease in TIT and TOT and thus decrease in flue gas temperature. This leads to a decrease in flue gas enthalpy, however due to increase in fuel flowrate in the CCGT, the flue gas flowrate is seen to increase as shown in Figure 7.6.

With an increase in the flue gas flowrate into the CO_2 capture plant, the thermal input into the HRSG is seen to increase, regardless of the reduction in the flue gas temperature. Also, with an increase in CO_2 content in the fuel, there is a noticeable increase in thermal consumption in the steam turbine section from the reboiler. This is due to an increase in the solvent flowrate in the capture plant and an increase in the CO_2 capture rate, as shown in Table 7.9, regardless of the increase in CO_2 partial pressures. This leads to the required thermal duty in the capture plant to increase, thus increasing the thermal consumption from the steam turbines.

With less thermal energy in the steam turbine section, there is less steam being used in the generators and as such, there is less power being generated in the steam turbine section.

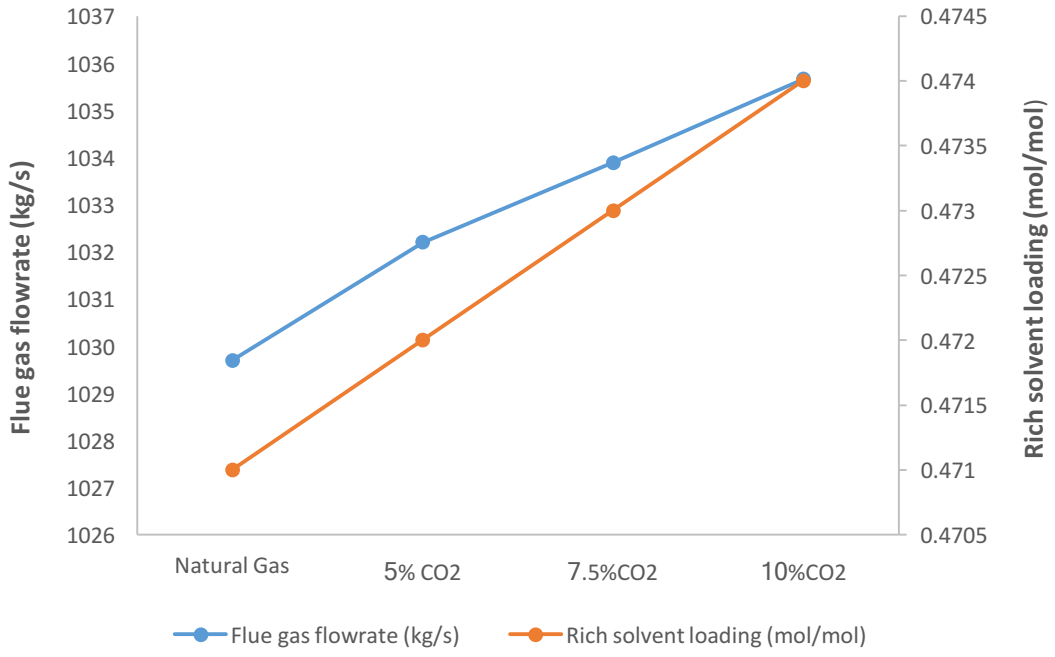

Figure 7.6: Relationship between the flue gas flowrate and the rich solvent loading in the amine capture plant.

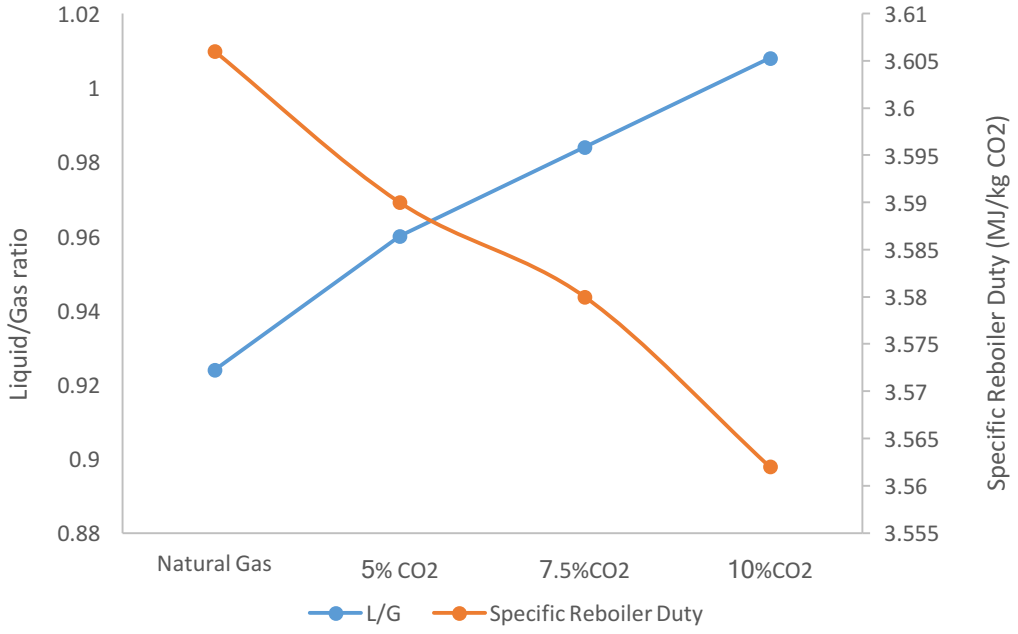

Figure 7.7: Relationship between the L/G ratio and reboiler duty in the amine capture plant.

As shown in Figure 7.6, the flue gas flowrate increases with an increase in CO_2 content in the fuel. Also, as shown in Figure 7.6, the rich solvent loading increases with an increase in

CO_2 content in the fuel. As mentioned earlier in Section 7.2, the lean solvent loading was maintained at a constant value of 0.2 mol CO_2/mol MEA, however, the CO_2 concentration in the flue gas, as well as the CO_2 capture rate is seen to increase. This leads to an increase in CO_2 being absorbed by the solvent in the absorber and thus the increase in CO_2 loading in the rich solvent.

An important parameter in analysing the techno-economic performance of the capture plant is the Liquid/Gas (L/G) ratio. As shown in Figure 7.7, the L/G ratio increases with the increase in the fuel CO_2 concentration. The increase in the L/G ratio is due to the increase in the flue gas flowrate as shown in Figure 7.6. This leads to an increase in the solvent flowrate required for CO_2 absorption. However, the regeneration energy required per kg of CO_2 (specific reboiler duty) decreases due to more CO_2 being present in the rich solvent, hence CO_2 being stripped more efficiently.

Another important parameter in analysing the techno-economic performance of the capture plant is the specific reboiler duty [183]. The specific reboiler duty is very sensitive to the solvent flowrate [159]. The relationship between the L/G ratio and the specific reboiler duty is shown in Figure 7.7. As the L/G ratio increases, the specific reboiler duty decreases with an increase in CO_2 content in the fuel and CO_2 concentration in the flue gas. This observation has been validated in the literature by Cifre et al. [159] and Akram et al. [120]. This is because the reboiler requires less energy to strip the CO_2 from the rich solvent.

As the L/G ratio increases, the flooding velocity increases. However, the optimum operating condition is at a flooding ratio of 80%. A further increase in the L/G ratio will lead to the column going beyond its flooding point. This will cause unstable CO_2 absorption in the capture plant. Also, there will be observed a rapid increase in the pressure drop in the column, the liquid carryover from the top of the column and instability in the column [185].

7.5.2. Economic study

In the economic study, the TPC and TOC were assumed to be constant for varying increases in CO_2 content in the fuel. This was to focus the study on the operational performance of the CCGT and ACP systems, thus removing any bias which could occur as a result of plant modifications to improve plant performance. Maintaining a constant TPC and TOC removes any bias in analysing the capital costs involved in the operation of the CCGT and ACP with different fuel compositions.

However, the COE and COA are affected by almost 10% when compared to the natural gas case, which is due to the cost of transport and storage for the CO_2. When operating with higher CO_2 content fuels, the amount of CO_2 leaving the CCGT will increase as well as the amount of CO_2 being captured.

Table 7.10

Results of the costing analysis (x$1000).

	Reference case	**Natural Gas**	**5% CO_2**	**7.5% CO_2**	**10% CO_2**
Total Plant Cost ($)	**758709**	**751765**	**751765**	**751765**	**751765**
Other costs ($)	166763	165274	165274	165274	165274
Total Overnight Cost ($)	**925472**	**917039**	**917039**	**917039**	**917039**
Operation and Maintenance Cost ($/y)	229115	228846	228846	228846	228846
CO_2 Transport and Storage ($/MWh)	**3.65**	**3.65**	**3.82**	**3.93**	**4.05**
COE ($/MWh) [with CO_2 T&S]	**84.27**	**83.98**	**84.15**	**84.26**	**84.37**
COA ($/tonne CO_2)	**86.59**	**85.85**	**82.63**	**80.62**	**78.60**

The results shown in Table 7.10 highlight the difference in TPC between the models developed in the gCCS and the reference case in the 2013 DOE/NETL report. The differences observed in the TPC are due to the different sizing and the different solvent used in the CO_2 capture plant in the gCCS model when compared to the 2013 DOE/NETL report. The TOC is expected to also be constant as the TOC is a function of the TPC as explained in Section 7.3 (Table 7.5).

Most of the variations that occur in the results in Table 7.10 are in the cooling systems, such as the cooling towers and connecting the steam turbines to the capture plant. As seen in Table 7.10, most of the parameters used for the cost analysis are constant for varying the increase in the CO_2 content in the fuel.

As shown in Table 7.10, operating with high CO_2 content fuels leads to an increase in the COE and a decrease in the COA. This is mainly due to the expected increase in CO_2 transport and storage cost shown in Table 7.10, which is a function of the flowrate of the condensed CO_2 exiting the stripper column for compression and storage.

The COA, which is costed per unit of CO_2 captured, reduces as the partial pressures of CO_2 within the flue gas increases. This leads to the capture plant's efficiency per unit of CO_2 increasing, hence, it becomes cheaper to avoid the emissions.

The use of fuels with high CO_2 content will incur higher COE prices, however this is marginally offset by the increase in the capture efficiency of the CO_2 capture plant, which makes CCS more applicable when fuel flexibility is desirable. Also, due to the observed approach of the amine solvent to flooding point in the columns, CO_2 concentrations in the fuel higher than 10% will result in the capture plant failing. To counter this, when operating with CO_2 content fuels higher than 10 mol%, a taller absorber and stripper column will be necessary to increase the residence time in the columns and also ensure that the appropriate capture efficiency is achieved.

7.6. EGR Fuel Flexibility

The second study in this chapter investigates the effect of fuel flexibility on EGR. In this study a similar variation in fuel composition, as shown in Table 7.8, is employed within a

CCGT modified with a 35% EGR ratio and coupled to the CO_2 capture plant. As mentioned in Section 7.1, 35% of the flue gas is redirected to the inlet of the compressor, whilst the remaining 65% is sent to the CO_2 capture plant for CO_2 capture. The required modifications to the CCGT for EGR are highlighted in Section 7.2 as well as the dimensions and operation of the capture plant coupled to the system.

7.6.1. Technical Study

With the introduction of EGR to the CCGT, the gas turbine power output is lower (as explained earlier in Section 7.2). However, the steam turbine power output is higher, hence increasing the gross power output. This is because with EGR there is more steam available in the steam turbine for generating power. This occurs due to the lower energy requirements of the CO_2 capture plant as a result of the decrease in the flowrate of the flue gas being stripped as well as the increase in CO_2 concentration of the flue gas [93].

Following a similar procedure as the CCGT fuel flexibility study in Section 7.5, the gas turbine power output was maintained at a constant value of 418.56 MWe. As shown in Table 7.11, the fuel flowrate increases with CO_2 content in the fuel, and this is due to the reduction in LHV. The TIT, TOT and steam turbine power output also follow a similar pattern as the CCGT fuel flexibility study. Furthermore, the CO_2 capture rate increases with an increase in the CO_2 content in the fuel. However, as shown in Table 7.11, the temperatures associated with the CCGT and with the EGR study are lower than the CCGT without EGR. This includes the TIT and the TOT. This is due to the increased presence of CO_2 in the working fluid that reduces the LHV and thus inhibits the combustion reaction in the combustion chamber as stated earlier in Section 7.5. The TOT entering the HRSG is lower with EGR, however, the flue gas temperature exiting the HRSG is higher in the CCGT with EGR when compared to the CCGT without EGR.

Table 7.11

Results with the use of various fuel compositions in the 35% EGR CCGT with CO_2 capture.

Parameters	**Natural Gas**	**5% CO_2**	**7.5% CO_2**	**10% CO_2**
Fuel flowrate (kg/s)	23.38	23.41	23.44	23.47
Gas turbine power output (MWe)	418.56	418.56	418.56	418.56
Steam turbine power output (MWe)	178.80	177.82	176.66	175.51
Total gross power output (MWe)	597.36	596.38	595.21	594.06
Auxiliary power (MWe)	51.00	51.21	51.43	51.65
Total net power plant output (MWe)	546.36	545.17	543.78	542.41
Net power plant efficiency [LHV] (%)	49.51	54.67	57.99	61.46
Turbine Inlet temperature (°C)	1260.89	1257.41	1255.11	1252.52
Turbine Outlet temperature (°C)	604.23	602.74	601.82	600.73
Flue gas temperature (°C)	96.72	98.42	100.16	101.85
CO_2 capture rate (%)	90	90.4	90.6	90.8
O_2 concentration in flue gas (mol %)	8.64	8.61	8.59	8.56
CO_2 concentration in flue gas (mol %)	5.99	6.21	6.35	6.50
Flue gas flowrate (kg/s)	1036.09	1041.98	1046.87	1051.96
Solvent rich loading (mol CO_2 /mol MEA)	0.481	0.482	0.483	0.483

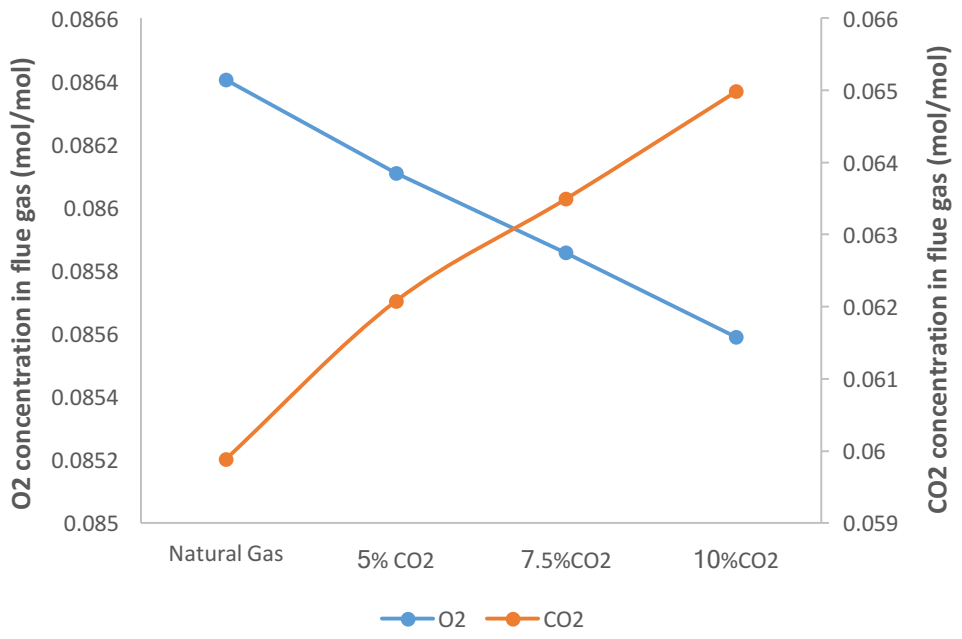

Figure 7.8: Relationship between the O_2 and CO_2 in the EGR flue gas.

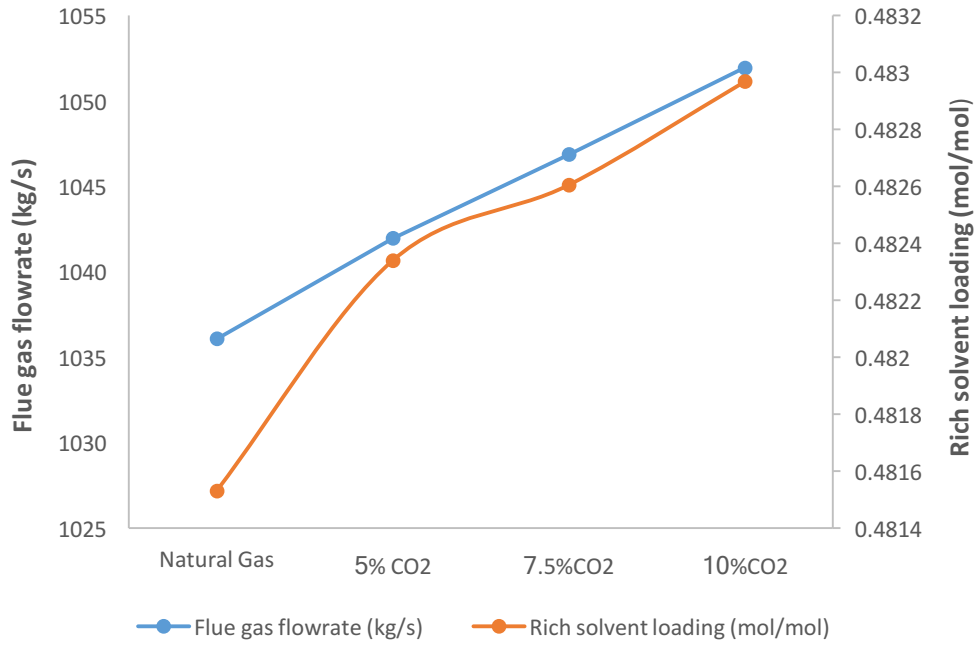

Figure 7.9: Relationship between the flue gas flowrate and the rich solvent loading in the amine capture plant.

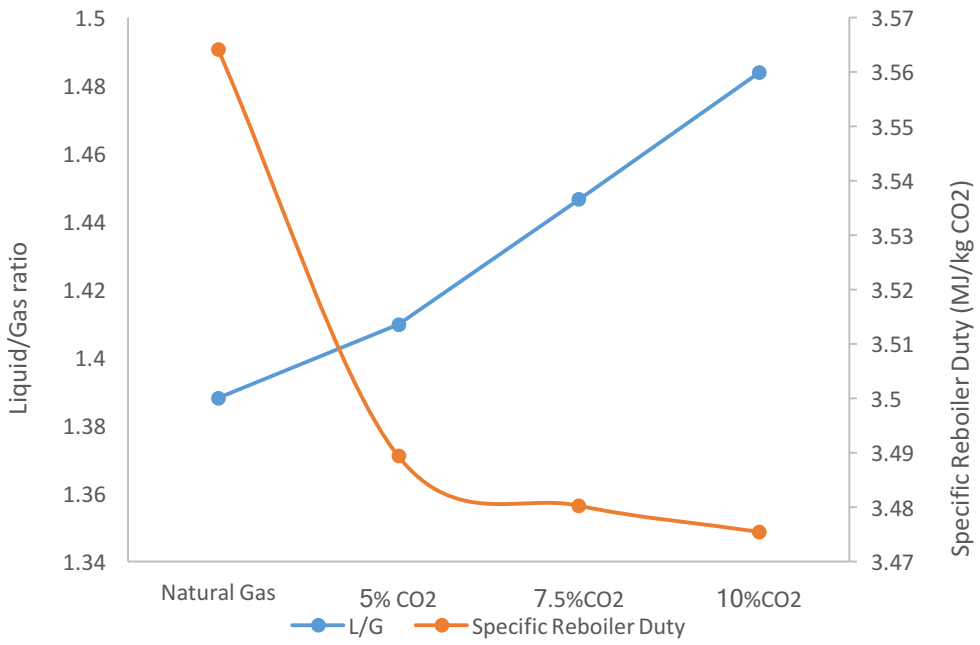

Figure 7.10: Relationship between the L/G ratio and reboiler duty in the amine capture plant.

The flue gas temperature exiting the HRSG is higher in the CCGT with EGR compared to without EGR because of the reduction in steam requirement by the capture plant from the steam turbine section. Thus, the enthalpy difference of the flue gas across the HRSG is lower.

Furthermore, the flue gas temperature exiting the HRSG is observed to increase with an increase in CO_2 content in the fuel. This occurs due to a reduction in thermal energy requirement in the HRSG. The main reason for the reduction in thermal requirement is the increase in CO_2 concentration in the flue gas. However, with an increase in CO_2 content in the fuel, the O_2 concentration in the flue gas reduces, whilst the CO_2 concentration increases by very small amounts as shown in Figure 7.8.

As shown in Figure 7.9, the rich solvent loading increases when operating with higher CO_2 content fuels. This is due to the increase in CO_2 content in the flue gas. With a constant lean solvent loading, higher CO_2 concentration in the flue gas and higher CO_2 capture rate, the rich solvent loading is expected to increase. As shown in Figure 7.9, there is a noticeably large increase in rich loading when the CO_2 concentration in the fuel increases from 1 mol% to 5 mol% CO_2, as a result of the increased absorption reactions in the

absorber column, due to larger amounts of CO_2 being introduced into the absorber column. This in turn affects the specific reboiler duty in the system, as there is large drop in specific reboiler duty when the CO_2 concentration in the fuel increases from 1 mol% to 5 mol% CO_2 as shown in Figure 7.10.

As shown in Figure 7.10, the L/G ratio increases when operating with higher CO_2 content fuels in a similar way as the CCGT fuel flexibility study, with the specific reboiler duty reducing. This is due to the increase in the flue gas flowrate and the increase in the flue gas CO_2 concentration. This leads to an increase in the solvent flowrate to maintain an appropriate CO_2 capture rate. Hence, the stripper requires less energy to strip the CO_2 rich solvent.

7.6.2. Economic study

In this economic study, the TPC and TOC were maintained at a constant value. Earlier stated in Section 7.5.2, the most important parameter contributing to the COE and COA is the cost of the CO_2 transport and storage, which is determined from the flowrate of the condensed CO_2 stripped from the flue gas and sent for compression and drying.

Table 7.12

Results of the costing analysis (x$1000).

	Natural Gas	**5% CO_2**	**7.5% CO_2**	**10% CO_2**
Total Plant Cost ($)	**722148**	**722148**	**722148**	**722148**
Other costs ($)	159464	159464	159464	159464
Total Overnight Cost ($)	**881612**	**881612**	**881612**	**881612**
Operation and Maintenance Cost ($/y)	228884	228884	228884	228884
CO_2 Transport and Storage ($/MWh)	**3.73**	**3.84**	**3.95**	**4.08**
COE ($/MWh) [with CO_2 T&S]	**83.11**	**83.21**	**83.33**	**83.46**
COA ($/tonne CO_2)	**83.06**	**79.73**	**77.85**	**75.97**

As shown in Table 7.12, the results show the TPC and TOC of the CCGT coupled with a CO_2 capture plant is more than the TPC and TOC in the CCGT modified with 35% EGR with a CO_2 capture plant. Although, there is a noticeable increase in cost associated with the cooling tower and additional equipment required in the exhaust gas recycle stream, however, this increased cost do not offset the cost savings as a result of the reduced volume of the absorber and stripper columns in the capture plant, as well as the improved performance of the capture plant as shown by the large decrease in specific reboiler duty. However, following the CCGT fuel flexibility methodology, the TPC and TOC are maintained at a constant value throughout this study. With the EGR integrated, there is more CO_2 being stripped in the stripper column, and as such, this incurs a higher cost for CO_2 transport and storage. However, due to the low TPC and TOC associated with EGR, the COE is lower when compared to the CCGT coupled with a capture plant. In a similar way as the CCGT fuel flexibility study, the cost of CO_2 transport and storage is seen to increase due to the increase in CO_2 content of the stripped gas. The leads to an increase in COE when operating with higher CO_2 content fuels.

The COA in this study is strongly dependent on the CO_2 emissions from the capture plant as well as the capture efficiency of the plant. With the CCGT modified with 35% EGR, the COA is lower. Furthermore, when operating with higher CO_2 content fuels in the EGR study, the COA further reduces. This is because of the increase in the capture efficiency and reduction in specific reboiler duty, hence making it cheaper to avoid the emissions.

7.7. Chapter Conclusion

This chapter provides much deeper insight into a study on the technical and economic performance of a CCGT integrated with a CO_2 capture plant. Two studies were carried, the first being a study on the impact of fuel flexibility in a CCGT coupled to a CO_2 capture plant and the second being a study on the operations of a CCGT, modified to operate at an EGR ratio of 35%, whilst coupled to a CO_2 capture plant. The models implemented in these studies were developed using the gCCS software, which is a CCS process modelling platform of the gPROMS modelling package. The CCGT model developed is validated using the 2013 DOE/NETL report as the reference case, with similar output results within an accuracy of 4.3%. However, with the integration of the CO_2 capture plant, there a larger discrepancy in output results due to differences in column dimensions and operating parameters as stated in Section 7.4.

Economically, the model illustrates that the TPC and TOC is 0.9% lower than the 2013 DOE/NETL reference case. However, the cost of CO_2 transport and storage is the same, hence there is a decrease of 0.3% in the COE from 84.27 to 83.98 $/MWh.

The first study in this chapter investigates an increase in the CO_2 content in the fuel in a CCGT, and the impact of this operation when coupled with a capture plant. The results from the CCGT show a decrease in steam turbine power, TOT and TIT. Regardless of the constant gas turbine power output for all the fuel scenarios, the gross power output of the plant was seen to decrease as well. The results from the capture plant show an expected increase in the capture efficiency and a decline in reboiler duty, whilst operating with fuels with a higher CO_2 content. This is due to the increase in CO_2 concentration in the flue gas, as such there is more CO_2 absorbed in the absorber column and the energy needed to regenerate the solvent is lower, however, the thermal consumption from the

steam turbine is higher due to the reduction in thermal input into the HRSG as shown by the decrease in TOT entering the HRSG.

With an increase in CO_2 content in the fuel, the COE increases up to 84.37 $/MWh for the 10% CO_2 concentration in the fuel. While the COA reduces from 85.85 $/tonne CO_2 in the natural gas case to 78.6 $/tonne CO_2 for the 10% CO_2 concentration in the fuel. This represents a 0.5% increase in COE and an 8% decrease in COA.

The results of the second study demonstrate the impact of 35% EGR in a CCGT coupled to a CO_2 capture plant. With the integration of EGR, there is an increase in TIT, TOT and steam turbine power output, however, the gas turbine power output is lower when compared to the 2013 DOE/NETL reference case. This occurs due to the increase in temperature of the working fluid and thus the increase in temperatures across the system. When operating with higher CO_2 content fuels, there is a decrease in steam turbine power, TIT and TOT in a similar way as the CCGT fuel flexibility study. In the EGR fuel flexibility study, the TPC and TOC reduce by 5% to M$722 and M$882 respectively, and the cost of CO_2 transport and storage is seen to increase by 2% from 3.65 $/MWh to 3.73 $/MWh. Despite the increase in additional equipment cost and increase in cooling water, the reduction in capital cost associated with the decrease in column sizing has shown to be an important factor in determining the TPC and TOC.

With higher CO_2 content fuels, the cost of transport and storage for CO_2 is seen to also increase, which leads to increase in COE. The COE increases by 0.4% from 83.11 $/MWh with natural gas to 83.46$/MWh when operating with a 10% CO_2 concentration in the fuel. However, the COA reduces by 9% from 83.06 $/tonne CO_2 to 75.97 $/tonne CO_2.

The decrease in COA in both studies indicates the lower efficiency losses in the CO_2 capture system, due to the increase of the CO_2 content in the flue gas, outweighing the negative effect associated with the increase in the cost of transport and storage for the CO_2 and the increase in COE. Hence, highlighting a trade-off associated with operating a CCGT with various CO_2 content in the fuel. Furthermore, whilst operating with high CO_2 content fuels has shown to have some benefits, it was worth noting that the limit of 10 mol% CO_2 in the fuel stated earlier in this chapter is necessary to ensure an efficient operation of the system. Also, operating with higher CO_2 content fuels increases the

flooding velocities in the absorber and stripper columns, thus pushing the columns towards the flooding point, at which point the plant will be inoperable. Beyond this point, modifications will have to be made to some components such as the combustion chamber to ensure complete combustion taking place. The heights of the absorber and stripper columns will have to be increased as well to accommodate the increasing liquid and gas flowrates.

From these studies, it can be depicted that it is economically beneficial to modify a CCGT with EGR and couple it to a CO_2 capture plant to increase the capture efficiency. This conclusion can be derived from the lower COE and COA associated with EGR when compared to the CCGT coupled to a CO_2 capture plant without EGR. When operating with higher CO_2 content fuels, the COE for the CCGT with EGR study increases at slower rate of 0.4% when compared to an increase of 0.5% in COE for the CCGT without EGR. Also, the COA decreases at a faster rate of 9% for the CCGT with EGR study compared to 8% for the CCGT without EGR study. This highlights that the implementation of EGR in a CCGT operating with higher CO_2 content fuels and coupled to a capture plant leads to lower capital cost and lower efficiency losses in the capture plant.

In this Chapter, the novelty includes; evaluating the performance of fuel flexibility via increasing the CO_2 concentration in the fuel on a commercial-scale CCGT modified with Exhaust Gas Recirculation (EGR), coupled to an amine capture plant, with techno-economic considerations.

8. Conclusion and Future work

The key issue in CCS implementation is the economic implication of the system due to its associated energy penalty which reduces its competitiveness compared to conventional fossil fuel energy generation processes. The proposed processes to overcome these issues are exhaust gas recirculation (EGR) and selective exhaust gas recirculation (S-EGR). Work from literature has shown that the performance of the CCS via chemical absorption process can be improved by CO_2 enhancement in the system Best et al., [193]. One of the advantages of S-EGR is the increase in CO_2 content in the flue gas whilst having little impact on the performance of the MGT. Further research was carried out on the impact of S-EGR on the CCS process, with the CO_2 capture plant subjected to different parameter changes such as changes in amine strength. The commercial implementation of EGR is also researched, as well as its implementation to a fuel flexibility gas turbine operation, in which the CO_2 concentration in the fuel is increased. A techno-economic analysis study was carried out for this process to determine the energy and cost savings when operating EGR with varying fuel compositions.

All research work carried out in this these involved the modelling of the afromentioned systems using process modelling software and when needed, an iterative process software (Matlab). With limited detailed modelling work carried out in this topic in the literature, this research work facilitates knowledge transfer regarding the techniques and methodology implemented in this study.

The final conclusion of the thesis involves the collation of data and analysis from the different topics being researched on. These are underlined, as well its novelty and contribution to knowledge. Future recommendations and work are also pointed out in the chapter, to create research suggestions and ideas for gas-CCS development purposes.

8.1. Selective Exhaust Gas Recirculation modelling

S-EGR process modelling of the MGT was performed using Aspen Plus. Modelling the MGT under S-EGR conditions involves the injection of CO_2 into the compressor inlet. Previous researchers such as Ali et al., [84], have come to the conclusion that the performance of the MGT with S-EGR can be easier analysed from the performance of the system by increasing the CO_2 content of the working fluid.

Characteristic maps were used to accurately analyse the effect of varying CO_2 injection flowrates on the performance of the MGT, thus producing comparable data to experiments. This process significantly increases the CO_2 concentration in the flue gas from 1.8 to 9.6 mol% while increasing the CO_2 injection flowrate from 0 to 300 kg/hr when operating at 100 kWe and also increases from 1.5 to 1.8 mol% between 60 to 100 kWe, with no CO_2 injection. The results are within a similar range to experimental data conducted by Bellas et al., [139] in literature. To perform this study, the MGT was modelled in accordance with the Tubrec T100 available at PACT, Shefffield. In developing the process model, the characteristic maps were scaled for each operating condition using Matlab and implemented in the software.

The increase in CO_2 injection flowrate changes the working fluid in the MGT and thus combustion parameters such as the air to fuel ratio, which increases with increase in CO_2 injection flowrate. Other parameters affected are the rotational speed of the shaft and the electrical efficiency of the system. There is an observed decrease of 2.4 - 6% in rotational speed with increase in CO_2 injection flowrate and a decrease of 0.3 - 12% in electrical efficiency with increase in CO_2 injection flowrate. This is as a result of the increase in density and heat capacity of the working fluid, hence affecting the work done by the compressor and consequently, the expansion being carried out in the turbine. Another parameter investigated is the recuperator effectiveness, which increases by 0.15% with increase in CO_2 injection flowrate from 0 to 300 kg/hr at a power output of 100 kWe and increase by 2.9% when decreasing the power outputs from 100 to 60 kWe with no CO_2 injection.

Under S-EGR conditions, the O_2 concentration in the combustor inlet also reduces with increase in CO_2 injection flowrate from 20.7 to 19.06 mol%, when operating at injection flowrates of 0 to 300kg/hr at 100kWe. This leads to changes in combustion characteristics such as flame speed and reaction rates of the species involved in combustion and consequently incomplete combustion, as explained earlier in Chapter 5 of the thesis. However, throughout the modelling, the O_2 concentration limit of 16 mol% recommended by literature was not reached. The decrease in O_2 concentration in the combustion chamber, also leads to a decrease in O_2 concentration in the flue gas from 17 to 15.4 mol%, when operating with a CO_2 injection flowrate of 0 to 300 kg/hr at 100kWe power output. With no CO_2 injection, the CO_2 concentration in the flue gas is observed to reduce from 17.7 to 17 mol% when increasing power outputs from 60 to 100kWe.

The variation in temperatures across the MGT is dependent on the changes in MGT performance characteristics such as the power output and in this study, the CO_2 injection flowrate, which affects the composition of the working fluid. The CDT and TIT were observed to reduce with increase in CO_2 injection flowrate and increase with increase in power output. The CDT and TIT reduces by 1.2% and 0.87% respectively, when the CO_2 injection flowrate is increased from 0 to 300 kg/hr at 100kWe power output. With no CO_2 injection, the CDT and TIT increase by 9.4% and 5.6% respectively, when increasing the power output of the MGT from 60 to 100 kWe.

In relation to the wider scope of the study, the increase in CO_2 concentration in the flue gas plays an important role in the future of CCS. As S-EGR is a widely researched method with its impact studied and analysed. Hence, the implementation of this strategy with carbon capture and storage (CCS) will aid in promoting the use of CCS in future energy generation techniques. S-EGR leads to an increase in the flue gas CO_2 concentration by 433% (in this study), which increases the capture rate in a CO_2 capture plant using amines and reduces the specific reboiler duty required for regenerating the amine. In a larger-scale system, such as a CCGT, there will be additional steam turbines used to increase the efficiency of the system. This set-up will further reduce the specific reboiler duty in the amine capture plant, as the steam can be fed to the reboiler to aid in regenerating the amine.

8.1.1. Novelty

The novelty in this Chapter include;

- Characteristic map scaling methodology and equations, developed for changes in working fluid composition and conditions in a simple gas turbine.
- The implementation of characteristic maps in modelling S-EGR in micro gas turbines via CO_2 injection.
- The influence of S-EGR on MGT performance by monitoring the rotational speed, electrical efficiency, compressor and turbine work and emissions.

8.1.2. Recommendation

The modelling of the MGT carried out in this Chapter involved an iterative process for scaling the characteristic maps, which was carried out using Matlab. This process was kept independent from the process modelling software used, and as such input data had to be copied from the process model into Matlab and vice versa for scaling purposes.

To further advance the model;

- A function should be developed to relay data between the process modelling software and Matlab.

The characteristic maps implemented in this study were acquired from the original equipment manufacturers, which were developed during start-up of the new device at baseload conditions. However, with increase in operational hours, there is observed decrease in performance of the system, due to component degradation.

To further improve the reliability of the model;

- The decrease in MGT performance should be accounted for and be considered in the model.

8.2. Pilot-scale amine capture plant with S-EGR modelling

In this study, a chemical absorption CO_2 capture pilot plant, involving the use of the amine MEA (monoethanolamine) to absorb the CO_2 from the flue gas is investigated. This process involves the capture of CO_2 whilst regenerating the amine for continuous use in the absorption process. To improve the absorption process, two absorber columns are implemented in this study. The process modelling of the capture plant was carried out using Aspen Plus, and the model is validated against experimental data obtained from a similar capture plant available at the PACT facility, Sheffield. To develop a detailed study of the capture plant, the flue gas composition and amine strength are varied.

The first parametric study involves the increase in CO_2 concentration in the flue gas whilst operating at 40 wt% MEA. This study concludes that increase in CO_2 concentration in the flue gas leads to increase in solvent flowrate, L/G ratio and CO_2 loadings, due to increase in CO_2 mass transfer in the absorber column. This leads to higher temperatures in the absorber column, thus a bigger temperature bulge. This indicates an increase in mass transfer with increase in CO_2 concentration in the flue gas. Nonetheless, the specific reboiler duty and CO_2 efficiency decrease due to the increase in driving force and decrease in CO_2 absorption capacity.

The second parametric study involves the variation in amine strength, in which the concentration of MEA was reduced from 40wt% to 30wt%. The results indicate that operating with higher concentration amines improves the absorption process due to increase in CO_2 capture efficiency, and lean and rich loadings. Furthermore, the specific reboiler duty is reduced when operating with high concentration amines, which is due to the CO_2 absorption performance and reduced required regeneration energy.

Both studies present the benefits and trade-offs associated with operating a two-absorber chemical absorption CO_2 capture plant. Operating with higher CO_2 concentration in the flue provides better operating conditions of the capture plant, which can be further improved by increasing the strength of the amine implemented.

8.2.1. Novelty

The novelty in this Chapter include;

- Modelling a two-absorber pilot-scale CO_2 capture plant with various CO_2 concentrations in the flue gas.
- Modelling a two-absorber pilot-scale CO_2 capture plant operating with different amine strengths.

8.2.2. Recommendation

In modelling the CO_2 capture plant, experimental data was used. However, due to lack of access to PACT, Sheffield, the data obtained was limited.

To further improve the reliability of the model developed;

- More experimental data points for different operating conditions such as changes in CO_2 loadings need to be investigated experimentally to further validate the model.

8.3. Economics

Performing a techno-economic study involves the technical and economic modelling of commercial-scale power plant and a CO_2 capture plant. Firstly, a combined cycle gas turbine operated by natural gas and other fuels are evaluated, followed by an exhaust gas recirculation modification and finally an integration to a MEA operated chemical absorption CO_2 capture plant. Both systems are modelled in gCCS, with the TPC and TOC in the model being 0.9% lower than the reference case, whilst the cost of CO_2 transport and storage being the same, thus leading to a 0.3% decrease in the COE, and a 0.85% decrease in COA.

In this study, the CO_2 concentration in the fuel is varied in a standalone CCGT and with a later modification with EGR, 35% of the flue gas is recycled into the compressor inlet. In both studies, the systems are integrated to a CO_2 capture plant.

The fuel flexibility study entails the variation in CO_2 concentration in the fuel. The results from this study indicate a decrease in gross power output, steam turbine power and temperature across the system with an increase in CO_2 content in the fuel, and with the integration of the CO_2 capture plant, the capture efficiency increases, whereas the reboiler duty decreases. However, the thermal consumption from the steam turbine is higher due to the reduction in thermal input into the HRSG as indicated by a decrease in temperature in the HRSG. Economically, with an increase in CO_2 content in the fuel, the COE increases up to 84.37 $/MWh for the 10% CO_2 concentration in the fuel, while the COA reduces to 78.6 $/tonne CO_2 for the 10% CO_2 concentration in the fuel. This represents a 0.5% increase in COE and an 8% decrease in COA.

In the second study, the CCGT is modified with EGR at a 35% EGR ratio. This leads to is an increase in TIT, TOT and steam turbine power output, however, the gas turbine power output is lower when compared to the 2013 DOE/NETL reference case. When operating with higher CO_2 content fuels in the CCGT with EGR, there is a decrease in steam turbine power, TIT and TOT. In the EGR fuel flexibility study, the TPC and TOC reduce by 5%, and the cost of CO_2 transport and storage is seen to increase by 2%. With higher CO_2 content fuels, the cost of transport and storage for CO_2 is seen to also increase. The causes the COE to increases by 0.4% from natural gas to 10% CO_2 in the fuel. However, this causes the COA to decrease by 9%.

The decrease in COA in both studies indicates the lower efficiency losses in the CO_2 capture system, due to the increase of the CO_2 content in the flue gas, outweighing the negative effect associated with the increase in COE and cost of transport and storage for the CO_2. Also, operating with higher CO_2 content fuels increases the flooding velocities in the absorber and stripper columns, thus pushing the columns towards the flooding point, at which point the plant will be inoperable. The heights of the absorber and stripper columns, therefore will have to be increased to accommodate the increase liquid and gas flowrates.

8.3.1. Novelty

The novelty in this Chapter include;

- Evaluating the effect of fuel flexibility via increasing the CO_2 concentration in the fuel on the performance of a commercial-scale CCGT integrated with CCS.
- Evaluating the effect of fuel flexibility via increasing the CO_2 concentration in the fuel on the techno-economics of a commercial-scale CCGT integrated with CCS.
- Evaluating the performance of fuel flexibility via increasing the CO_2 concentration in the fuel on a commercial-scale CCGT modified with Exhaust Gas Recirculation (EGR), coupled to an amine capture plant.
- Evaluating the effect of fuel flexibility via increasing the CO_2 concentration in the fuel on the techno-economics of a commercial-scale CCGT modified with Exhaust Gas Recirculation (EGR), coupled to an amine capture plant.

8.3.2. Recommendation

In modelling the CO_2 capture plant, chemical absorption with monoethanolamine (MEA) was implemented based on recommendation form literature and the DOE report used in the modelling process. However, there are other commercially used amines for chemical absorption process of CO_2 such as DEA (diethanolamine).

Work carried out by Xue et al., [113] has compared the performance of MEA and DEA, in which it has been shown that DEA has less impact on important parameters for CO_2 capture such as lean loading, which affects the rebuilder duty and as such, the reboiler duty in operating with DEA as the amine is low compared to MEA. This reduces the overall energy penalty in the coupled system, thus leading to observable reductions in COE and COA.

9. References

1. Data.giss.nasa.gov. (Accessed 20 Jan, 2020). *Data.GISS: GISS Surface Temperature Analysis: Analysis Graphs and Plots*. [online] Available at: https://data.giss.nasa.gov/gistemp/graphs/.
2. IPCC, 2014: *Climate Change 2014: Synthesis Report. Contribution of Working Groups I, II and III to the Fifth Assessment Report of the Intergovernmental Panel on Climate Change* [Core Writing Team, R.K. Pachauri and L.A. Meyer (editions.)]. IPCC, Geneva, Switzerland, 151 pp.
3. Metz, B., Davidson, O., De Coninck, H., Loos, M., & Meyer, L. (2005). *IPCC special report on carbon dioxide capture and storage*. Intergovernmental Panel on Climate Change, Geneva (Switzerland). Working Group III.
4. Team, E. (Accessed 10 Jun. 2019). ESRL Global Monitoring Division - Global Greenhouse Gas Reference Network. [online] Esrl.noaa.gov. Available at: https://www.esrl.noaa.gov/gmd/ccgg/trends/full.html.
5. *Forests and energy*, 2008. , 1. Rome : Food and agriculture organization of the United nations (FAO).
6. U.S. Energy Information Administration. International Energy Outlook 2013 – With Projections to 2040. DOE/EIA-0484 2013.
7. Outlook, B. E. 2019 edition. *London, United Kingdom2019*.
8. International Energy Outlook 2017. (2019). Retrieved from https://www.eia.gov/outlooks/ieo/pdf/0484(2017).pdf
9. Leung, D. Y., Caramanna, G., & Maroto-Valer, M. M. (2014). An overview of current status of carbon dioxide capture and storage technologies. *Renewable and Sustainable Energy Reviews*, *39*, 426-443.
10. Wall TF. *Combustion processes for carbon capture*. In: Proceedings of the combustion institute, vol. 31; 2007. p. 31–47.
11. U.S. Energy Information Administration. International Energy Outlook 2016 – With Projections to 2040. DOE/EIA-0484 2016.

12. *2016-2020 Strategic Plan And Implementing Framework*, 1st edition (Washington, D.C.: United States. Dept. of Energy. Office of Energy Efficiency and Renewable Energy, 2015).
13. Heuberger, C. F., Staffell, I., Shah, N., & Mac Dowell, N. (2016). Quantifying the value of CCS for the future electricity system. *Energy & Environmental Science*, *9*(8), 2497-2510.
14. "Wind Power Reassessed: A Review Of The UK Wind Resource For Electricity Generation". *ADAMSMITHINSTITUTE*,2017,https://static1.squarespace.com/static/56eddde762cd9413e151ac92/t/56f71e527c65e4881ff6eac2/1459035746943/Assessment7.pdf.
15. Annual Energy Outlook. 2019 (2019). Retrieved from https://www.eia.gov/outlooks/aeo/pdf/aeo2019.pdf
16. Metz, B., Davidson, O., Bosch, P., Dave, R., & Meyer, L. (2007). *Climate Change 2007: Mitigation* (No. C048. 060). Intergovernmental Panel on Climate Change.
17. Energy demand in the world in 2004: *A global energy database including OECD data*. Enerta, Grenoble, France, 2004.
18. Schade, W., Jochem, E., Barker, T., Catenazzi, G., Eichhammer, W., Fleiter, T., ... & Mima, S. (2009). ADAM 2-degree scenario for Europe-policies and impacts (No. D-M1. 3). Alterra.
19. Mantripragada, H. C., Zhai, H., & Rubin, E. S. (2019). Boundary Dam or Petra Nova–Which is a better model for CCS energy supply?. International Journal of Greenhouse Gas Control, 82, 59-68.
20. Olajire, A. A. (2010). CO2 capture and separation technologies for end-of-pipe applications–a review. *Energy*, *35*(6), 2610-2628.
21. Kanniche, M., Gros-Bonnivard, R., Jaud, P., Valle-Marcos, J., Amann, J. M., & Bouallou, C. (2010). Pre-combustion, post-combustion and oxy-combustion in thermal power plant for CO2 capture. *Applied Thermal Engineering*, *30*(1), 53-62.
22. Hendriks, C. (1995). Energy conversion: CO 2 removal from coal-fired power plant. *Netherlands: Kluwer Academic Publishers*.

23. Corradetti, A., & Desideri, U. (2004). Analysis of Gas-Steam Combined Cycles with Natural Gas Reforming and CO2 Capture. In *ASME Turbo Expo 2004: Power for Land, Sea, and Air* (pp. 613-622). American Society of Mechanical Engineers.
24. GHG, I. (2006). CO2 capture as a factor in power station investment decisions. IEA GHG (IEA Greenhouse Gas R&D Programme) Report, (2006/8).
25. Buhre, B. J., Elliott, L. K., Sheng, C. D., Gupta, R. P., & Wall, T. F. (2005). Oxy-fuel combustion technology for coal-fired power generation. *Progress in energy and combustion science*, *31*(4), 283-307.
26. Folger, P. (2013). Carbon capture: A technology assessment. LIBRARY OF CONGRESS WASHINGTON DC CONGRESSIONAL RESEARCH SERVICE.
27. Pfaff, I., & Kather, A. (2009). Comparative thermodynamic analysis and integration issues of CCS steam power plants based on oxy-combustion with cryogenic or membrane based air separation. *Energy Procedia*, *1*(1), 495-502.
28. Mattisson, T., & Lyngfelt, A. (2001). Applications of chemical-looping combustion with capture of CO2. Second Nordic Minisymposium on Carbon Dioxide Capture and Storage, 46-51.
29. Ishida, M., Yamamoto, M., & Ohba, T. (2002). Experimental results of chemical-looping combustion with NiO/NiAl2O4 particle circulation at 1200 C. *Energy Conversion and Management*, *43*(9-12), 1469-1478.
30. Cho, P., Mattisson, T., & Lyngfelt, A. (2002). Reactivity of iron oxide with methane in a laboratory fluidized bed-application of chemical looping combustion. In *7th International Conference on Circulating Fluidised Beds, Niagara Falls, Ontario* (pp. 599-606).
31. Figueroa, J. D., Fout, T., Plasynski, S., McIlvried, H., & Srivastava, R. D. (2008). Advances in CO2 capture technology—the US Department of Energy's Carbon Sequestration Program. *International journal of greenhouse gas control*, *2*(1), 9-20.
32. Li, H., Haugen, G., Ditaranto, M., Berstad, D., & Jordal, K. (2011). Impacts of exhaust gas recirculation (EGR) on the natural gas combined cycle integrated with chemical absorption CO2 capture technology. *Energy Procedia*, *4*, 1411-1418.

33. Eckardt, D. and P. Rufli, *Advanced gas turbine technology: ABB/BCC historical firsts. Journal of engineering for gas turbines and power, 2002.* 124(3): p. 542-549.
34. "The History of Aircraft Gas Turbine Development in the United States", St. Peter, J., Published IGTI, ASME, 1999.
35. Poullikkas, A. (2005). An overview of current and future sustainable gas turbine technologies. *Renewable and Sustainable Energy Reviews*, *9*(5), 409-443.
36. Langston, L.S., Opdyke, G. and Dykewood, E.,. Introduction to gas turbines for non-engineers. *Global Gas Turbine News*, 1997; *37*(2), pp.1-9.
37. Kurz, R. and Brun, K., September. Gas Turbine Performance—What Makes the Map. In *29th Texas A&M Turbomachinery Symposium, Houston, TX, September* 2000; pp. 18-21.
38. De Sa, A. and Al Zubaidy, S., Gas turbine performance at varying ambient temperature. *Applied Thermal Engineering*, 2011; *31*(14), pp.2735-2739.
39. Ibrahim, T.K. and Rahman, M.M., Thermal impact of operating conditions on the performance of a combined cycle gas turbine. *Journal of applied research and technology*, 2012; *10*(4), pp.567-577.
40. Cameretti, M.C., R. Tuccillo, and R. Piazzesi, Study of an EGR Equipped Micro Gas Turbine supplied with bio-fuels. Applied Thermal Engineering, 2013.
41. Flavio Caresana, Gabriele Comodi, Leonardo Pelagalli and Sandro Vagni. Micro Gas Turbines, Gas Turbines, Gurrappa Injeti (Ed.), InTech, DOI: 10.5772/10211 (2010). Available from:https://www.intechopen.com/books/gas-turbines/micro-gasturbines-mgts-
42. Saravanamuttoo, H. *Gas turbine theory*. 1st ed. Harlow, England: Prentice Hall, Financial Times, 2009.
43. Mohanty, D.K. and Venkatesh, V., Performance Analysis Of a Combined Cycle Gas Turine Under Varying Operating Conditions. *Mechanical Engineering: An International Journal (MEIJ)*, 2014; *1*(2).
44. Kaushika S.C., Reddya V.S., Tyagi S.K., "Energy and exergy analyses of thermal power plants: A review" Renewable Sustainable Energy Review, 2011; Vol. 15, pp. 1857–1872.

45. Vaccarelli, M., Sammak, M., Jonshagen, K., Carapellucci, R., & Genrup, M. (2016). Combined cycle power plants with post-combustion CO_2 capture: Energy analysis at part load conditions for different HRSG configurations. *Energy*, *112*, 917-925.

46. Boyce, M. *Gas turbine engineering handbook*. 1st ed. Amsterdam: Elsevier Butterworth-Heinemann, 2012; p.51.

47. Tiwari, A.K., Hasan, M.M. and Islam, M., Effect of ambient temperature on the performance of a combined cycle power plant. *Transactions of the Canadian Society for Mechanical Engineering*, 2013; *37*(4), pp.1177-1188.

48. Tiwari, A.K., Hasan, M.M. and Islam, M., Energy analysis of combined cycle power plant: NTPC Dadri, India. *International Journal of Thermodynamics*, 2013; *16*(1), pp.36-42.

49. Ganapathy V., Waste Heat Boiler Deskbook. Indian Trail: 1991; Fairmont Press, Inc.

50. do Nascimento, M.R., de Oliveira Rodrigues, L., dos Santos, E.C., Gomes, E.B., Dias, F.G., Velásques, E.G. and Carrillo, R.M., Micro gas turbine engine: a review. 2013; *DOI*, *10*, p.54444.

51. Liss, W.E., Natural Gas Power Systems for the Distributed Generation Market. Power-Gen International '99 Conference. CD-Rom. New Orleans, Louisiana, USA, 1999.

52. Pilavachi, P.A., Mini-and micro-gas turbines for combined heat and power. *Applied thermal engineering*, 2002; *22*(18), pp.2003-2014.

53. Ali, U., Palma, C.F., Hughes, K.J., Ingham, D.B., Ma, L. and Pourkashanian, M., Impact of the operating conditions and position of exhaust gas recirculation on the performance of a micro gas turbine. *Computer Aided Chemical Engineering*, 2015; *37*, pp.2417-2422.

54. Nikpey, H., Majoumerd, M.M., Assadi, M. and Breuhaus, P., June. "Thermodynamic analysis of innovative micro gas turbine cycles" 2014; In *ASME Turbo Expo 2014: Turbine Technical Conference and Exposition* (pp. V03AT07A029-V03AT07A029). American Society of Mechanical Engineers.

55. Nascimento, M. A. R.; Santos, E. C., Biofuel and Gas Turbine Engines, Advances in Gas Turbine Technology, InTech, ISBN 978-953-307-611-9, Chapter 6, 2011.

56. Rodgers, C.; Watts, J.; Thoren, D.; Nichols, K. & Brent, R. Microturbines, Distributed Generation – The Power Paradigm for the New Millennium, edited by Anne-Marie Borbely & Jan F. Kreider, cap. 5, pp. 120 – 148, CRC Press LLC. USA, 2001.
57. Pact.ac.uk. (2020). *Gas Turbine*. [online] Available at: http://www.pact.ac.uk/facilities/PACT-Core-Facilities/Gas-Turbine/gas-turbine-system [Accessed 10 Dec 2020].
58. Capstone Turbine Corporation, Capstone Low Emissions Microturbine Tecnology, White Paper, USA, 2000.
59. Lee, J.J., Yoon, J.E., Kim, T.S. and Sohn, J.L., Performance test and component characteristics evaluation of a micro gas turbine. *Journal of Mechanical Science and Technology*, 2007; *21*(1), pp.141-152.
60. Badran, O.O., Gas-turbine performance improvements. *Applied Energy*, 1999; *64*(1), pp.263-273.
61. S. Minett, Thematic network on combined heat and power—CHAPNET, EC ENERGY contract no. ENK5- CT2001-00155, 2001.
62. Li, H., Ditaranto, M., & Berstad, D. (2011). Technologies for increasing CO2 concentration in exhaust gas from natural gas-fired power production with post-combustion, amine-based CO2 capture. *Energy*, *36*(2), 1124-1133.
63. Rao, A. D., 1989, US patent 4829763, USA.
64. Jonsson M, Yan J. Humidified gas turbines - a review of proposed and implemented cycles. Energy 2005; 30(7):1013e78.
65. Carrero, M. M., Paepe, W. D., Contino, F., Ferrari, M. L., Parente, A., & Bram, S. (2015). Transient simulations of a T100 micro gas turbine converted into a micro humid air turbine. In *ASME Turbo Expo 2015*.
66. Parente, J., Traverso, A., and Massardo, A., "Micro Humid Air Cycle Part A: Thermodynamic and Technical Aspects," 2003; ASME Paper No. GT2003-38326. ASME Turbo Expo, Atlanta, Georgia, USA.
67. Kiameh, P. (2002). *Power generation handbook: selection, applications, operation, and maintenance*. McGraw-Hill Professional.

68. Díaz, A. G., Fernández, E. S., Gibbins, J., & Lucquiaud, M. (2016). Sequential supplementary firing in natural gas combined cycle with carbon capture: A technology option for Mexico for low-carbon electricity generation and CO2 enhanced oil recovery. *International Journal of Greenhouse Gas Control*, *51*, 330-345.

69. Li, H., Ditaranto, M., & Yan, J. (2012). Carbon capture with low energy penalty: supplementary fired natural gas combined cycles. *Applied energy*, *97*, 164-169.

70. Carapellucci, R., Giordano, L., & Vaccarelli, M. (2015). Studying heat integration options for steam-gas power plants retrofitted with CO2 post-combustion capture. *Energy*, *85*, 594-608.

71. Biliyok, C., Canepa, R., & Hanak, D. P. (2015). Investigation of alternative strategies for integrating post-combustion CO2 capture to a natural gas combined cycle power plant. *Energy & Fuels*, *29*(7), 4624-4633.

72. Diego, M. E., Akram, M., Bellas, J. M., Finney, K. N., & Pourkashanian, M. (2017). Making gas-CCS a commercial reality: The challenges of scaling up. *Greenhouse Gases: Science and Technology*, *7*(5), 778-801.

73. Ditaranto, M., Hals, J., & Bjørge, T. (2009). Investigation on the in-flame NO reburning in turbine exhaust gas. *Proceedings of the Combustion Institute*, *32*(2), 2659-2666.

74. Gnanapragasam, N. V., Reddy, B. V., & Rosen, M. A. (2009). Optimum conditions for a natural gas combined cycle power generation system based on available oxygen when using biomass as supplementary fuel. *Energy*, *34*(6), 816-826.

75. Datta, A., Mondal, S., & Gupta, S. D. (2008). Perspectives for the direct firing of biomass as a supplementary fuel in combined cycle power plants. *International journal of energy research*, *32*(13), 1241-1257.

76. Bhattacharya, A., & Datta, A. (2013). Effects of supplementary biomass firing on the performance of combined cycle power generation: A comparison between NGCC and IGCC plants. *Biomass and bioenergy*, *54*, 239-249.

77. Jansohn, P., Griffin, T., Mantzaras, I., Marechal, F., & Clemens, F. (2011). Technologies for gas turbine power generation with CO2 mitigation. *Energy Procedia*, *4*, 1901-1908.

78. Akram, M., B. Khandelwal, S. Blakey, and C.W. Wilson. Preliminary Calculations on Post Combustion Carbon Capture from Gas Turbines With Flue Gas Recycle. in ASME Turbo Expo 2013: Turbine Technical Conference and Exposition. 2013. American Society of Mechanical Engineers.

79. Cameretti, M. C., Tuccillo, R., Reale, F., and Piazzesi, R., "Combustion Simulation of an EGR Operated Micro-Gas Turbine," 2008; ASME Paper No. GT2008-50692. ASME Turbo Expo, Berlin, Germany.

80. Cameretti, M. C., Tuccillo, R., & Piazzesi, R. (2012, June). Fuelling an EGR Equipped Micro Gas Turbine With Bio-Fuels. In *Turbo Expo: Power for Land, Sea, and Air* (Vol. 44717, pp. 629-640). American Society of Mechanical Engineers.

81. Majoumerd, M. M., Nikpey, H., Assadi, M., & Breuhaus, P. (2014). Micro gas turbine configurations with carbon capture–Performance assessment using a validated thermodynamic model. *Applied Thermal Engineering*, *73*(1), 172-184.

82. Nikpey, H., Ali, U., Font-Palma, C., Majoumerd, M. M., Akram, M., Pourkashanian, M., & Assadi, M. (2017, June). Evaluation of a Micro Gas Turbine With Post-Combustion CO2 Capture for Exhaust Gas Recirculation Potential With Two Experimentally Validated Models. In *Turbo Expo: Power for Land, Sea, and Air* (Vol. 50831, p. V003T06A007). American Society of Mechanical Engineers.

83. Ali, U., Palma, C. F., Hughes, K. J., Ingham, D. B., Ma, L., & Pourkashanian, M. (2015, June). Thermodynamic analysis and process system comparison of the exhaust gas recirculated, steam injected and humidified micro gas turbine. In *Turbo Expo: Power for Land, Sea, and Air* (Vol. 56673, p. V003T06A011). American Society of Mechanical Engineers.

84. Ali, U., Hughes, K. J., Ingham, D. B., Ma, L., & Pourkashanian, M. (2017). Effect of the CO2 enhancement on the performance of a micro gas turbine with a pilot-scale CO2 capture plant. *Chemical Engineering Research and Design*, *117*, 11-23.

85. Best, T., Finney, K. N., Ingham, D. B., & Pourkashanian, M. (2016). Impact of CO2-enriched combustion air on micro-gas turbine performance for carbon capture. *Energy*, *115*, 1138-1147.

86. Ali, U., Agbonghae, E. O., Hughes, K. J., Ingham, D. B., Ma, L., & Pourkashanian, M. (2016). Techno-economic process design of a commercial-scale amine-based CO2 capture system for natural gas combined cycle power plant with exhaust gas recirculation. *Applied Thermal Engineering*, *103*, 747-758.

87. Adams, T., & Mac Dowell, N. (2016). Off-design point modelling of a 420 MW CCGT power plant integrated with an amine-based post-combustion CO2 capture and compression process. *Applied Energy*, *178*, 681-702.

88. Sipöcz, N., & Tobiesen, F. A. (2012). Natural gas combined cycle power plants with CO2 capture–Opportunities to reduce cost. *International Journal of Greenhouse Gas Control*, *7*, 98-106.

89. Herraiz, L., Fernández, E. S., Palfi, E., & Lucquiaud, M. (2018). Selective exhaust gas recirculation in combined cycle gas turbine power plants with post-combustion CO2 capture. *International Journal of Greenhouse Gas Control*, *71*, 303-321.

90. Herraiz, L., Palfi, E., & Lucquiaud, M. (2018, October). A Regenerative Adsorption Wheel: Conceptual Design for CO2 Recycling in Combined Cycle Gas Turbine with CO2 Capture. In *14th Greenhouse Gas Control Technologies Conference Melbourne* (pp. 21-26).

91. Sander, F., Carroni, R., Rofka, S., & Benz, E. (2011, January). Flue gas recirculation in a gas turbine: Impact on performance and operational behavior. In *Turbo Expo: Power for Land, Sea, and Air* (Vol. 54648, pp. 123-132).

92. Qureshi, Y., Ali, U., & Sher, F. (2021). Part load operation of natural gas fired power plant with CO2 capture system for selective exhaust gas recirculation. *Applied Thermal Engineering*, *190*, 116808.

93. Diego, M. E., Bellas, J. M., & Pourkashanian, M. (2017). Process analysis of selective exhaust gas recirculation for CO_2 capture in natural gas combined cycle power plants using amines. *Journal of Engineering for Gas Turbines and Power*, *139*(12), 121701.

94. Diego, M. E., Bellas, J. M., & Pourkashanian, M. (2018). Techno-economic analysis of a hybrid CO2 capture system for natural gas combined cycles with selective exhaust gas recirculation. *Applied Energy*, *215*, 778-791.

95. Merkel, T. C., Wei, X., He, Z., White, L. S., Wijmans, J. G., & Baker, R. W. (2013). Selective exhaust gas recycle with membranes for CO2 capture from natural gas combined cycle power plants. *Industrial & Engineering Chemistry Research*, *52*(3), 1150-1159.

96. Russo, G., Prpich, G., Anthony, E. J., Montagnaro, F., Jurado, N., Di Lorenzo, G., & Darabkhani, H. G. (2018). Selective-exhaust gas recirculation for CO2 capture using membrane technology. *Journal of Membrane Science*, *549*, 649-659.

97. Baker, R. W., Freeman, B., Kniep, J., Wei, X., & Merkel, T. (2017). CO2 capture from natural gas power plants using selective exhaust gas recycle membrane designs. *International Journal of Greenhouse Gas Control*, *66*, 35-47.

98. Elkady A, Evulet A, Brand A, Ursin TP, Lynghjem A. Application of exhaust gas recirculation in a DLN F-Class combustion system for post combustion carbon capture. J Eng Gas Turbines Power 2009; 131(3):034505.

99. Moliere, M. (2005). Expanding fuel flexibility of gas turbines. *Proceedings of the Institution of Mechanical Engineers, Part A: Journal of Power and Energy*, *219*(2), 109-119.

100. Majoumerd, M. M., Breuhaus, P., Smrekar, J., Assadi, M., Basilicata, C., Mazzoni, S., ... & Cerri, G. (2012, June). Impact of Fuel Flexibility Needs on a Selected GT Performance in IGCC Application. In *Turbo Expo: Power for Land, Sea, and Air* (Vol. 44670, pp. 593-601). American Society of Mechanical Engineers.

101. Nikpey, H., Assadi, M., Breuhaus, P., & Mørkved, P. T. (2014). Experimental evaluation and ANN modeling of a recuperative micro gas turbine burning mixtures of natural gas and biogas. *Applied Energy*, *117*, 30-41.

102. Bohn, D., & Lepers, J. (2003, January). Effects of biogas combustion on the operation characteristics and pollutant emissions of a micro gas turbine. In *Turbo Expo: Power for Land, Sea, and Air* (Vol. 36843, pp. 247-257).

103. Nikpey, H., Majoumerd, M. M., Breuhaus, P., & Assadi, M. (2014). Performance analysis of a biogas-fueled micro gas turbine using a validated thermodynamic model. *Applied thermal engineering*, *66*(1-2), 181-190.

104. Kang, J. Y., Kim, T. S., & Hur, K. B. (2014). Comparative economic analysis of gas turbine-based power generation and combined heat and power systems using biogas fuel. *Energy*, *67*, 309-318.

105. Abbott, D. J., Bowers, J. P., & James, S. R. (2012, October). The impact of natural gas composition variations on the operation of gas turbines for power generation. In *Proceedings of the 6th International Conference on the Future of Gas Turbine Technology, Brussels, Belgium* (pp. 17-18).

106. Wasiu, A. B., & Heikal, M. R. (2012). The effect of carbon dioxide content-natural gas on the performance characteristics of engines: a review.

107. IEA Greenhouse Gas R&D Programme, *Improvement in power generation with post-combustion capture of CO2*. 2004.

108. Brunetti, A., Scura, F., Barbieri, G., & Drioli, E. (2010). Membrane technologies for CO2 separation. *Journal of Membrane Science*, *359*(1-2), 115-125.

109. Bounaceur, R., Lape, N., Roizard, D., Vallieres, C., & Favre, E. (2006). Membrane processes for post-combustion carbon dioxide capture: a parametric study. *Energy*, *31*(14), 2556-2570.

110. Korelskiy, D., Ye, P., Fouladvand, S., Karimi, S., Sjöberg, E., & Hedlund, J. (2015). Efficient ceramic zeolite membranes for CO 2/H 2 separation. *Journal of Materials Chemistry A*, *3*(23), 12500-12506.

111. Fu, Y., Jiang, Y. B., Dunphy, D., Xiong, H., Coker, E., Chou, S. S., ... & Rempe, S. B. (2018). Ultra-thin enzymatic liquid membrane for CO 2 separation and capture. *Nature communications*, *9*(1), 1-12.

112. Trachtenberg, M. C., Cowan, R. M., Smith, D. A., Horazak, D. A., Jensen, M. D., Laumb, J. D., & Wu, X. (2009). Membrane-based, enzyme-facilitated, efficient carbon dioxide capture. *Energy Procedia*, *1*(1), 353-360.

113. Xue, B., Yu, Y., Chen, J., Luo, X., & Wang, M. (2017). A comparative study of MEA and DEA for post-combustion CO 2 capture with different process configurations. *International Journal of Coal Science & Technology*, *4*(1), 15-24.

114. De Ávila, S. G., Logli, M. A., & Matos, J. R. (2015). Kinetic study of the thermal decomposition of monoethanolamine (MEA), diethanolamine (DEA), triethanolamine (TEA) and methyldiethanolamine (MDEA). *International Journal of Greenhouse Gas Control*, *42*, 666-671.

115. Fredriksen, S. B., & Jens, K. J. (2013). Oxidative degradation of aqueous amine solutions of MEA, AMP, MDEA, Pz: A review. *Energy Procedia*, *37*, 1770-1777.

116. Koronaki, I. P., Prentza, L., & Papaefthimiou, V. D. (2017). Parametric analysis using AMP and MEA as aqueous solvents for CO2 absorption. *Applied Thermal Engineering*, *110*, 126-135.

117. Rodríguez, N., Mussati, S., & Scenna, N. (2011). Optimization of post-combustion CO2 process using DEA–MDEA mixtures. *Chemical engineering research and design*, *89*(9), 1763-1773.

118. Agbonghae, E. O., Hughes, K. J., Ingham, D. B., Ma, L., & Pourkashanian, M. (2014). Optimal process design of commercial-scale amine-based CO2 capture plants. *Industrial & Engineering Chemistry Research*, *53*(38), 14815-14829.

119. Rezazadeh, F., Gale, W. F., Akram, M., Hughes, K. J., & Pourkashanian, M. (2016). Performance evaluation and optimisation of post combustion CO2 capture processes for natural gas applications at pilot scale via a verified rate-based model. *International Journal of Greenhouse Gas Control*, *53*, 243-253.

120. Akram, M., Ali, U., Best, T., Blakey, S., Finney, K. N., & Pourkashanian, M. (2016). Performance evaluation of PACT Pilot-plant for CO2 capture from gas turbines with Exhaust Gas Recycle. *International Journal of Greenhouse Gas Control*, *47*, 137-150.

121. Akram, M., Blakey, S., & Pourkashanian, M. (2015, June). Influence of gas turbine exhaust CO2 concentration on the performance of post combustion carbon capture plant. In *Turbo Expo: Power for Land, Sea, and Air* (Vol. 56673, p. V003T08A005). American Society of Mechanical Engineers.

122. Amrollahi, Z., Ertesvåg, I. S., & Bolland, O. (2011). Optimized process configurations of post-combustion CO2 capture for natural-gas-fired power plant—Exergy analysis. *International Journal of Greenhouse Gas Control*, *5*(6), 1393-1405.

123. Le Moullec, Y., Neveux, T., Al Azki, A., Chikukwa, A., & Hoff, K. A. (2014). Process modifications for solvent-based post-combustion CO2 capture. *International Journal of Greenhouse Gas Control*, *31*, 96-112.

124. Bek-Pedersen, E., & Gani, R. (2004). Design and synthesis of distillation systems using a driving-force-based approach. *Chemical Engineering and Processing: Process Intensification*, *43*(3), 251-262.

125. Knudsen, J. N., Andersen, J., Jensen, J. N., & Biede, O. (2011). Evaluation of process upgrades and novel solvents for the post combustion CO2 capture process in pilot-scale. *Energy Procedia*, *4*, 1558-1565.

126. Li, K., Cousins, A., Yu, H., Feron, P., Tade, M., Luo, W., & Chen, J. (2016). Systematic study of aqueous monoethanolamine-based CO2 capture process: model development and process improvement. *Energy Science & Engineering*, *4*(1), 23-39.

127. Giannaris, S., Jacobs, B., Srisang, W., Bruce, C., & Janowczyk, D. (2019). Heat integration analysis and optimization for a post combustion CO2 capture retrofit study of SaskPower's Shand Power Station. *International Journal of Greenhouse Gas Control*, *84*, 62-71.

128. Mosher, Mel. "Organic Chemistry. (Morrison, Robert Thornton; Boyd, Robert Neilson)." (1992): A305.

129. Kohl, Arthur L., and Richard Nielsen. *Gas purification*. Gulf Professional Publishing, 1997.

130. Caresana, F., Comodi, G., Pelagalli, L. and Vagni, S., 2010. Micro gas turbines. In *Gas Turbines*. IntechOpen.

131. Turbec, A.B., Technical description - T100 microturbine system. Turbec Company. Italy. Turbec AB, 2000

132. Wang, M., Joel, A. S., Ramshaw, C., Eimer, D., & Musa, N. M. (2015). Process intensification for post-combustion CO2 capture with chemical absorption: A critical review. *Applied Energy*, *158*, 275-291.

133. Edris, M. (2010). Comparison between ingle-shaft and mutli-shaft gas fired 800 MWel combined cycle power plant. *Applied thermal engineering*, *30*(16), 2339-2346.

134. Ali, U., Font-Palma, C., Somehsaraei, H.N., Majoumerd, M.M., Akram, M., Finney, K.N., Best, T., Said, N.B.M., Assadi, M. and Pourkashanian, M., 2017. Benchmarking of a micro gas turbine model integrated with post-combustion CO2 capture. *Energy*, *126*, pp.475-487.

135. Tait, P., Buschle, B., Milkowski, K., Akram, M., Pourkashanian, M., & Lucquiaud, M. (2018). Flexible operation of post-combustion CO2 capture at pilot scale with demonstration of capture-efficiency control using online solvent measurements. *International Journal of Greenhouse Gas Control*, *71*, 253-277.

136. Bui, M., Tait, P., Lucquiaud, M., & Mac Dowell, N. (2018). Dynamic operation and modelling of amine-based CO2 capture at pilot scale. *International Journal of Greenhouse Gas Control*, *79*, 134-153.

137. Gasmet Technologies - Know What's In the Air. (2021). Retrieved 12 April 2021, from https://www.gasmet.com/.

138. (2021). Retrieved 14 April 2021, from http://www.sanhuatai.com/Private/Files/20180730/636685580740907981292756 9.pdf

139. Bellas, J. M., Finney, K. N., Diego, M. E., Ingham, D., & Pourkashanian, M. (2019). Experimental investigation of the impacts of selective exhaust gas recirculation on a micro gas turbine. *International Journal of Greenhouse Gas Control*, *90*, 102809.

140. Process Industry Leadership | About AspenTech. (2020). Retrieved 3 July 2020, from https://www.aspentech.com/en/about-aspentech/industry-leadership

141. Suppes, G. J. (2002). Selecting thermodynamic models for process simulation of organic VLE and LLE systems. *ChapterONE Online (2002)*.

142. 3977-2:1997, I. *ISO 3977-2:1997 - Gas turbines -- Procurement -- Part 2: Standard reference conditions and ratings*. [online] Iso.org. Available at: https://www.iso.org/standard/24755.html?browse=tc [Accessed 3 Nov. 2020].

143. Kurzke, J. (1996). How to get component maps for aircraft gas turbine performance calculations. In *ASME 1996 International Gas Turbine and Aeroengine Congress and Exhibition* (pp. V005T16A001-V005T16A001). American Society of Mechanical Engineers.

144. Rademaker, E. R. (2012). Scaling of compressor and turbine maps on basis of equal flow Mach numbers and static flow parameters.

145. Kurzke, J. (2011). Correlations hidden in compressor maps. In *ASME 2011 Turbo Expo: Turbine Technical Conference and Exposition* (pp. 161-170). American Society of Mechanical Engineers.

146. Razak, A. M. Y. (2007). *Industrial gas turbines: performance and operability*. Elsevier.

147. Sabia, P., Lavadera, M. L., Giudicianni, P., Sorrentino, G., Ragucci, R., & de Joannon, M. (2015). CO2 and H2O effect on propane auto-ignition delay times under mild combustion operative conditions. *Combustion and flame*, *162*(3), 533-543.

148. Bolland, O., & Mathieu, P. (1998). Comparison of two CO2 removal options in combined cycle power plants. *Energy Conversion and Management*, *39*(16-18), 1653-1663.

149. Nguyen, T. H., Park, J., Jung, S., & Kim, S. (2019). A numerical study on NO x formation behavior in a lean-premixed gas turbine combustor using CFD-CRN method. *Journal of Mechanical Science and Technology*, *33*(10), 5051-5060.

150. Aspen Plus Carbon Capture | AspenTech. (2020). Retrieved 10 October 2020, from https://www.aspentech.com/en/products/pages/aspen-plus-carbon-capture

151. Arachchige, U. S. P., & Melaaen, M. C. (2012). Aspen plus simulation of CO2 removal from coal and gas fired power plants. *Energy Procedia*, *23*, 391-399.

152. Abu-Zahra, M. R., Schneiders, L. H., Niederer, J. P., Feron, P. H., & Versteeg, G. F. (2007). CO2 capture from power plants: Part I. A parametric study of the technical

performance based on monoethanolamine. *International Journal of Greenhouse gas control*, *1*(1), 37-46.

153. Zhang, Y., & Chen, C. C. (2013). Modelling CO2 absorption and desorption by aqueous monoethanolamine solution with Aspen rate-based model. *Energy Procedia*, *37*, 1584-1596.

154. Yeh, J. T., Pennline, H. W., & Resnik, K. P. (2001). Study of CO2 absorption and desorption in a packed column. *Energy & fuels*, *15*(2), 274-278.

155. Zhang, Y., & Chen, C. C. (2011). Thermodynamic modelling for CO2 absorption in aqueous MDEA solution with electrolyte NRTL model. *Industrial & engineering chemistry research*, *50*(1), 163-175.

156. Kvamsdal, H. M., & Rochelle, G. T. (2008). Effects of the temperature bulge in CO2 absorption from flue gas by aqueous monoethanolamine. *Industrial & Engineering Chemistry Research*, *47*(3), 867-875.

157. Austgen, D. M., Rochelle, G. T., Peng, X., & Chen, C. C. (1989). Model of vapor-liquid equilibria for aqueous acid gas-alkanolamine systems using the electrolyte-NRTL equation. *Industrial & engineering chemistry research*, *28*(7), 1060-1073.

158. Lim, Y., Kim, J., Jung, J., Lee, C. S., & Han, C. (2013). Modeling and simulation of CO2 capture process for coal-based power plant using amine solvent in South Korea. *Energy Procedia*, *37*, 1855-1862.

159. Cifre, P. G., Brechtel, K., Hoch, S., García, H., Asprion, N., Hasse, H., & Scheffknecht, G. (2009). Integration of a chemical process model in a power plant modelling tool for the simulation of an amine based CO2 scrubber. *Fuel*, *88*(12), 2481-2488.

160. Rochelle, G., Chen, E., Freeman, S., Van Wagener, D., Xu, Q., & Voice, A. (2011). Aqueous piperazine as the new standard for CO2 capture technology. *Chemical engineering journal*, *171*(3), 725-733.

161. Jilvero, H., Eldrup, N. H., Normann, F., Andersson, K., Johnsson, F., & Skagestad, R. (2014). Techno-economic evaluation of an ammonia-based post-combustion process integrated with a state-of-the-art coal-fired power plant. *International Journal of Greenhouse Gas Control*, *31*, 87-95.

162. Huang, W., Mi, Y., Li, Y., & Zheng, D. (2015). An aprotic polar solvent, diglyme, combined with monoethanolamine to form CO2 capture material: solubility measurement, model correlation, and effect evaluation. *Industrial & Engineering Chemistry Research*, *54*(13), 3430-3437.

163. Dinca, C., & Badea, A. (2013). The parameters optimization for a CFBC pilot plant experimental study of post-combustion CO2 capture by reactive absorption with MEA. *International Journal of Greenhouse Gas Control*, *12*, 269-279.

164. Agbonghae, E. O., Best, T., Finney, K. N., Palma, C. F., Hughes, K. J., & Pourkashanian, M. (2014). Experimental and process modelling study of integration of a micro-turbine with an amine plant. *Energy Procedia*, *63*, 1064-1073.

165. DOE/NETL. (2013). Current and Future Technologies for Natural Gas Combined Cycle (NGCC) Power Plants. Report No. DOE/NETL-341/061013. Retrieved from https://www.netl.doe.gov/energy-analysis/details?id=607

166. Turner, M. J., & Pinkerton, L. L. (2013). Quality Guidelines for Energy System Studies: Capital Cost Scaling Methodology. In *Final Report DOE/NETL-341/013113*.

167. Gerdes, K., Summers, W. M., & Wimer, J. (2011). Cost Estimation Methodology for NETL assessments of power plant performance. *US Department of Energy, National Energy Technology Laboratories, Report No. DOE/NETL-2011/1455.*

168. Basher, S. A., & Raboy, D. G. (2018). The misuse of net present value in energy efficiency standards. *Renewable and Sustainable Energy Reviews*, *96*, 218-225.

169. Díaz-Herrera, P. R., Alcaraz-Calderón, A. M., González-Díaz, M. O., & González-Díaz, A. (2020). Capture level design for a natural gas combined cycle with post-combustion CO2 capture using novel configurations. *Energy*, *193*, 116769.

170. Omehia, K. C., Clements, A. G., Michailos, S., Hughes, K. J., Ingham, D. B., & Pourkashanian, M. (2020). Techno-economic assessment on the fuel flexibility of a commercial scale combined cycle gas turbine integrated with a CO2 capture plant. *International Journal of Energy Research*, *44*(11), 9127-9140.

171. PSE: Products - Power & CCS - gCCS product overview. (2020). Retrieved 7 April 2020, from https://www.psenterprise.com/products/gccs.

172. Del Rio, M. S., Gibbins, J., & Lucquiaud, M. (2017). On the retrofitting and repowering of coal power plants with post-combustion carbon capture: An advanced integration option with a gas turbine windbox. *International Journal of Greenhouse Gas Control*, *58*, 299-311.

173. Dettori, S., Colla, V., Salerno, G., & Signorini, A. (2017). Steam Turbine models for monitoring purposes. *Energy Procedia*, *105*, 524-529.

174. Afkhamipour, M., & Mofarahi, M. (2017). Review on the mass transfer performance of CO 2 absorption by amine-based solvents in low-and high-pressure absorption packed columns. *RSC advances*, *7*(29), 17857-17872.

175. Zhao, M., Minett, A. I., & Harris, A. T. (2013). A review of techno-economic models for the retrofitting of conventional pulverised-coal power plants for post-combustion capture (PCC) of CO 2. *Energy & Environmental Science*, *6*(1), 25-40.

176. Laribi, S., Dubois, L., De Weireld, G., & Thomas, D. (2017). Post-combustion CO 2 capture process applied to flue gases with high CO 2 contents: Micro-pilot experiments and simulations. In *2017 International Conference on ENERGY and ENVIRONMENT (CIEM)* (pp. 500-504). IEEE.

177. Feron, P., Cousins, A., Jiang, K., Zhai, R., & Garcia, M. (2020). An update of the benchmark post-combustion CO2-capture technology. *Fuel*, *273*, 117776. doi: 10.1016/j.fuel.2020.117776

178. Ustadi, I., Mezher, T., & Abu-Zahra, M. R. (2017). Potential for Hybrid-Cooling system for the CO2 Post-Combustion capture technology. *Energy Procedia*, *114*, 6348-6357.

179. Joel, A. S., Wang, M., & Ramshaw, C. (2015). Modelling and simulation of intensified absorber for post-combustion CO2 capture using different mass transfer correlations. *Applied Thermal Engineering*, *74*, 47-53.

180. Heischkamp, E., Varlik, M., Korkmaz, Ö., Oeljeklaus, G., & Görner, K. (2011). Analysis of operating conditions of a flue gas scrubbing process for CO2 separation in a coal-fired power plant. *Energy Procedia*, *4*, 1377-1384.

181. Vaccarelli, M., Carapellucci, R., & Giordano, L. (2014). Energy and economic analysis of the CO2 capture from flue gas of combined cycle power plants. Energy Procedia, 45, 1165-1174.

182. Luo, X., Wang, M., & Chen, J. (2015). Heat integration of natural gas combined cycle power plant integrated with post-combustion CO_2 capture and compression. *Fuel*, *151*, 110-117.

183. Canepa, R., & Wang, M. (2015). Techno-economic analysis of a CO_2 capture plant integrated with a commercial scale combined cycle gas turbine (CCGT) power plant. *Applied Thermal Engineering*, *74*, 10-19.

184. Kale, C., Górak, A., & Schoenmakers, H. (2013). Modelling of the reactive absorption of CO2 using mono-ethanolamine. *International Journal of Greenhouse Gas Control*, *17*, 294-308.

185. Perry, R. H., & Green, D. W., (2007). Perry's chemical engineers' handbook, 8th illustrated edition.

186. Kister, H. (2013). *Distillation design*. New York: McGraw-Hill.

187. Billet, R., & Schultes, M. (1999). Prediction of mass transfer columns with dumped and arranged packings: updated summary of the calculation method of Billet and Schultes. *Chemical Engineering Research and Design*, *77*(6), 498-504.

188. Lawal, A., Wang, M., Stephenson, P., & Obi, O. (2012). Demonstrating full-scale post-combustion CO_2 capture for coal-fired power plants through dynamic modelling and simulation. *Fuel*, *101*, 115-128.

189. Olaleye, A. K., Wang, M., & Kelsall, G. (2015). Steady state simulation and exergy analysis of supercritical coal-fired power plant with CO2 capture. *Fuel*, *151*, 57-72.

190. Wolf-Zöllner, V., Seibert, F., & Lehner, M. (2019). Extended performance comparison of different pressure drop, hold-up and flooding point correlations for packed columns. *Chemical Engineering Research and Design*, *147*, 699-708.

191. Sipöcz, N., Tobiesen, A., & Assadi, M. (2011). Integrated modelling and simulation of a 400 MW NGCC power plant with CO2 capture. *Energy Procedia*, *4*, 1941-1948.

192. Nørstebø, V. S., Midthun, K. T., Bjørkvoll, T. H., & Kolbeinsen, L. (2012). Use of Natural Gas with High CO2 Content in an Integrated Industrial Park. ISIJ international, 52(8), 1439-1446.

193. Best, T., Finney, K. N., Santis, A. D., Ingham, D. B., & Pourkashanian, M. (2016). Exhaust gas recirculation and selective Exhaust gas recirculation on a micro-gas turbine for enhanced CO2 Capture performance. In *The future of gas turbine technology: 8th International gas turbine conference, Brussels, Belgium. Paper ID Number (31-IGTC16)*.

10. Appendix

10.1. Appendix A1

The stoichiometric reactions modelled in the in the combustion chamber between the natural gas and the air are highlighted in table 10.1.

Table 10.1

Stoichiometric reaction

Species	Reaction
Methane (CH4)	$CH_4 + 2O_2 \rightarrow CO_2 + 2H_2O$
Ethane (C2H6)	$C_2H_6 + 3.5O_2 \rightarrow 2CO_2 + 3H_2O$
Propane (C3H8)	$C_3H_8 + 5O_2 \rightarrow 3CO_2 + 4H_2O$
Butane (C4H10)	$C_4H_{10} + 6.5O_2 \rightarrow 4CO_2 + 5H_2O$
Pentane (C5H12)	$C_5H_{12} + 8O_2 \rightarrow 5CO_2 + 6H_2O$
Hexane (C6H14)	$C_6H_{14} + 9.5O_2 \rightarrow 6CO_2 + 7H_2O$
Methane (CH4)	$CH_4 + 2O_2 \rightarrow CO_2 + 2H_2O$

10.2. Appendix A2

The Matlab script used to modify the compressor characteristic maps which were implemented in the process modelling software. The data for the compressor maps have been removed for confidentiality purposes.

```
function output = co2(Filename)
Speed =;
%Design Speed without CO2
co2_flowrate = ;
airmassflowrate = ;
air_molarflowrate = (airmassflowrate -((co2_flowrate*10)/36))/28.9604;
co2_mole = co2_flowrate/(3600*0.044);

Nitrogen0 = n2*air_molarflowrate;
Oxygen0 = o2*air_molarflowrate;
Argon0 = ar*air_molarflowrate;
Carbondioxide0 = co2*air_molarflowrate + co2_mole;
H2O0 = h2o*air_molarflowrate;
Normalisation = Nitrogen0 + Oxygen0 + Argon0 + Carbondioxide0 + H2O0;

Nitrogen = Nitrogen0/Normalisation;
Oxygen = Oxygen0/Normalisation;
Argon = Argon0/Normalisation;
Carbondioxide = Carbondioxide0/Normalisation;
H2O = H2O0/Normalisation;

%Fluid properties entering the compressor
MWfluid = 28.0134.*(Nitrogen) + 31.998.*(Oxygen) + 39.95.*(Argon) + 44.01.*(Carbondioxide) +
18.*(H2O);% molecular weight of fluid
tair =;%temperature of the air
ref1 =;%reference pressure
ref2 =;%reference temperature
Dair = ((101325.*MWfluid)/(8.314.*tair))./1000;%Density of air
```

```
Rco2 = 8.3145/MWfluid;

mfi_Nitrogen = (28.0134.*Nitrogen)/MWfluid;
mfi_Oxygen = (31.998.*Oxygen)/MWfluid;
mfi_Argon = (39.95.*Argon)/MWfluid;
mfi_Carbondioxide = (44.01.*Carbondioxide)/MWfluid;
mfi_H2O = (18.*H2O)/MWfluid;

cp = 1.041333.*(mfi_Nitrogen) + 0.9182564.*(mfi_Oxygen) + 0.5217955.*(mfi_Argon) +
0.8362184.*(mfi_Carbondioxide) + 1.888586.*(mfi_H2O);
Gammaco2 = cp/(cp-(8.3145/MWfluid));
%Gamma for the co2 injected air
Gamma_air =;
Rair =;

%Compressor map data which includes the corrected parameters
N = [N1; N2; N3; N4; N5; N6; N7; N8; N9; N10; N11];
% Corrected Rotational Speed
out = N*sqrt(ref2);
%corrected speed
output0 = out.*sqrt((Gammaco2.*Rco2)/(Gamma_air.*Rair));
%scaled speed
output0_speed = interp1 (out,output0,Speed,'spline');
%Getting the New operating Speed
Design_Speed = output0_speed

m1 = [];
m2 = [];
m3 = [];
m4 = [];
m5 = [];
m6 = [];
m7 = [];
m8 = [];
m9 = [];
```

```
m10 = [];
m11 = [];

A = [m1; m2; m3; m4; m5; m6; m7; m8; m9; m10; m11];

mass0 = A*ref1/(sqrt(ref2));
mass1 = (mass0*sqrt((Gammaco2*Rair)/(Gamma_air*Rco2)));
%corrected mass flow rate

mass1_Design_Speed = interp1 (output0,mass1,Design_Speed, 'spline');
%interpolating the corrected mass flow rate at design speed in rpm
mass1_Design_Speed = mass1_Design_Speed';
Cs = sqrt((Rair*tair)/Gamma_air);
Mx = mass0.*Cs.*(1./(101325.*0.13));
%Dimensionless parameters

PR1 = [];
PR2 = [];
PR3 = [];
PR4 = [];
PR5 = [];
PR6 = [];
PR7 = [];
PR8 = [];
PR9 = [];
PR10 = [];
PR11 = [];

B = [PR1; PR2; PR3; PR4; PR5; PR6; PR7; PR8; PR9; PR10; PR11];

New_B = ((((Gammaco2-1).*(1+(((Gamma_air-1)./2).*Mx.^2))).*(B.^((Gamma_air-1)./Gamma_air)-
1)./((Gamma_air-1).*(1+(((Gammaco2-1)./2).*Mx.^2))))+1).^(Gammaco2./(Gammaco2-1));

EFF1 = [];
```

```
EFF2 = [];
EFF3 = [];
EFF4 = [];
EFF5 = [];
EFF6 = [];
EFF7 = [];
EFF8 = [];
EFF9 = [];
EFF10 = [];
EFF11 = [];
C = [EFF1; EFF2; EFF3; EFF4; EFF5; EFF6; EFF7; EFF8; EFF9; EFF10; EFF11];
mass_in = Dair*mass1_Design_Speed';
%Getting the operating air flowrate

TestT = tair*(New_B.^((Gamma_air-1)/Gamma_air)./C-1./C+1);
%Outlet temperature of the compressor
TestE = (1-(log(TestT./tair)./log(New_B))).^-1;
Exponent = TestE;
%Polytropic exponent calculation

PEff = ((Gamma_air-1)/Gamma_air).*(Exponent./(Exponent-1));
%polytropic efficiency

PEff_Design_Speed = interp1 (output0,PEff,Design_Speed);
%interpolating the polytropic efficiency at design speed in rpm
PEff_Design_Speed = PEff_Design_Speed';
H1 = Exponent./(Exponent-1);
H2 = (8.314.*tair)./MWfluid;
H3 = New_B.^(1./H1)-1;
Head = H1.*H2.*H3.*1000;
%Head calculation

Head_Design_Speed = interp1 (output0,Head,Design_Speed);
%interpolating the Head at design speed in rpm
Head_Design_Speed = Head_Design_Speed'
```

10.3. Appendix A3

The Matlab script used to modify the turbine characteristic maps which were implemented in the process modelling software. The data for the turbine maps have been removed for confidentiality purposes.

```
function output = Tco2(Filename)

Design_Speed = ;
%Design Speed

co2_flowrate = 0;

%Air composition and properties
FA = ;

%air flowrate
air_molarflowrate = (FA -((co2_flowrate*10)/36))/28.9615;

co2_mole = co2_flowrate/(3600*0.04401);
%co2 molarflowrate

Nitrogen0 = n2*air_molarflowrate;
Oxygen0 = o2*air_molarflowrate;
Argon0 = ar*air_molarflowrate;
Carbondioxide0 = co2*air_molarflowrate + co2_mole;
H2O0 = h2o*air_molarflowrate;
Normalisation = Nitrogen0 + Oxygen0 + Argon0 + Carbondioxide0 + H2O0;

Nitrogen = Nitrogen0/Normalisation;
Oxygen = Oxygen0/Normalisation;
Argon = Argon0/Normalisation;
Carbondioxide = Carbondioxide0/Normalisation;
H2O = H2O0/Normalisation;
```

```
MWair = 28.0134.*(Nitrogen) + 31.998.*(Oxygen) + 39.95.*(Argon) + 44.01.*(Carbondioxide) +
18.01528.*(H2O);% molecular weight of air

%Fuel composition and properties
FF = ;
%fuel flowrate
CH4 = ;
C2H6 = ;
C3H8 = ;
C4H10 = ;
CO2 = ;
N2 = ;

MWfuel = 16.04.*(CH4) + 30.07.*(C2H6) + 44.1.*(C3H8) + 58.124.*(C4H10) + 44.01.*(CO2) + 28.0134.*(N2);

N_R = Nitrogen/Oxygen;
C_R = Carbondioxide/Oxygen;
A_R = Argon/Oxygen;
H_R = H2O/Oxygen;

%Combustion Product and properties
C_CO2 = (1+2*C_R).*CH4 + (2+(3.5*C_R)).*C2H6 + (3+(5*C_R)).*C3H8 + (4+(6.5*C_R)).*C4H10 + CO2;
C_H2O = (2+(2*H_R)).*CH4 + (3+(3.5*H_R)).*C2H6 + (4+(5*H_R)).*C3H8 + (5+(6.5*H_R)).*C4H10;
C_N2 = (2*N_R).*CH4 + (3.5*N_R).*C2H6 + (5*N_R).*C3H8 + (6.5*N_R).*C4H10 + N2;
C_Ar = (2*A_R).*CH4 + (3.5*A_R).*C2H6 + (5*A_R).*C3H8 + (6.5*A_R).*C4H10;
%Stoichiometric reactions in combustor

C_O2 = 2.*CH4 + 3.5.*C2H6 + 5.*C3H8 + 6.5.*C4H10;
%Required O2

tgas = ;%Turbine Inlet Temperature
ref1 = ;%reference pressure for the gas entering the turbine
ref2 = ;%reference temperature for the gas entering the turbine

%Excess Air calculation
R_O2 = (FF/MWfuel)*C_O2;
```

```
R_air = (R_O2./Oxygen)*MWair;
Excess_air = (FA-R_air)/R_air

Excess_O2 = Excess_air.*C_O2;
Excess_H2O = ((Excess_air+1).*(C_H2O -(2.*CH4)-(3.*C2H6)-(4.*C3H8)-(5.*C4H10))) + ((2.*CH4) +
(3.*C2H6)+(4.*C3H8)+(5.*C4H10));
Excess_N2 = ((Excess_air+1).*(C_N2-N2)) + N2;
Excess_CO2 = ((Excess_air+1).*(C_CO2-CO2-CH4-(2.*C2H6)-(3.*C3H8)-(4.*C4H10))) +
(CO2+CH4+(2.*C2H6)+(3.*C3H8)+(4.*C4H10));
Excess_Ar = (Excess_air+1).*C_Ar;
Total_Product = Excess_H2O + Excess_O2 + Excess_N2 + Excess_CO2 + Excess_Ar;

%Normalisation of the gas products
N_CO2 = Excess_CO2/Total_Product;
N_O2 = Excess_O2/Total_Product;
N_H2O = Excess_H2O/Total_Product;
N_N2 = Excess_N2/Total_Product;
N_Ar = Excess_Ar/Total_Product;
%Number of moles of each product

MWproduct = 44.01.*N_CO2 + 18.01528.*N_H2O + 28.0134.*N_N2 + 31.998.*N_O2 + 39.95.*N_Ar;
mfi_CO2 = (44.01.*N_CO2)/MWproduct;
mfi_O2 = (31.998.*N_O2)/MWproduct;
mfi_H2O = (18.01528.*N_H2O)/MWproduct;
mfi_N2 = (28.0134.*N_N2)/MWproduct;
mfi_Ar = (39.95.*N_Ar)/MWproduct;
%mass fractions of the individual products of combustion

cp = 1.1955.*(mfi_CO2) + 2.22692.*(mfi_H2O) + 1.15073.*(mfi_N2) + 1.07805.*(mfi_O2) +
0.52072.*(mfi_Ar);
Gamma = cp/(cp-(8.3145/MWproduct));
%Gamma for the product
D_product = (pressure*MWproduct)/(8.314*tgas)/1000;

%Turbine map data which includes the corrected parameters
N1 = ;
```

```
N2 = ;
N3 = ;
N4 = ;
N5 = ;
N6 = ;
N7 = ;
N8 = ;
N9 =;
N10 =;
N11 =;

N = [N1; N2; N3; N4; N5; N6; N7; N8; N9; N10; N11];

output0 = N*sqrt(ref2);
%corrected speed

m1 = [];
m2 = [];
m3 = [];
m4 = [];
m5 = [];
m6 = [];
m7 = [];
m8 = [];
m9 = [];
m10 = [];
m11 = [];

A = [m1; m2; m3; m4; m5; m6; m7; m8; m9; m10; m11];

PR1 = [];
PR2 = [];
PR3 = [];
PR4 = [];
PR5 = [];
PR6 = [];
```

```
PR7 = [];
PR8 = [];
PR9 = [];
PR10 = [];
PR11 = [];

B = [PR1; PR2; PR3; PR4; PR5; PR6; PR7; PR8; PR9; PR10; PR11];

EFF1 = [];
EFF2 = [];
EFF3 = [];
EFF4 = [];
EFF5 = [];
EFF6 = [];
EFF7 = [];
EFF8 = [];
EFF9 = [];
EFF10 = [];
EFF11 = [];

C = [EFF1; EFF2; EFF3; EFF4; EFF5; EFF6; EFF7; EFF8; EFF9; EFF10; EFF11];

mass1 = A*ref1/(D_product.*sqrt(ref2));
%corrected mass flow rate

mass1_Design_Speed = interp1 (output0,mass1,Design_Speed, 'spline');
%interpolating the corrected mass flow rate at design speed in rpm
mass1_Design_Speed = mass1_Design_Speed';

OutletT = tgas.*(1-(C.*(1-(B.^((1-Gamma)/Gamma)))));
% %Outlet temperature of the turbine

Exponent = (1-(log(OutletT./tgas)./log(1./B))).^-1;
%Polytropic exponent calculation

PEff = (Gamma./(Gamma-1)).*((Exponent-1)./Exponent);
```

```
%polytropic efficiency

PEff_Design_Speed = interp1 (output0,PEff,Design_Speed);
%interpolating the polytropic efficiency at design speed in rpm
PEff_Design_Speed = PEff_Design_Speed';

H1 = Exponent./(Exponent-1);
H2 = (8.314.*tgas)./MWproduct;
H3 = B.^(1./H1)-1;
Head = H1.*H2.*H3.*1000;
%Head calculation

Head_Design_Speed = interp1 (output0,Head,Design_Speed);
%interpolating the Head at design speed in rpm
Head_Design_Speed = Head_Design_Speed';
```